Marine Geology, 98 (1991) 201–239
Elsevier Science Publishers B.V., Amsterdam

Petrology and geochemistry of the central North Fiji Basin spreading centre (Southwest Pacific) between 16°S and 22°S

Jean-Philippe Eissen[a,1], Christian Lefèvre[b], Patrick Maillet[c], Gilles Morvan[d] and Masato Nohara[e]

[a]*Centre ORSTOM, BP A5, Nouméa Cedex, New Caledonia*
[b]*Université des Sciences et Techniques de Lille, Sciences de la Terre, 59655 Villeneuve d'Ascq Cedex, France*
[c]*ORSTOM, La Trobe University, Geology Department, Bundoora, Vic. 3083, Australia*
[d]*Université de Bretagne Occidentale, Faculté des Sciences, 6 Avenue Le Gorgeu, 29263 Brest Cedex, France*
[e]*Geological Survey of Japan, Tsukuba, Ibaraki 305, Japan*

(Received March 5, 1990; revision accepted September 17, 1990)

ABSTRACT

Eissen, J.-P., Lefèvre, C., Maillet, P., Morvan, G. and Nohara, M., 1991. Petrology and geochemistry of the central North Fiji Basin spreading centre (Southwest Pacific) between 16°S and 22°S. In: K.A.W. Crook (Editor), The Geology, Geophysics and Mineral Resources of the South Pacific. Mar. Geol., 98: 201–239.

The North Fiji Basin (NFB) is a 12 m.y. old back-arc basin that has a complex multi-stage history. The presently active spreading system can be divided into four segments between 16°S and 22°S, which from north to south trend N160, N15 and N–S (the fourth segment is the N–S trending segment located near 174E). The main N–S segment is morphologically similar to other medium-rate oceanic ridges, whereas the other segments have rougher morphologies which have been severely disturbed by a triple junction at 16°45'S and several instability features such as overlapping spreading centres (OSCs) and propagating rifts. The spreading rate seems to diminish from 7.8 cm/yr near 20°S to 4.6 cm/yr near 18°S. Mineralogical, petrological and geochemical data were obtained on 24 new stations located along all the four segments. The petrogenesis of the basalts collected is essentially controlled by low-pressure crystal fractionation of plagioclase ± olivine ± clinopyroxene (*plagioclase > olivine > clinopyroxene*) with 52% of the NFB basalts reaching the four-phase cotectic. Locally, some magma mixing occurs, but this is limited to magma batches of closely related composition, as might be expected to occur inside a magma reservoir. The N–S segment, which, since 3 m.y., is the only steady-state segment, is also petrologically and geochemically very comparable to other medium-rate oceanic spreading centres, producing moderately evolved LILE and LREE-depleted N-MORB. In contrast, the three other segments produce basalts of much more variable petrology and geochemistry characterized by LILE and slightly LREE-enriched magmas of back-arc basin basalt (BABB) affinity (but not as enriched as, for example, the Mariana BABB); MORB is, however, also found on the N160, N15 and 174E segments. Diagrams using Ba, Rb, K/P and $(K/Ti)_N$ (normalized to the chondrites) plotted against latitude clearly show along-strike variations. Beneath the recently formed segments, the mantle source is heterogeneous, and locally has some BABB affinities, whereas beneath the more steady-state N–S segment the magma source is more homogeneous, being generally depleted in LILE and REE as is the case for classical N-MORB mantle sources. Simple evolution from an early stage of BABB production to MORB described in the Lau basin and proposed for the NFB does not seem to occur. Present-day activity still produces large amounts of BABB along the less-stable and more recently created segments, and MORB was produced in the earlier stages of the development of the NFB.

Introduction

Located in a back-arc environment, the North Fiji Basin (hereafter, NFB) spreading centre is probably the largest if not the oldest active back-arc basin on earth. Early work (Chase, 1971; Karig, 1971, 1974) explains its formation by active spreading (Fig.1). Subsequent geomagnetic, heat flow, seismic reflection, refraction and bathymetric surveys confirmed the present activity of the NFB and roughly located its main spreading areas (Ma-

[1]Member of GDR 910, "Genèse et Evolution des Domaines Océaniques", Brest

0025-3227/91/$03.50

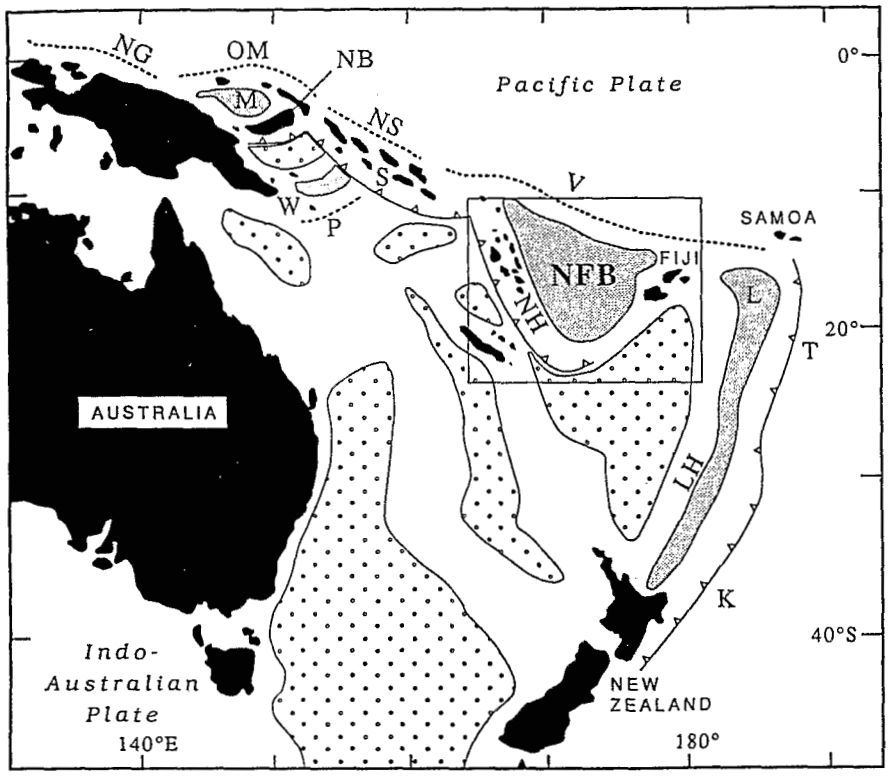

Fig.1. Geodynamic features of the Southwest Pacific. Active subduction zones dipping towards the continent: *T*=Tonga; *K*=Kermadec. Active subduction zones dipping towards the ocean: *NB*=New Britain; *S*=Solomon; *NH*=New Hébrides. Paleo-subduction zones: *NG*=New-Guinea; *OM*=West Melanesia; *NS*=North Solomon; *V*=Vitiaz; *P*=Pocklington. Active marginal basins (grey stipple): *M*=Manus; *W*=Woodlark; *NFB*=North Fiji; *L*=Lau; *LH*=Le Havre. Inactive marginal basins are shown with coarse stippling. The box delineates the area of Fig.2.

lahoff et al., 1982; Larue et al., 1982; Brocher, 1985; Maillet et al., 1986). However, samples from this spreading centre were hitherto almost non-existent except from north of 16°S (Aggrey et al., 1988; Sinton et al., 1991).

Eissen et al. (1990) have published a short note dealing with petrological along-strike variations in the NFB spreading centre between 16 and 20°S, and this paper presents some general results obtained on "zero-age" volcanic rocks collected on or close to the NFB spreading centre between 16°18′S and 21°26′S during the SEAPSO Leg 3 cruise (Auzende et al., 1986, 1988a) and the subsequent KAIYO 87 (Auzende et al., 1988b) and KAIYO 88 (Ruellan et al., 1989) cruises. The mineralogy, petrology and geochemistry of the samples are discussed, with a special emphasis on the along-strike variations. In addition we will compare these basalts with samples from other Pacific back-arc basins, and discuss their petrogenesis.

Geological setting

Previous work

The opening of the NFB results from the break up of the old Vitiaz lineament (Fig.1). Rapidly changing stress regimes within the Southwest Pacific approximately 12 m.y. ago led to the reversal of the subduction polarity along the Vitiaz–New Hebrides Island Arc. As a consequence, the NFB back-arc spreading began between 12 and 8 m.y., and this was followed by several reorganizations (Falvey, 1978; Kroenke, 1984; Brocher, 1985; Auzende et al., 1988c; Pelletier et al., 1988; Charvis and Pelletier, 1989). The presently active spreading centre was identified by roughly N–S trending

magnetic anomalies (Chase, 1971; Cherkis, 1980; Malahoff et al., 1982).

The NFB spreading centre was located precisely between 20° and 21°S near 173°20'E using the bathymetric and geomagnetic survey carried out during EVA 12 cruise of R.V. *Coriolis* (Maillet et al., 1986, 1989). During the SEAPSO Leg 3 cruise of R.V. *Jean Charcot*, the ridge location was defined between 16°18'S and 20°10'S and two precise full-coverage Seabeam maps (30 × 10 miles) were completed near 18°25'S and 20°05'S (Auzende et al., 1986, 1988a). Ten bottom water, dredge and deep-tow stations along the active ridge were also surveyed during this cruise. The KAIYO 87 cruise completed this first detailed survey. A full Seabeam mapping of the axis was carried out between 16°30'S and 18°10'S, accompanied by water and hard rock sampling (Auzende et al., 1988b). Detailed photo and video work near the sea bottom around a newly discovered active hydrothermal site near 17°S was also conducted. The subsequent KAIYO 88 cruise was mainly devoted to the area south of 21°S, where Seabeam mapping of the axis and sampling were conducted (Ruellan et al., 1989). This southernmost segment completes the junction between the spreading system of the NFB and the subduction zone of the southern New Hebrides Trench (Fig.2) (Maillet et al., 1989).

Morphology of the NFB spreading ridge

Between 16°S and 22°S, the roughly N–S oriented presently active spreading system was created approximately 3 m.y. ago, with a local reorganization around 1 m.y. ago (Auzende et al., 1988a,c; Tanahashi et al., this issue). It may be divided into four segments displaying different structural orien-

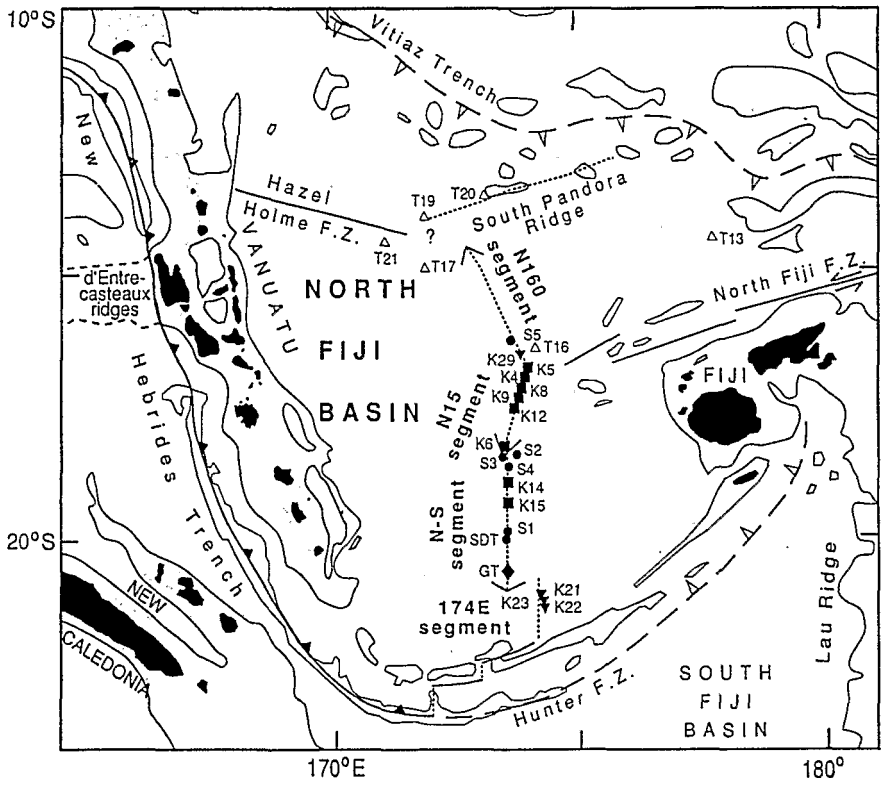

Fig.2. North Fiji Basin map with sample locations used in this study. Black diamond = GEOTRANSIT (GT) cruise; dots = SEAPSO cruise; black squares = KAIYO 87 cruise; black triangles = KAIYO 88 cruise. Data from the literature: white triangles = KANA KEOKI 1982 tripartite cruise (T13 to T21, from Sinton et al., 1991). *F.Z.* = fracture zone. Dashed lines = spreading centres. Arrow at the tip of a spreading centre indicates a propagating rift. Areas in less than 2000 m of water are shown in grey stipple. The active New Hebrides subduction zone is shown. Dashed lines with white triangles are paleo-subduction zones.

tations and morphologies. From north to south, they are as follows (Fig.2):

(1) *A N160 segment between ca.15°S and 16°40'S.* This segment is marked by a complex cross section, with high scarps, alternation of ridges and grabens, and at least one overlapping spreading centre (OSC) near 16°20'S. The spreading axis is situated in a deep asymmetrical rift (Kroenke and Eade, 1991) rather than on top of a wide ridge (Lafoy, 1989).

(2) *A N15 segment between 16°50'S and 18°20'S.* The spreading axis is situated on a small, 10 km wide symmetrical ridge, but is frequently offset by non-transform offsets or by OSCs (e.g. near 17°16'S, 17°48'S and 17°52'S). Both the N160 and N15 segments are marked by a sharp decrease in the water depth towards 16°45'S. Here, the two spreading ridges and the westernmost part of the North Fiji Fracture Zone meet at a triple junction (Lafoy et al., 1987; Lafoy, 1989; Tanahashi et al., this issue) (Fig.2).

(3) *A N–S segment between 18°10'S and ca.21°S.* Compared to the other segments, the morphology of this segment is relatively flat, the axis being situated on a 7–8 km wide and 200–400 m high ridge. Very few offsets are observed and only one OSC occurs, near 19°50'S. The morphology of this segment is very similar to that observed along the East Pacific Rise near 13°N (Gente, 1987).

(4) *A 174E segment, oriented N5–N15 between 20°40'S and 21°30'S, and offset eastwards along the 174°10'E meridian.* Although highly variable, the morphology of this segment often corresponds to a wide dome bounded by two elongate deep troughs.

The relative instability of the NFB, which has known several reorganizations in less than 12 m.y., is marked by the presence of several propagating rifts (Hey, 1977), which are, from north to south:

(1) The northernmost part of the N160 segment, propagating northward (Kroenke and Eade, 1991).

(2) The southernmost part of the N15 segment, propagating southward (Lafoy, 1989), whereas the northernmost part of the N–S segment is dying.

(3) The southernmost part of the N–S segment, propagating southward, whereas the northernmost part of the 174E segment is dying (Maillet et al., 1989).

Geomagnetic data enable the calculation of a spreading rate of 7.8 cm/yr at 20°S for the period represented by magnetic anomalies 1 and 2A (Maillet et al., 1986), 5.2 cm/yr at 18°10'S (Auzende et al., 1988a) and 4.6 cm/yr along the N15 segment for anomalies 1 and J (Lafoy, 1989). Thus, the spreading rate seems to decrease significantly from 21°S towards the 16°45'S triple junction.

In summary, the NFB is a large, old, structurally mature back-arc basin. Its long (ca.12 m.y.) and complex development is probably the result of unstable regional stress regimes.

Sample preparation and analytical procedure

The hard rock recovery from the 24 new sampling sites (Fig.2, Table 1) was highly variable (ranging from less than 1 kg to more than 200 kg depending on the success of the sampling technique), these techniques include conventional dredging during the SEAPSO Leg 3 cruise and chain-bag dredging or use of small dredges attached to the deep tow during the KAIYO 87 and 88 cruises. Table 1 sumarizes the sampling locations, briefly describes the structural environment of the sampling sites, and the relative recovery. When enough material was recovered, eight to twelve samples were selected aboard the ship as the representative set of each site depending on the macroscopic differences observed. One hundred and twenty four samples were thus selected, photographed and described (Table 2), and all the subsequent studies were carried out on these samples. From each of them, at least one polished thin section was made for petrographic and microprobe analysis. Model analyses were obtained, with at least 1000 point counting, on six thin sections (Table 2), using internally consistent definitions of phenocrysts and microphenocrysts based not only on the size of the mineral grains, but also on texture, shapes, and intergrowths of the coexisting phases as described by Bryan (1983) and already used in other petrological studies (Staudigel and Bryan, 1981; Eissen et al., 1989). All the other modes given in Table 2 indicate occurrence of the different mineral phases and microscopically estimated modal contents. For a volume percentage of total phenocrysts and microphenocrysts, lavas

are defined as aphyric, sub-aphyric, moderately phyric, phyric and highly phyric as follows: of <1%, between 1 and 5%, between 5 and 15%, between 15 and 25%, and >25% respectively. Each sample was crushed in an agate mortar for bulk rock geochemical analysis (except sample GT 104, which is only made up of a few glass chips). Major and trace element analyses were performed by atomic absorption spectrometry at the *Université de Bretagne Occidentale* at Brest by Joseph Cotten. Rare earth element analyses for eight samples were obtained by ICP at the Geological Survey of Japan at Tsukuba. Microprobe analyses were made using the fully automated CAMEBAX microprobe at the IFREMER Centre at Brest. Glasses were analyzed using hand-picked glass chips from 89 samples and mounted on 25-hole brass supports containing one reference glass. Individual minerals were analyzed on polished thin sections from 56 selected samples. We used the usual three-step procedure for silicate analysis: (1) Fe, Na, Si and K, (2) Mn, Mg, Al and Ca, and (3) Cr and Ti (the peak and background counting times was 6 s and the filament current 15 kV). The accuracy was controlled during a single probe session or from one session to another, by analyzing homogeneous reference minerals or USNM reference glasses numbers 111240 (VG-2) and 113498 (VG-A99). Some complementary mineral analyses was performed on the JEOL 744 superprobe at the Geological Survey of Japan at Tsukuba.

Petrology of the lavas

The rocks collected along the NFB spreading centre present a typical basaltic plagioclase ± olivine ± clinopyroxene (± spinel) mineralogy. Plagioclase is the dominant phase, and occurs either as phenocrysts or microphenocrysts. Olivine is frequently associated with it, but at a much lower volume percent; moreover, phyric olivine basalt is completely absent from this rock collection. Clinopyroxene rarely appears as phenocrysts, but is frequently intimately associated with plagioclase and sometimes olivine in skeletal microphenocrysts or glomerocrysts. Spinels are scarce, and are generally associated with plagioclase or olivine phenocrysts or xenocrysts in the most phyric lavas.

These dredged basalts can be separated into different petrochemical types on the basis of their mineralogical assemblage, their modal content, and their geochemistry. However, as the observed variations differs from one segment to another, we will describe these samples according to their structural location, from the northern segment to the southernmost one. The various types probably represent individual magma batches, much of the observed scattering within each type being explained by low-pressure fractionation, with some occasional magma mixing.

N160 segment

This spreading centre has been sampled only near its southern tip at four stations (S5, K29, K17 and K5 in Fig.2). (Its northern part was surveyed during other cruises (Aggrey et al., 1988; Sinton et al., 1991; Kroenke and Eade, 1991).) The three most northerly stations (S5, K29 and K17) were probably not directly on the active volcanic zone as no very fresh basalts with shining glass were recovered. Indeed, bulk rock analyses (Table 3a) always show a positive H_2O^+ content (between 0.02 and 0.58%), indicating incipient alteration. This weak alteration was confirmed by the observation in thin sections of palagonite and Fe–Mn hydroxides along cracks and in vesicles, even in cases where minerals such as olivine were still not transformed. The two most southerly stations (K17 and K5) are in the triple junction area, which probably explains their peculiar petrology, with the presence of highly phyric lavas. Four types can be recognized in these samples:

Type 1-I: Highly phyric plagioclase + olivine ± clinopyroxene basalts from station K5. These lavas exhibit a relatively unevolved bulk rock, with low FeO*/MgO (0.85 ± 0.03) and TiO_2% (0.80 ± 0.10), relatively high Cr (246 ± 39 ppm) and Ni (113 ± 11 ppm) contents (Table 3a), and glass (Table 4a) compositions.

Type 1-II: Highly phyric or sub-aphyric plagioclase–olivine–clinopyroxene basalts from station K17. Despite a large difference in crystals, the two lavas exhibit a moderately evolved bulk rock, with

TABLE I

Summary of the 24 sampling locations used in this study with: abridged station number, position, water depth, description of the structure of the sampling sites, and description of the recovered samples. SPS 3=SEAPSO 3 cruise; K 87=KAIYO 87 cruise; K 88=KAIYO 88 cruise; GT104=GEOTRANSIT cruise; *ST*=station; *D*=dredge; *DT*=deep tow. The abridged station number given in station number column will hereafter be used

Station Number	Latitude South	Longitude East	Water Depth	Site	Recovery
N160 segment :					
SPS 3 D 5	=S5	16°18.18′ to 16°18.77′	173°33′13 to 173°31′10	3930 to 3500	western flank of the ridge	60 kg of pillows and lava with slight Mn coating and sediment traces
K 88 ST 29 D 6	=K29	16°39.89′ to 16°40.45′	173°49.24′ to 173°49.07′	2580 to 2498	ridge near the N160 graben axis	40 kg of Mn coated aphyric to phyric pillow basalts, 50 kg of consolidated sediments
K 88 ST 17 D 1	=K17	16°47.54′ to 16°47.90′	174°01.46′ to 174°01.69′	2778 to 2667	triple junction area	one highly phyric and one sub-aphyric basaltic pillow
K 87 ST 5 D 3	=K5	16°53.60′ to 16°53.42′	173°54.39′ to 173°54.57′	2205 to 2101	triple junction area	1.5 kg of highly phyric basaltic pillow
N15 segment :					
K 87 ST 4 D 2	=K4	16°54.66′ to 16°58.67′	173°54.66′ to 173°55.02′	1979 to 1960	axial graben	61 kg of fresh to lightly altered pillows and crusts of sub-aphyric basalt
K 87 ST 4 DT A	=K4A	16°57.85′ to 16°58.50′	173°54.97′ to 173°55.64′	1964 to 1970	axial graben	0.2 kg of Mn crust fragments 1 kg of altered basalt 0.5 kg of glass scree
K 87 ST 4 DT B	=K4B	16°58.57′ to 16°59.07′	173°54.76′ to 173°55.48′	1935 to 1970	axial graben	0.5 kg of Mn crust fragments 0.5 kg of light brown ooze 0.3 kg of basalt, 2 kg scree
K 87 ST 8 D 5	=K8	17°09.50′ to 17°09.17′	173°52.32′ to 173°52.41′	2306 to 2323	axial graben	24 kg of fresh sub-aphyric glassy crust of basalt 1 kg of sedimentry mud
K 87 ST 9 D 6	=K9	17°19.86′ to 17°19.22′	173°49.29′ to 173°48.60′	2506 to 2539	small axial graben	36 kg of aphyric to moderately phyric glassy pillow basalt with limited alteration
K 87 ST 12 D 9	=K12	17°36.05′ to 17°34.16′	173°46.15′ to 173°45.49′	2517 to 2494	axial ridge	1 kg of glassy phyric basalt crust basalt 0.5 kg light brown mud 0.5 kg of pumices
K 87 ST 6 DT A	=K6A	18°06.65′ to 18°07.68′	173°28.62′ to 173°29.98′	2696 to 2820	axial ridge	17 kg of sub-aphyric to moderatly phyric lightly altered basalt + sediment traces
K 87 ST 6 D 4	=K6	18°05.96′ to 18°08.93′	173°28.98′ to 173°29.45′	2816 to 2638	axial ridge	10 kg of relatively fresh aphyric pillow basalt
SPS 3 D 3	=S3	18°12.84′ to 18°13.61′	173°24′01 to 173°25′15	2940 to 2660	on-axis volcano	80 kg of pillows and lava crusts with slight Mn coating

TABLE 1 (*continued*)

Station Number	Latitude South	Longitude East	Water Depth	Site	Recovery
N-S segment :					
SPS 3 D 2	=S2 18°11.34′ to 18°12.04′	173°34′96 to 173°36′90	2800 to 2550	off-axis ridge	25 kg : 1 massive bloc and 1 pillow of basalt slightly altered + sediment traces
SPS 3 D 4	=S4 18°34.00′ to 18°32.62′	173°31′32 to 173°31′09	2870 to 2800	axial graben	50 kg of fresh pillow and glassy lava crust of basalt
K 87 ST 14 D 10	=K14 18°49.51′ to 18°48.72′	173°29.83′ to 173°29.53′	2729 to 2713	axial ridge	33 kg fresh aphyric glassy basaltic pillow, crust and protuberance
K 87 ST 15 D 11	=K15 19°17.08′ to 19°15.44′	173°27.33′ to 173°27.64′	2755 to 2696	axial ridge	200 kg fresh aphyric glassy basaltic pillow, crust and protuberance
SPS 3 DT	=SDT 19°59.6 ′ to 19°52.7 ′	173°22.5 ′ to 173°23.1 ′	2900 to 2700	axial graben	60 kg of fresh pillows and glassy protuberances of basalts
SPS 3 D 1	=S1 19°57.87′ to 19°57.20′	173°22′46 to 173°22′10	2900 to 2770	axial graben	50 kg of fresh pillows, glassy crusts and protuberances of basalts
GT104	=GT 20°26′	173°24′	2840	ridge axis	few glass fragments
174° East segment :					
K 88 ST 21 D 3	=K21 21°02.18′ to 21°01.86′	174°08.87′ to 174°08.83′	2844 to 2820	axial ridge	50 kg of fresh glassy pillow and lightly altered basaltic pillow with thin Mn coating
K 88 ST 23 D 4	=K23 21°10.74′ to 21°10.29′	174°11.03′ to 174°10.29′	2834 to 2844	axial ridge	22 kg of sub-aphyric lightly altered basaltic pillow and crust with thin Mn coating
K 88 ST 22 D 5	=K22 21°23.76′ to 21°22.63′	174°11.93′ to 174°11.63′	2653 to 2501	axial ridge	1 large pillow (70 kg) and 1 small pillow (2 kg) of aphyric basalt
K 88 ST 22 DT DT 9-10	=K22 21°26.70′ to 21°24.33′	174°10.73′ to 174°10.20′	2218 to 2563	axial ridge and seamount	33 kg aphyric sheeted lavas and basaltic pillow with thin Mn coating

low FeO*/MgO (1.26±0.03) and Ni content (72±1 ppm) (Table 3a) and glass (Table 4a) compositions. The lower Cr (140 ppm) and TiO_2% (1.27) of the most phyric basalt is the result of the plagioclase accumulation of a magma of similar composition to sample K17-1-2 (Table 3a).

Type 1-III: Moderately phyric to phyric basalts from site S5 with plagioclase, olivine phenocrysts and rare clinopyroxene microphenocrysts. These lavas are characterized by the occasional occurrence of clinopyroxene. They comprise a moderately evolved bulk rock, with low FeO*/MgO (1.05±0.05) and TiO_2% (1.58±0.03) (Table 3a), and glass (Table 4a) compositions, despite relatively high Cr (286±37 ppm), Ni (117±6 ppm) and Ba (57±21 ppm) contents.

TABLE 2

Summary of the sample morphology, mineralogy and modal content; lava types as distinguished in the text. *Sample morphology*: *pillow* = pillow lava; *crust* = lava crust; *massive* = pillow interior or massive flow; *protub.* = large pillow protuberance. *Mineralogy*: phenocrysts = more or less equidimensional crystals, euhedral to xenomorphic with a length of > 500 μm; microphenocrysts = small euhedral to skeletal crystals with a length of between 100 and 500 μm; *PL* = plagioclase; *OL* = olivine; *CPX* =

St. Nb.	Sa. Nb.	Morphology	PHENOCRYSTS PL	PHENOCRYSTS OL	PHENOCRYSTS CPX	MICROPHENOCRYSTS PL	MICROPHENOCRYSTS OL	MICROPHENOCRYSTS CPX	SP	Alt	Mode	Lava Type
N160 segment :												
S5	01	pillow	PL			PL	OL			+	MPH	1-III
S5	02	pillow	14	4		4	1	1	+	+	PH	1-III
S5	03	pillow	PL	OL		PL	OL	(CPX)		+	MPH	1-III
S5	04	pillow	3	1		11	1	1	+		MPH	1-III
S5	05	pillow	PL	OL		PL	OL	CPX			MPH	1-III
S5	06	pillow	PL	OL		PL	OL			+	MPH	1-III
S5	07	pillow	PL	OL		PL	OL			+	MPH	1-III
S5	08	pillow	PL	OL		PL	OL				MPH	1-III
K29	2	pillow	(PL)			PL	OL	CPX			MPH	1-IV
K29	3	pillow	PL	OL		PL	OL	(CPX)		+	MPH	1-IV
K29	4	pillow				PL	OL	CPX			SA	1-IV
K29	5	pillow	(PL)			PL	OL	CPX		+	MPH	1-IV
K29	8	pillow	(PL)			PL	OL	CPX			MPH	1-IV
K29	11	pillow				PL	OL	CPX		+	SA	1-IV
K17	1	pillow	PL	OL	(CPX)	PL	OL	CPX	+		HPH	1-II
K17	2	pillow				PL	OL	(CPX)	+	+	SA	1-II
K5	1	pillow	PL	OL		PL	OL	CPX	+		HPH	1-I
K5	2	pillow	PL	OL		(PL)	(OL)		+		HPH	1-I
N15 segment :												
K4	1	crust				(PL)					A	2-IV
K4	2	crust				(PL)					A	2-IV
K4	3	crust	(PL)			PL					SA	2-IV
K4	4	crust				PL					SA	2-IV
K4	5	pillow		(OL)		PL	OL	CPX			SA	2-IV
K4	6	pillow				PL	(OL)				SA	2-IV
K4	7	pillow				PL					A	2-IV
K4	8	pillow				PL					A	2-IV
K4	9	pillow				PL					A	2-IV
K4A	3	crust				(PL)				H	A	-
K4A	4	crust				(PL)				H	A	-
K4A	7	pillow	PL			(PL)				H	SA	-
K4B	1	crust				(PL)				+	A	-
K4B	2	crust				PL				H	SA	-
K8	1	crust	(PL)			PL	OL	CPX			SA	2-VI
K8	2	crust	PL			PL	OL	CPX			SA	2-VI
K8	3	crust	PL			PL	OL	CPX			SA	2-VI
K8	4	crust	PL			PL	OL	CPX			SA	2-VI
K8	5	crust	PL		(CPX)	PL	OL	CPX			SA	2-VII
K8	6	crust	PL	(OL)	(CPX)	PL	OL	CPX			SA	2-VII
K9	1	pillow	PL	OL		PL	OL	CPX		+	MPH	2-III
K9	2	pillow	PL	OL	CPX	PL	OL	CPX			MPH	2-III
K9	3	pillow	PL		(CPX)	PL	OL	CPX			SA	2-III
K9	4	pillow	PL	OL		PL	OL	CPX			MPH	2-III
K9	5	pillow				PL	OL	CPX			SA	2-VI
K9	6	pillow	(PL)	(OL)		PL	OL	CPX			MPH	2-VI
K12	1	crust	PL			PL	OL				MPH	2-I
K12	2	crust	PL			PL	OL			•	MPH	2-I
K12	3	crust	PL	OL		PL	OL			+	MPH	2-I
K12	4	crust	PL			PL	OL			+	MPH	2-I
K12	5	crust	PL			PL	OL				MPH	2-I
K12	6	crust	(PL)			PL	OL			+	MPH	2-I
K12	7	crust	PL			PL	OL			·	MPH	2-I
K12	8	crust	(PL)			PL	OL				MPH	2-I
K6A	1	pillow				PL	OL			+	SA	2-III
K6A	2	pillow	(PL)	(OL)		PL	OL			+	SA	2-III
K6A	3	pillow	PL	OL		PL	OL			+	SA	2-III
K6	1	pillow	PL	OL		PL	OL	CPX			SA	2-III
K6	2	horn	PL	OL		PL	OL	CPX			SA	2-III
K6	3	pillow	PL	(OL)		PL	OL	CPX			SA	2-III
K6	4	pillow	PL	(OL)		PL	OL	CPX			SA	2-III
K6	5	pillow	PL	OL		PL	OL	CPX			SA	2-III
K6	6	pillow	PL	OL		PL	OL	CPX			SA	2-III
S3	01	crust	22	1	0	1	0	1	+		PH	2-V
S3	02	pillow	PL	OL		PL	OL	(CPX)			MPH	2-V
S3	03	pillow	PL	OL		PL	OL				MPH	2-II
S3	04	pillow	PL	OL		PL	OL	(CPX)		+	MPH	2-II
S3	05	pillow	PL	OL		PL	OL				PH	2-II
S3	06	pillow	PL	OL		PL	OL		+		PH	2-V
S3	07	pillow	PL	OL	CPX	PL	OL	CPX			PH	2-V
S3	08	pillow	PL	OL		PL	OL	CPX			MPH	2-V
S3	09	pillow	PL	OL		PL	OL		+	+	PH	2-II
S3	10	pillow	PL	OL	CPX	PL	OL	CPX			PH	2-V

TABLE 2 (*continued*)

clinopyroxene (between parentheses = low occurrence); *SP* = spinels; *Alt* = alteration; + = traces; *H* = hydrothermal alteration. The six modal analyses were obtained by counting at least 1000 points (mineral abundances are given in volume percent); *t* = traces. All other mineral occurrences are estimated. Mode: *A* = aphyric lava (less than 1% of crystals); *SA* = sub-aphyric lava (1% < crystals < 5%); *MPH* = moderately phyric lava (5% < crystals < 15%); *PH* = phyric lava (15% < crystals < 25%); *HPH* = highly phyric lava (25% < crystals). Lava types are discussed in the text

St. Nb.	Sa. Nb.	Morphology	PHENOCRYSTS PL	PHENOCRYSTS OL	PHENOCRYSTS CPX	MICROPHENOCRYSTS PL	MICROPHENOCRYSTS OL	MICROPHENOCRYSTS CPX	SP	Alt	Mode	Lava Type
N-S segment :												
S2	1	massive	PL	OL	CPX	PL	OL	CPX		+	MPH	3-III
S2	2	crust	PL	OL		PL	OL	CPX		+	SA	3-III
S4	01	crust	PL	(OL)		PL	OL				SA	3-II
S4	02	pillow	PL			PL	OL				SA	3-II
S4	03	pillow	PL			PL	OL				SA	3-II
S4	04	pillow	1	0	0	3	1	0			SA	3-II
S4	05	crust	(PL)			PL	OL				SA	3-II
S4	06	crust	PL			PL	OL				SA	3-II
S4	07	crust	PL			PL	OL				SA	3-II
S4	08	crust	PL			PL	OL				SA	3-II
S4	09	crust	(PL)			PL	OL				SA	3-II
S4	10	crust	(PL)			PL	OL				SA	3-II
K14	1	pillow				PL	OL				SA	3-II
K14	2	pillow				PL	OL				SA	3-II
K14	5	crust				PL	OL				SA	3-II
K14	6	horn				(PL)					A	3-IV
K14	7	horn				PL	OL				SA	3-II
K14	8	crust	(PL)			PL	OL				SA	3-II
K14	10	crust				(PL)					A	3-IV
K15	2	pillow				PL	OL				SA	3-III
K15	5	pillow				PL	OL				SA	3-III
K15	6	pillow				PL	OL				SA	3-III
K15	7	pillow		(OL)		PL	OL	(CPX)			SA	3-III
K15	8	pillow				PL	OL				SA	3-III
K15	9	pillow				PL	OL				SA	3-III
K15	10	pillow				PL	OL				SA	3-II
K15	13	horn	(PL)			PL	OL				SA	3-III
SDT	01	protub.				PL	(OL)	(CPX)			A	3-II
SDT	02	protub.	PL	OL		PL	OL	(CPX)			SA	3-II
SDT	03	pillow	PL	OL		PL	OL	(CPX)			SA	3-II
SDT	04	pillow				(PL)		(CPX)			A	3-III
SDT	05	pillow	PL	OL		PL	OL	CPX			SA	3-II
SDT	06	pillow	PL	OL		PL	OL	(CPX)			SA	3-II
SDT	07	pillow	PL	OL		PL	OL	CPX			SA	3-II
SDT	08	massive	PL	OL		PL	OL	(CPX)			SA	3-II
SDT	09	protub.	PL	OL		PL	OL	(CPX)			SA	3-II
SDT	10	pillow	PL	OL		PL	OL	(CPX)			SA	3-II
S1	01	pillow	PL			PL	OL	(CPX)			SA	3-II
S1	02	crust	PL	OL		PL	OL	CPX			SA	3-II
S1	03	crust	t	t	t	2	1	0			SA	3-II
S1	04	crust	PL			PL	OL	CPX			SA	3-II
S1	05	pillow	PL			PL	OL	CPX			SA	3-II
S1	06	crust	PL	OL		PL	OL	CPX			SA	3-II
S1	07	protub.	1	0	0	1	t	t			SA	3-II
S1	08	protub.	PL			PL	OL	CPX			SA	3-II
S1	09	pillow				PL	OL	CPX			SA	3-II
S1	10	pillow	PL		CPX	PL	OL	CPX			SA	3-II
S1	11	pillow	PL		CPX	PL	OL	CPX			SA	3-II
GT104		glass				PL	OL	CPX			SA	3-I
174° East segment :												
K21	1	pillow		OL		PL	OL				SA	4-I
K21	2	pillow	PL	OL		PL	OL				SA	4-I
K21	6	pillow	PL			PL					SA	4-I
K21	8	pillow		OL		PL	OL				SA	4-I
K21	27	pillow				PL	OL				SA	4-I
K21	28	pillow		OL		PL	OL				SA	4-I
K21	29	pillow		OL		PL	OL				SA	4-I
K23	14	pillow	PL	OL	CPX	PL	(OL)	CPX		+	MPH	4-II
K23	15	pillow	PL	OL		PL	OL	CPX			MPH	4-II
K23	16	pillow	PL	OL		PL	OL				SA	4-II
K23	17	crust	PL	OL		PL	OL			+	SA	4-II
K23	18	crust	PL	OL		PL	OL				SA	4-II
K23	19	pillow	PL	OL		PL	OL				SA	4-II
K23	20	pillow	PL	OL		PL	OL	CPX			MPH	4-II
K22	1	pillow	(PL)			PL	(OL)	CPX		+	MPH	4-IV
K22	2	pillow	PL		CPX	PL	OL	CPX		+	MPH	4-IV
K22	3	pillow	PL	OL		PL	(OL)	CPX		+	SA	4-IV
K22DT2		pillow				PL		CPX		+	SA	4-III

TABLE 3a

Bulk rock analyses for the N160 segment. The analyst for Tables 3a–d was J. Cotten, *Université de Bretagne Occidentale*, Brest. In all tables, FeO*=total iron expressed as FeO ($=0.9\times Fe_2O_3$)

Station	S5	S5	S5	S5	S5	S5	S5	S5	K29	K29	K29	K29	K29	K29	K17	K17	K5	K5
Sample	01	02	03	04	05	06	07	08	2	3	4	5	8	11	1	2	1	2
Lava type	1-III	1-III	1-III	1-III	1-III	1-III	1-III	1-III	1-IV	1-IV	1-IV	1-IV	1-IV	1-IV	1-II	1-II	1-I	1-I
Mode	MPH	PH	MPH	MPH	MPH	MPH	MPH	MPH	MPH	MPH	SA	MPH	MPH	SA	HPH	SA	HPH	HPH
SiO_2	49.10	49.80	50.00	50.00	50.00	50.00	49.80	50.10	49.50	49.30	50.10	50.15	49.50	49.60	49.30	49.80	48.80	49.50
TiO_2	1.61	1.59	1.63	1.54	1.61	1.58	1.53	1.57	1.87	1.80	1.78	1.77	1.76	1.74	1.27	1.47	0.69	0.90
Al_2O_3	16.02	16.02	16.29	15.92	15.99	16.09	16.00	15.78	14.71	15.65	14.86	14.73	14.52	14.54	18.48	14.81	23.96	20.20
Fe_2O_3	8.98	8.79	8.65	9.84	9.00	9.04	8.72	9.62	10.49	10.83	10.05	10.43	10.63	10.85	8.96	10.62	5.00	7.17
MnO	0.15	0.15	0.15	0.17	0.16	0.15	0.14	0.17	0.20	0.18	0.17	0.17	0.18	0.18	0.15	0.18	0.09	0.14
MgO	7.43	7.54	7.09	7.69	7.97	7.49	7.78	7.64	7.27	7.08	7.37	7.24	7.18	7.00	6.11	7.63	5.38	7.20
CaO	12.13	12.22	12.23	12.04	12.18	12.33	12.34	12.08	11.66	11.36	11.80	11.64	11.50	11.54	12.41	11.93	13.86	12.62
Na_2O	2.66	2.55	2.60	2.50	2.58	2.54	2.53	2.55	2.82	2.57	2.86	2.86	2.87	2.82	2.51	2.91	1.79	2.06
K_2O	0.31	0.36	0.31	0.29	0.39	0.40	0.34	0.42	0.26	0.28	0.22	0.29	0.33	0.37	0.19	0.11	0.06	0.08
P_2O_5	0.20	0.10	0.10	0.10	0.10	0.10	0.10	0.10	0.10	0.20	0.20	0.20	0.20	0.20	0.05	0.05	0.10	0.10
H_2O^+	0.58	0.35	0.43	0.12	0.02	0.20	0.56	0.14	0.06	0.32	0.03	0.22	0.15	0.25	0.22	0.54	-0.22	-0.35
H_2O^-	0.41	0.27	0.41	0.19	0.15	0.15	0.43	0.21	0.11	0.21	0.11	0.12	0.12	0.17	0.07	0.05	0.08	0.12
Total	99.58	99.74	99.89	100.40	100.15	100.07	100.27	100.38	99.05	99.78	99.55	99.82	98.94	99.26	99.72	100.10	99.59	99.74
FeO*/MgO	1.06	1.03	1.07	1.13	0.99	1.06	0.99	1.11	1.27	1.35	1.20	1.27	1.30	1.36	1.29	1.22	0.82	0.88
Rb	5.0	6.0	5.0	5.0	7.0	7.0	6.0	9.0	6.0	5.0	4.0	6.0	7.0	8.0	4.0	3.0	2.5	3.0
Sr	191	190	211	175	181	217	184	178	185	158	185	184	185	181	141	131	127	116
Ba	45	70	70	64	64	70	70	58	27	42	30	27	27	30	24	26	15	15
V	237	246	239	239	249	236	237	230	268	272	270	275	257	263	223	258	124	175
Cr	303	308	306	292	305	300	294	300	200	253	208	204	205	225	140	259	207	282
Co	46	46	43	41	43	44	46	45	41	42	40	41	39	40	36	43	23	33
Ni	119	128	120	104	114	116	118	114	84	100	71	76	70	92	73	71	101	124
Cu	71	71	69	68	70	73	68	70	72	61	60	70	76	70	65	94	50	67
Zn	76	75	74	77	74	76	73	73	81	88	80	79	79	81	66	75	44	60

TABLE 3b

Bulk rock analyses for the N15 segment

Station	K4	K4	K4	K4	K4	K4	K4	K4	K4	K4A	K4A	K4A	K4B	K4B	K8	K8	K8	K8	K8	K8	K9	K9	K9	K9	K9	K9
Sample	1	2	3	4	5	6	7	8	9	3	4	7	1	2	1	2	3	4	5	6	1	2	3	4	5	6
Lava type	2-IV	2-IV	2-IV	2-IV	2-IV	2-IV	2-IV	2-IV	2-IV	-	-	-	-	-	2-VI	2-VI	2-VI	2-VI	2-VII	2-VII	2-III	2-III	2-III	2-III	2-VI	2-VI
Mode	A	A	SA	SA	SA	SA	A	A	A	A	A	SA	A	SA	SA	SA	SA	SA	SA	SA	MPH	MPH	SA	MPH	SA	MPH
SiO_2	51.20	51.30	51.35	51.60	50.50	51.20	51.40	50.90	51.50	49.00	49.80	49.25	51.30	49.60	51.50	51.50	51.50	51.30	50.10	50.15	50.35	50.50	51.00	50.75	51.15	51.00
TiO_2	1.53	1.55	1.55	1.51	1.50	1.57	1.58	1.58	1.55	1.85	1.87	1.90	1.66	1.84	1.47	1.44	1.44	1.47	2.47	2.48	1.34	1.52	1.24	1.41	1.59	1.62
Al_2O_3	14.24	14.27	14.17	14.27	14.80	14.20	14.10	14.30	14.09	16.55	15.90	15.70	14.23	16.82	13.78	13.92	13.68	13.70	13.90	13.92	14.67	14.78	14.24	14.44	13.68	13.66
Fe_2O_3	11.20	11.31	11.17	11.22	10.80	11.14	11.07	11.08	11.13	8.20	9.07	9.24	11.32	7.82	12.47	12.51	12.32	12.31	12.90	12.71	11.08	10.99	10.73	11.18	12.55	12.88
MnO	0.19	0.19	0.19	0.19	0.18	0.19	0.19	0.19	0.19	0.20	0.16	0.13	0.19	0.14	0.21	0.21	0.21	0.21	0.20	0.20	0.17	0.17	0.18	0.17	0.21	0.21
MgO	6.90	6.84	6.94	7.04	7.11	6.93	7.13	6.84	6.89	8.13	8.07	7.30	6.72	7.89	6.78	6.67	6.65	6.72	6.87	6.76	7.38	7.48	7.39	7.43	6.38	6.41
CaO	11.19	11.22	11.22	11.16	11.35	11.08	11.06	11.21	11.03	10.64	10.69	10.65	10.60	10.16	11.05	10.98	10.78	10.85	11.06	11.03	11.84	11.97	11.76	11.98	10.47	10.53
Na_2O	2.90	2.92	2.91	2.88	2.90	2.89	2.87	2.88	2.89	2.31	2.76	2.88	3.08	2.89	2.95	2.97	2.92	2.92	2.88	2.85	2.75	2.76	2.81	2.76	2.97	2.94
K_2O	0.17	0.17	0.17	0.13	0.14	0.18	0.22	0.17	0.16	0.76	0.77	0.78	0.45	0.87	0.20	0.20	0.20	0.15	0.19	0.21	0.13	0.13	0.12	0.13	0.26	0.19
P_2O_5	0.10	0.12	0.10	0.10	0.10	0.10	0.10	0.10	0.10	0.35	0.35	0.35	0.20	0.40	0.10	0.12	0.12	0.12	0.10	0.10	0.10	0.10	0.10	0.10	0.12	0.12
H_2O^+	-0.50	-0.51	-0.57	-0.73	-0.24	-0.43	-0.37	-0.43	-0.46	0.47	0.09	0.68	-0.44	0.33	-0.47	-0.44	-0.45	-0.61	-0.56	-0.50	-0.09	-0.43	-0.40	-0.40	-0.47	-0.57
H_2O^-	0.11	0.14	0.09	0.05	0.19	0.17	0.18	0.16	0.21	0.24	0.09	0.25	0.09	0.26	0.13	0.14	0.16	0.10	0.19	0.17	0.11	0.10	0.10	0.09	0.15	0.09
Total	99.23	99.52	99.36	99.42	99.33	99.22	99.51	98.98	99.28	99.20	99.62	99.11	99.40	99.02	100.17	100.22	99.53	99.24	100.30	100.08	99.83	100.07	99.27	100,04	99.06	99.08
FeO*/MgO	1.43	1.46	1.42	1.40	1.34	1.41	1.37	1.43	1.42	0.89	0.89	1.11	1.48	0.87	1.62	1.65	1.63	1.61	1.65	1.65	1.32	1.29	1.18	1.32	1.73	1.72
Rb	4.5	4.5	5.0	5.0	4.0	5.0	5.0	5.0	5.0	16.0	17.0	17.0	11.0	18.0	5.0	5.0	5.0	4.0	5.0	5.0	4.0	3.5	3.5	4.0	5.0	5.0
Sr	130	130	126	125	138	129	128	129	128	260	260	267	160	269	110	113	109	112	114	113	121	121	118	123	120	118
Ba	35	30	30	30	25	30	35	30	40	180	199	191	140	232	57	33	25	33	25	25	10	20	45	25	66	49
V	290	285	285	285	280	293	300	295	285	220	202	220	245	180	275	273	260	255	316	326	270	257	232	254	290	266
Cr	135	129	129	129	246	128	126	123	126	213	215	209	56	220	110	109	106	108	93	92	159	160	183	162	115	116
Co	40	40	40	40	38	40	41	43	41	32	31	32	44	36	46	46	46	47	43	43	40	41	46	40	46	46
Ni	50	50	50	49	59	53	51	50	50	159	157	145	45	150	43	40	41	40	42	42	49	50	49	49	41	42
Cu	88	87	88	86	98	82	82	84	83	57	57	67	78	53	80	81	82	80	78	77	91	91	93	90	74	114
Zn	86	86	87	86	79	86	86	86	86	67	67	122	90	93	99	94	95	98	98	97	79	82	79	80	97	96

Station	K12	K12	K12	K12	K12	K12	K12	K12	K6A	K6A	K6A	K6	K6	K6	K6	K6	K6	S3	S3	S3	S3	S3	S3	S3	S3	S3
Sample	1	2	3	4	5	6	7	8	1	2	3	1	2	3	4	5	6	01	02	03	04	05	06	07	08	09	10
Lava type	2-I	2-I	2-I	2-I	2-I	2-I	2-I	2-I	2-III	2-III	2-III	2-III	2-III	2-III	2-III	2-III	2-III	2-V	2-V	2-II	2-II	2-II	2-II	2-V	2-V	2-II	2-V
Mode	MPH	MPH	MPH	MPH	MPH	MPH	MPH	MPH	SA	SA	SA	SA	SA	SA	SA	SA	SA	PH	MPH	MPH	MPH	PH	PH	PH	MPH	PH	PH
SiO_2	50.00	43.50	48.30	48.00	49.10	49.60	49.75	49.40	50.30	51.30	51.15	51.50	51.80	51.50	51.30	51.40	51.20	50.50	50.40	50.00	50.10	49.70	50.00	50.20	50.60	49.60	50.20
TiO_2	0.95	0.95	0.89	0.93	0.93	1.02	0.94	0.93	1.33	1.22	1.23	1.39	1.42	1.55	1.48	1.39	1.42	1.68	1.58	1.10	1.20	1.10	1.09	1.59	1.66	1.14	1.64
Al_2O_3	17.38	14.35	16.98	16.26	16.87	16.10	16.69	17.00	14.83	15.04	15.08	14.33	14.47	14.50	14.33	14.43	14.41	15.25	15.67	17.27	16.20	17.45	17.73	15.70	14.59	17.21	15.53
Fe_2O_3	8.70	11.15	9.30	9.62	9.04	9.60	9.20	9.04	10.54	10.18	10.22	11.20	11.11	11.25	11.24	11.22	11.55	11.49	11.33	8.85	9.22	8.88	8.34	11.21	12.29	8.93	11.38
MnO	0.17	2.99	0.58	0.56	0.34	0.45	0.39	0.34	0.16	0.17	0.17	0.18	0.18	0.18	0.18	0.18	0.18	0.18	0.18	0.15	0.16	0.15	0.14	0.18	0.19	0.15	0.18
MgO	7.35	6.72	7.16	7.23	7.30	7.48	7.40	7.56	7.48	7.47	7.47	7.51	7.60	7.58	7.52	7.43	7.64	6.50	6.35	7.26	7.55	6.95	6.92	6.41	6.53	6.66	6.42
CaO	12.35	10.66	11.94	12.02	12.11	11.89	12.08	12.21	11.12	10.84	10.79	11.35	11.31	11.33	11.36	11.28	11.68	11.90	12.03	13.06	12.99	13.15	13.43	12.02	11.67	12.97	12.02
Na_2O	2.39	2.30	2.36	2.40	2.42	2.49	2.41	2.38	2.61	2.62	2.65	2.41	2.38	2.39	2.33	2.33	2.39	2.35	2.43	2.37	2.36	2.28	2.31	2.34	2.39	2.31	2.40
K_2O	0.11	0.17	0.12	0.16	0.13	0.15	0.13	0.11	0.55	0.51	0.51	0.10	0.10	0.10	0.11	0.10	0.10	0.13	0.14	0.06	0.08	0.12	0.07	0.11	0.13	0.18	0.14
P_2O_5	0.05	0.20	0.12	0.10	0.10	0.12	0.10	0.08	0.30	0.25	0.20	0.10	0.08	0.08	0.08	0.10	0.10	0.10	0.10	0.05	0.05	0.05	0.05	0.08	0.10	0.05	0.05
H_2O^+	-0.44	2.25	0.39	0.68	0.04	0.21	0.15	-0.12	-0.11	-0.06	-0.06	-0.44	-0.58	-0.49	-0.57	-0.62	-0.56	-0.50	-0.43	-0.23	-0.36	-0.16	-0.37	-0.50	-0.30	0.04	-0.42
H_2O^-	0.06	4.25	0.36	0.62	0.28	0.27	0.20	0.12	0.34	0.20	0.18	0.11	0.12	0.14	0.13	0.12	0.14	0.10	0.10	0.12	0.07	0.09	0.04	0.09	0.18	0.12	0.11
Total	99.07	99.49	98.50	98.58	98.66	99.38	99.44	99.05	99.45	99.75	99.59	99.74	99.99	100.11	99.49	99.36	100.25	99.68	99.88	100.06	99.62	99.76	99.75	99.43	100.03	99.36	99.65
FeO*/MgO	1.04	1.46	1.14	1.17	1.09	1.13	1.09	1.05	1.24	1.20	1.20	1.31	1.29	1.31	1.32	1.33	1.33	1.56	1.57	1.07	1.07	1.12	1.06	1.54	1.66	1.18	1.56
Rb	3.0	3.5	3.0	3.5	3.5	3.5	3.5	3.0	10.0	10.0	10.0	4.0	4.0	3.5	3.5	3.5	3.5	2.5	2.5	1.5	1.5	2.5	1.5	2.5	3.0	4.0	2.5
Sr	145	269	172	178	157	166	160	153	134	129	130	91	93	93	93	93	93	108	108	110	104	112	110	109	109	111	110
Ba	43	136	77	77	34	60	43	51	85	125	109	15	15	10	10	10	10	15	35	20	20	32	17	24	25	10	10
V	166	198	174	180	167	175	178	187	241	230	247	305	295	313	320	300	314	304	282	221	240	213	230	285	314	219	306
Cr	322	285	284	315	315	322	313	322	256	285	284	286	292	287	282	283	283	134	134	303	325	296	295	135	136	294	129
Co	40	84	48	52	48	51	50	45	38	40	40	38	41	40	43	41	41	40	39	46	39	37	37	40	40	37	41
Ni	88	193	117	106	101	101	101	102	115	110	108	78	86	79	75	78	76	52	56	86	81	80	81	57	56	87	55
Cu	86	194	94	160	144	135	127	104	66	66	65	73	73	74	74	74	75	68	64	84	81	86	74	62	70	78	65
Zn	64	119	78	86	78	79	74	70	89	87	89	89	89	89	89	86	90	91	90	64	74	66	66	86	93	65	90

TABLE 3c

Bulk rock analyses for the N–S segment

Station	S2	S2	S4	S4	S4	S4	S4	S4	S4	S4	S4	S4	K14	K14	K14	K14	K14	K14	K15	K15	K15	K15	K15
Sample	1	2	01	02	03	04	05	06	07	08	09	10	1	2	5	6	8	10	2	5	7	8	9
Lava type	3-III	3-III	3-II	3-II	3-II	3-II	3-II	3-II	3-II	3-II	3-II	3-II	3-II	3-II	3-II	3-IV	3-II	3-IV	3-III	3-III	3-III	3-III	3-III
Mode	MPH	SA	SA	SA	SA	SA	SA	SA	SA	SA	SA	SA	SA	SA	SA	A	SA	A	SA	SA	SA	SA	SA
SiO_2	50.35	50.00	50.00	49.00	49.50	49.75	49.95	49.80	49.90	50.00	48.75	50.00	49.80	50.50	50.30	50.30	50.00	50.00	49.20	49.70	49.75	49.75	49.25
TiO_2	1.79	1.79	1.59	1.53	1.55	1.56	1.57	1.48	1.50	1.56	1.58	1.55	1.54	1.58	1.48	1.80	1.48	1.80	1.82	1.82	1.89	1.85	1.78
Al_2O_3	14.55	14.48	14.92	14.88	14.88	14.93	14.92	14.61	14.87	14.87	14.93	14.89	14.43	14.22	14.38	14.25	14.10	14.20	14.80	14.76	14.79	14.95	14.56
Fe_2O_3	11.68	11.83	11.65	11.59	11.72	11.66	11.52	11.91	11.64	11.75	11.56	11.67	12.20	12.17	12.14	12.40	12.40	12.37	11.69	11.75	11.69	11.75	11.81
MnO	0.18	0.18	0.18	0.19	0.18	0.18	0.18	0.19	0.18	0.18	0.18	0.18	0.19	0.19	0.19	0.19	0.19	0.19	0.18	0.18	0.18	0.18	0.18
MgO	6.99	7.12	7.40	7.77	7.78	7.80	7.73	7.85	7.84	7.81	7.89	7.87	7.74	7.77	7.82	7.30	7.84	7.30	7.73	7.73	7.69	7.71	7.77
CaO	11.43	11.45	12.12	12.19	12.19	12.15	12.06	11.21	12.06	12.10	12.17	12.23	11.69	11.73	11.72	11.21	11.74	11.21	11.47	11.45	11.39	11.37	11.61
Na_2O	2.55	2.52	2.46	2.50	2.52	2.51	2.49	2.44	2.49	2.49	2.53	2.52	2.31	2.32	2.31	2.59	2.34	2.56	2.65	2.65	2.69	2.67	2.67
K_2O	0.20	0.21	0.07	0.06	0.07	0.07	0.07	0.10	0.07	0.07	0.07	0.07	0.09	0.09	0.09	0.22	0.10	0.22	0.16	0.16	0.16	0.16	0.16
P_2O_5	0.10	0.10	0.10	0.10	0.10	0.10	0.10	0.10	0.10	0.10	0.10	0.10	0.10	0.08	0.10	0.20	0.12	0.15	0.20	0.20	0.15	0.15	0.20
H_2O^+	-0.28	-0.32	-0.80	-0.88	-0.68	-0.64	-0.64	-0.60	-0.68	-0.72	-0.65	-0.53	-0.83	-0.64	-0.82	-0.64	-0.64	-0.64	-0.50	-0.62	-0.52	-0.53	-0.53
H_2O^-	0.12	0.15	0.07	0.07	0.10	0.10	0.11	0.03	0.09	0.08	0.08	0.07	0.04	0.06	0.04	0.07	0.06	0.05	0.11	0.07	0.07	0.12	0.11
Total	99.66	99.51	99.76	99.00	99.91	100.17	100.06	99.12	100.06	100.29	99.19	100.62	99.30	100.07	99.75	99.89	99.73	99.73	99.51	99.85	99.93	100.13	99.57
FeO*/MgO	1.47	1.46	1.39	1.31	1.33	1.32	1.31	1.34	1.31	1.32	1.29	1.30	1.39	1.38	1.37	1.49	1.39	1.49	1.33	1.34	1.34	1.34	1.34
Rb	3.6	4.5	2.0	2.0	2.0	2.0	2.0	2.4	2.0	2.0	2.0	2.0	3.0	3.5	3.0	5.0	3.5	5.5	3.5	3.5	3.5	3.5	3.5
Sr	117	117	96	94	94	96	96	95	93	96	97	96	84	84	83	141	83	141	117	116	118	118	120
Ba	20	20	40	25	30	23	17	10	17	30	35	25	20	20	30	49	15	40	20	20	20	25	20
V	295	300	292	294	285	287	291	300	285	290	291	293	300	307	305	306	312	298	291	301	289	292	280
Cr	232	232	299	295	297	295	297	315	297	297	295	297	272	272	273	137	284	148	264	265	265	262	268
Co	44	43	44	44	43	43	44	45	44	44	44	44	41	40	42	40	43	44	40	39	40	40	42
Ni	106	104	92	97	94	93	93	102	93	94	93	94	98	98	98	69	100	71	101	101	103	104	104
Cu	78	79	71	71	71	71	73	68	91	72	72	75	76	71	73	68	76	69	69	70	71	70	69
Zn	99	99	87	87	86	85	85	89	86	86	86	86	95	94	93	97	96	97	93	92	95	91	92

Station	K15	K15	SDT	SDT	SDT	SDT	SDT	SDT	SDT	SDT	SDT	SDT	S1	S1	S1	S1	S1	S1	S1	S1	S1	S1	S1
Sample	10	13	01	02	03	04	05	06	07	08	09	10	01	02	03	04	05	06	07	08	09	10	11
Lava type	3-II	3-III	3-II	3-II	3-II	3-III	3-II	3-II	3-II	3-II	3-II	3-II	3-II	3-II	3-II	3-II	3-II	3-II	3-II	3-II	3-II	3-II	3-II
Mode	SA	SA	A	SA	SA	A	SA	SA	SA	SA	SA	SA	SA	SA	SA	SA	SA	SA	SA	SA	SA	SA	SA
SiO_2	50.00	49.50	49.80	50.55	50.20	49.20	50.00	50.20	49.50	49.80	49.75	50.25	50.20	50.20	50.00	50.50	50.60	50.60	50.00	50.10	50.50	50.00	50.50
TiO_2	1.58	1.88	1.61	1.38	1.37	1.80	1.47	1.42	1.44	1.36	1.38	1.34	1.53	1.54	1.54	1.67	1.63	1.54	1.53	1.55	1.55	1.66	1.66
Al_2O_3	14.59	13.79	14.43	14.86	14.71	14.04	14.54	14.59	14.65	14.66	14.51	14.65	14.58	14.49	14.51	14.13	14.15	14.47	14.53	14.38	14.50	14.06	14.14
Fe_2O_3	11.50	12.80	11.79	11.07	11.03	11.76	11.17	11.18	11.25	11.21	11.21	11.16	11.32	11.53	11.61	12.15	12.03	11.52	11.40	11.31	11.33	12.15	12.05
MnO	0.19	0.20	0.19	0.18	0.18	0.19	0.18	0.18	0.18	0.18	0.18	0.18	0.18	0.18	0.18	0.19	0.19	0.19	0.20	0.20	0.20	0.19	0.19
MgO	7.74	7.49	7.57	7.86	7.83	7.55	7.89	7.81	7.86	7.88	7.84	7.92	7.85	7.76	7.85	7.51	7.51	7.74	7.85	7.86	7.73	7.44	7.47
CaO	11.11	11.60	12.50	12.72	12.74	12.30	12.68	12.62	12.59	12.53	12.55	12.57	12.26	12.04	12.06	11.70	11.74	11.93	12.06	12.01	11.99	11.68	11.77
Na_2O	2.72	2.51	2.47	2.35	2.21	2.54	2.34	2.36	2.35	2.37	2.36	2.34	2.51	2.55	2.53	2.58	2.56	2.55	2.52	2.50	2.51	2.54	2.55
K_2O	0.15	0.09	0.11	0.08	0.08	0.14	0.09	0.10	0.10	0.10	0.08	0.08	0.10	0.09	0.08	0.09	0.10	0.08	0.07	0.07	0.08	0.09	0.10
P_2O_5	0.15	0.12	0.10	0.10	0.10	0.10	0.10	0.10	0.10	0.10	0.10	0.10	0.10	0.10	0.10	0.10	0.10	0.10	0.10	0.10	0.10	0.10	0.10
H_2O^+	-0.69	-0.89	-0.57	-0.78	-0.52	-0.29	-0.60	-0.48	-0.47	-0.39	-0.79	-0.68	-0.47	-0.59	-0.75	-0.75	-0.69	-0.79	-0.84	-0.83	-0.79	-0.64	-0.58
H_2O^-	0.06	0.08	0.09	0.05	0.06	0.20	0.06	0.10	0.11	0.12	0.06	0.06	0.08	0.06	0.03	0.05	0.06	0.04	0.02	0.02	0.03	0.09	0.10
Total	99.10	99.17	100.09	100.42	99.99	99.53	99.92	100.18	99.66	99.92	99.23	99.97	100.24	99.95	99.74	99.92	99.98	99.97	99.44	99.27	99.73	99.36	100.05
FeO*/MgO	1.31	1.50	1.37	1.24	1.24	1.37	1.25	1.26	1.26	1.25	1.26	1.24	1.27	1.31	1.30	1.42	1.41	1.31	1.28	1.27	1.29	1.44	1.42
Rb	4.0	3.0	2.5	2.0	2.0	2.5	2.0	2.0	2.0	2.0	2.0	2.5	2.0	2.0	2.0	2.0	2.0	2.0	2.0	2.0	2.0	2.0	2.0
Sr	116	95	112	105	105	111	104	104	104	104	104	104	112	110	112	106	108	111	112	112	112	105	107
Ba	66	10	20	23	30	23	15	20	25	17	23	14	30	25	20	17	17	17	10	10	10	20	20
V	270	340	302	282	287	308	290	285	285	280	263	266	280	294	285	294	296	285	278	281	278	300	303
Cr	290	224	240	201	200	241	197	197	197	199	198	196	298	278	277	213	224	272	287	289	290	225	235
Co	44	42	43	43	42	44	44	42	44	44	44	46	44	44	44	44	43	44	43	43	44	44	43
Ni	105	83	71	80	79	72	75	78	79	83	78	80	93	91	90	74	79	86	89	89	88	72	70
Cu	74	69	82	82	82	80	83	88	81	81	86	81	77	82	80	76	84	83	88	81	81	77	73
Zn	89	102	86	81	82	88	82	80	81	82	81	80	80	84	84	89	90	83	81	80	81	91	89

TABLE 3d

Bulk rock analyses for the 174E segment

Station	K21	K21	K21	K21	K21	K21	K21	K23	K23	K23	K23	K23	K23	K23	K22	K22	K22	K22DT
Sample	1	2	6	8	27	28	29	14	15	16	17	18	19	20	1	2	3	2
Lava type	4-I	4-I	4-I	4-I	4-I	4-I	4-I	4-II	4-II	4-II	4-II	4-II	4-II	4-II	4-IV	4-IV	4-IV	4-III
Mode	SA	SA	SA	SA	SA	SA	SA	MPH	MPH	SA	SA	SA	SA	MPH	MPH	MPH	SA	SA
SiO_2	48.50	48.20	49.00	49.00	49.40	49.20	48.30	50.40	50.00	51.40	50.20	49.50	49.80	49.75	52.45	51.85	52.65	50.60
TiO_2	2.26	2.25	2.29	1.80	1.81	1.99	1.94	1.40	1.40	1.50	1.49	1.49	1.41	1.40	1.17	1.19	1.22	1.57
Al_2O_3	15.40	15.27	15.35	15.37	15.51	15.38	15.30	15.50	15.10	14.90	15.35	15.00	15.66	15.10	15.48	15.30	15.60	14.40
Fe_2O_3	10.39	10.38	10.42	10.26	9.92	10.25	10.20	9.56	9.98	10.64	11.00	10.64	10.24	10.51	9.85	10.10	9.80	10.79
MnO	0.18	0.18	0.18	0.18	0.17	0.17	0.18	0.17	0.18	0.18	0.26	0.21	0.20	0.18	0.17	0.17	0.16	0.18
MgO	9.00	8.93	9.11	9.42	9.32	9.32	9.41	7.20	7.53	7.99	7.46	7.81	7.76	7.73	5.50	5.70	5.55	6.50
CaO	10.16	10.08	10.12	10.47	10.39	10.44	10.46	12.51	12.27	11.90	11.57	11.97	12.09	12.15	10.42	9.94	10.15	11.03
Na_2O	3.02	3.07	3.04	2.88	2.95	2.83	2.86	2.59	2.47	2.47	2.36	2.42	2.30	2.44	3.18	3.18	3.17	2.80
K_2O	0.42	0.43	0.41	0.37	0.39	0.40	0.37	0.14	0.12	0.07	0.21	0.13	0.07	0.14	0.45	0.46	0.46	0.30
P_2O_5	0.25	0.25	0.25	0.25	0.20	0.25	0.25	0.05	0.08	0.08	0.10	0.10	0.10	0.10	0.12	0.12	0.10	0.10
H_2O^+	-0.14	0.07	-0.14	-0.11	-0.19	-0.03	-0.15	0.29	-0.25	-0.53	0.53	-0.03	-0.27	-0.13	0.83	1.01	0.67	0.55
H_2O^-					0.07			0.06									0.21	0.23
Total	99.44	99.11	100.03	99.89	99.94	100.20	99.12	99.87	99.88	100.60	100.53	99.24	99.36	99.37	99.62	99.02	99.74	99.05
FeO*/MgO	1.02	1.02	1.01	0.96	0.94	0.97	0.95	1.17	1.17	1.17	1.30	1.20	1.16	1.20	1.58	1.56	1.55	1.46
Rb	6.9	7.0	7.2	6.2	7.0	6.6	6.4	3.0	2.8	2.2	4.3	3.4	2.0	3.6	6.5	6.3	7.0	5.5
Sr	254	252	253	250	240	246	250	113	115	120	127	122	118	115	360	358	336	148
Ba	100	60	60	80	60	70	80	36	50	50	50	60	60	60	80	100	61	36
V	305	250	250	250	256	250	250	268	280	260	240	260	250	265	260	260	257	280
Cr	293	298	226	299	286	231	300	231	236	273	269	258	267	237	7	5	3	151
Co	41	41	41	42	43	41	43	41	41	40	42	42	39	39	33	33	35	40
Ni	178	174	182	184	190	184	184	75	69	70	70	68	72	56	25	25	31	62
Cu	51	51	51	52	54	54	57	80	77	75	85	76	64	73	100	93	98	76
Zn	81	77	80	73	75	76	76	79	88	89	88	79	77	80	78	79	75	83

TABLE 4a

Electron microprobe glass analyses for the N160 and 174E (last two columns only) segments. Major and minor elements in glass rims in a few samples from the North Fiji Basin. Analysis performed on the CAMEBAX microprobe at the IFREMER Centre at Brest (analysts J.P. Eissen and M. Bohn). FeO* = total iron expressed as FeO. Fo% and An% = calculated forsteritic content (for $K_D = 0.3$) of the olivine and anorthite content (for $K_D = 1.3$) of the plagioclase, respectively, at equilibrium with this magmatic composition

Station	S5	S5	S5	S5	S5	K29	K29	K5	K5	K21	K22
Sample	01	02	03	04	05	3	5	1	2	27	3
Lava Type	1-III	1-III	1-III	1-III	1-III	1-IV	1-IV	1-I	1-I	4-I	4-IV
Mode	MPH	PH	MPH	MPH	MPH	MPH	MPH	HPH	HPH	SA	MPH
SiO_2	49.55	50.41	50.17	49.74	50.01	51.38	50.83	48.91	48.77	50.11	54.04
TiO_2	1.53	1.86	1.63	1.49	1.56	1.64	1.83	1.06	1.02	1.78	1.19
Al_2O_3	14.85	15.01	15.43	15.61	15.49	13.96	14.15	17.11	17.29	15.81	15.11
FeO *	10.15	9.93	9.86	9.75	9.72	9.14	9.69	8.25	8.04	6.90	8.03
MnO	0.20	0.24	0.15	0.15	0.16	0.30	0.29	0.17	0.16	0.22	0.26
MgO	7.83	7.43	7.69	8.31	7.77	7.02	7.10	9.34	9.63	8.04	5.25
CaO	12.03	11.48	12.03	12.14	12.33	11.66	12.01	12.10	11.94	10.89	9.68
Na_2O	2.80	2.39	2.60	2.34	2.63	2.88	2.99	2.78	2.77	2.99	3.03
K_2O	0.08	0.30	0.28	0.22	0.28	0.17	0.16	0.07	0.07	0.33	0.29
P_2O_5	0.08	0.27	0.16	0.12	0.15	0.02	0.01	0.06	0.06	0.03	0.01
Cr_2O_3	0.05	0.02	0.01	0.01	0.01	0.02	0.01	0.03	0.03	0.00	0.01
Total	99.15	99.36	100.00	99.88	100.12	98.18	99.07	99.88	99.78	97.11	96.90
FeO*/MgO	1.30	1.34	1.28	1.17	1.25	1.30	1.36	0.88	0.83	0.86	1.53
Fo%	82.1	82.6	82.3	83.5	82.6	82.0	81.3	87.1	87.7	87.4	79.5
An%	75.5	77.6	76.9	78.9	77.6	74.4	74.3	75.8	75.6	72.3	69.6

Type 1-IV: Moderately phyric to sub-aphyric basalts with plagioclase, olivine and clinopyroxene from site K29. These lavas are dominantly composed of euhedral to skeletal microphenocrysts, with isolated occurrences of plagioclase and the occasional olivine phenocryst. They are moderately evolved lavas, with medium FeO*/MgO (1.29 ± 0.05) and relatively high TiO_2% (1.79 ± 0.04), and low Cr (216 ± 18 ppm) and Ni (82 ± 11 ppm) contents (Table 3a).

Mineralogical assemblages and geochemistry show that the basalts of type 1-IV are more evolved: they all reached the invariant point of low-pressure (< 1 kbar) co-crystallization of plagioclase + olivine + clinopyroxene (Bender et al., 1978; Presnall et al., 1979; Walker et al., 1979). This is not the case for the majority of samples from the other basalt types. The four groups could be well distinguished on some FeO*/MgO variation diagrams (Fig.3a). The highly phyric basalts from station K5, with their lower FeO*/MgO ratio, often show element contents which differ from the others with their element dilution or concentration consequent upon plagioclase enrichment. At a similar FeO*/MgO ratio, basalts from station K17 show TiO_2% and K_2O% contents which are similar to those of the other NFB basalts, whereas, also at a similar FeO*/MgO ratio, basalts from stations S5 and K29 exhibit TiO_2% and K_2O% contents which are higher than those of the other NFB basalts. The K17, S5, K29 and K5 basalts line up in two separate groups, along a fractional trend parallel to the one observed for the other NFB basalts. The limited alteration is not strong enough to explain the K_2O% gain, which could correspond to a smaller degree of partial melting of the mantle source and/or to a different mantle source.

N15 segment

Six stations were established along this 160 km long segment (Fig.2). The northernmost station is just south of the triple junction area, the southernmost one near the propagating rift tip; all others occur in the recently active volcanic spreading zone (Table 1). Several deposits or indications of hydrothermal activity are now known all along this segment, especially near 17°S (Auzende et al., 1988b; Auzende et al., this issue) and 18°10'S (Craig and Poreda, 1987). Some basaltic samples collected close to these hydrothermal sites have

TABLE 4b

Electron microprobe glass analyses for the N15 segment. For details, see Table 4a

Station	K4	K4	K4	K4	K4	K4	K4	K4	K4	K4A	K4A	K4A	K4B	K4B	K8	K8	K8	K8	K8	K8	K9	K9	K9
Sample	1	2	3	4	5	6	7	8	9	3	4	7	1	2	1	2	3	4	5	6	1	2	3
Lava Type	2-IV	2-IV	2-IV	2-IV	2-IV	2-IV	2-IV	2-IV	2-IV	-	-	-	-	-	2-VI	2-VI	2-VI	2-VI	2-VII	2-VII	2-III	2-III	2-III
Mode	A	A	SA	SA	SA	SA	A	A	A	A	A	SA	A	SA	SA	SA	SA	SA	SA	SA	MPH	MPH	SA
SiO_2	50.15	50.29	50.04	50.22	50.30	50.34	50.48	49.87	49.93	48.28	50.65	50.04	49.65	48.42	51.02	50.04	50.66	48.49	48.78	49.92	50.27	48.83	49.74
TiO_2	1.50	1.51	1.53	1.55	1.51	1.52	1.54	1.53	1.54	2.00	1.83	1.83	1.10	2.00	1.77	1.45	1.07	1.97	2.08	1.82	1.48	1.64	1.09
Al_2O_3	15.34	15.03	14.99	15.11	14.91	15.01	14.98	15.31	15.05	17.76	14.53	14.30	15.74	18.05	14.33	14.84	15.88	18.10	17.53	14.29	15.04	16.20	15.25
FeO *	10.02	9.92	9.68	9.74	9.86	9.98	10.08	9.88	9.66	6.96	11.83	11.50	8.88	6.80	11.30	9.78	8.77	6.94	7.09	11.31	9.91	8.62	8.85
MnO	0.17	0.20	0.22	0.21	0.16	0.21	0.19	0.17	0.21	0.15	0.21	0.16	0.15	0.14	0.28	0.16	0.17	0.13	0.12	0.21	0.19	0.16	0.15
MgO	7.56	7.70	7.31	7.44	7.67	7.65	7.82	7.47	7.48	9.16	7.47	7.48	10.03	9.01	6.85	8.57	9.13	8.93	8.85	7.48	8.63	9.47	9.81
CaO	11.58	11.60	11.59	11.67	11.52	11.71	11.67	11.47	11.56	10.76	11.35	11.29	12.56	11.07	10.84	12.19	12.21	10.87	10.83	11.27	12.36	11.53	12.49
Na_2O	3.39	3.29	3.14	3.27	3.29	3.43	3.04	3.42	3.34	2.56	1.80	2.73	1.92	2.43	2.56	2.57	2.36	2.50	2.51	2.49	2.49	2.44	1.63
K_2O	0.12	0.13	0.11	0.13	0.14	0.10	0.11	0.12	0.11	0.78	0.17	0.15	0.08	0.78	0.14	0.11	0.06	0.74	0.94	0.14	0.09	0.25	0.07
P_2O_5	0.10	0.10	0.12	0.13	0.12	0.11	0.10	0.12	0.12	0.29	0.12	0.15	0.08	0.29	0.13	0.10	0.07	0.30	0.32	0.13	0.10	0.15	0.09
Cr_2O_3	0.02	0.01	0.02	0.02	0.02	0.02	0.02	0.02	0.02	0.03	0.02	0.01	0.06	0.04	0.01	0.02	0.06	0.04	0.04	0.01	0.02	0.05	0.06
Total	99.94	99.79	98.76	99.48	99.49	100.08	100.03	99.38	99.03	98.73	99.97	99.65	100.24	99.02	99.24	99.83	100.44	98.99	99.08	99.08	100.56	99.34	99.22
FeO*/MgO	1.33	1.29	1.32	1.31	1.29	1.31	1.29	1.32	1.29	0.76	1.58	1.54	0.89	0.75	1.65	1.14	0.96	0.78	0.80	1.51	1.15	0.91	0.90
Fo%	81.8	82.2	81.8	81.9	82.2	82.0	82.2	81.8	82.1	88.7	78.9	79.5	87.0	88.7	78.3	83.9	86.1	88.4	88.1	79.7	83.8	86.7	86.8
An%	81.0	71.7	72.6	71.9	71.5	71.0	73.4	70.7	71.3	75.1	81.9	74.8	82.4	76.6	75.2	77.3	78.8	75.8	75.6	76.5	78.1	77.3	84.6

Station	K9	K9	K9	K12	K12	K12	K12	K12	K12	K12	K12	K6A	K6A	K6A	K6	K6	K6	K6	K6	K6	S3	S3	S3	S3
Sample	4	5	6	1	2	3	4	5	6	7	8	1	2	3	1	2	3	4	5	6	01	02	03	06
Lava Type	2-III	2-VI	2-VI	2-I	2-I	2-I	2-I	2-I	2-I	2-I	2-I	2-III	2-III	2-III	2-III	2-III	2-III	2-III	2-III	2-III	2-V	2-V	2-II	2-V
Mode	MPH	SA	MPH	MPH	MPH	MPH	MPH	MPH	MPH	MPH	MPH	SA	SA	SA	SA	SA	SA	SA	SA	SA	PH	MPH	MPH	MPH
SiO_2	48.58	49.96	49.67	48.90	48.80	49.32	48.67	48.94	48.47	48.62	49.24	49.19	49.28	49.80	49.66	49.83	50.18	50.03	50.44	50.81	50.57	50.88	50.35	51.00
TiO_2	1.92	1.81	1.46	1.24	1.26	1.29	1.25	1.23	1.23	1.23	1.23	1.34	1.34	1.37	1.40	1.40	1.39	1.39	1.39	1.38	1.86	1.72	1.12	1.73
Al_2O_3	18.01	14.05	14.81	15.84	15.85	15.74	16.03	16.06	15.74	15.98	16.11	16.35	16.37	16.43	14.92	15.04	14.99	15.37	15.02	15.12	14.57	13.92	14.20	13.86
FeO *	6.83	11.21	9.90	8.80	8.72	9.24	8.88	8.78	8.64	8.86	9.04	9.03	9.07	8.95	9.96	10.05	9.89	9.86	9.62	9.73	10.18	12.23	10.10	12.16
MnO	0.13	0.21	0.19	0.18	0.19	0.16	0.16	0.17	0.19	0.19	0.18	0.13	0.22	0.23	0.13	0.20	0.18	0.17	0.23	0.31	0.21	0.20	0.13	0.21
MgO	8.63	7.49	8.56	8.61	8.58	8.45	8.49	8.69	8.36	8.79	8.97	7.99	7.81	7.79	8.14	8.11	7.98	8.06	8.12	8.02	7.10	6.98	9.12	6.72
CaO	10.83	11.46	12.00	12.11	12.15	11.94	12.19	12.18	12.09	12.07	12.15	10.95	11.02	10.65	11.45	11.70	11.56	11.60	11.42	11.49	11.65	11.69	12.95	11.85
Na_2O	2.52	2.69	2.60	2.91	2.98	2.92	2.91	2.91	2.83	3.02	2.86	2.98	2.94	2.85	2.67	2.69	2.74	2.85	2.84	2.84	2.67	1.96	2.14	1.73
K_2O	0.70	0.11	0.11	0.11	0.13	0.11	0.11	0.10	0.11	0.11	0.10	0.43	0.44	0.47	0.03	0.06	0.05	0.07	0.04	0.04	0.31	0.09	0.04	0.10
P_2O_5	0.33	0.13	0.11	0.08	0.08	0.09	0.09	0.08	0.08	0.08	0.08	0.21	0.20	0.20	0.10	0.08	0.08	0.09	0.08	0.08	0.27	0.11	0.07	0.13
Cr_2O_3	0.02	0.01	0.01	0.04	0.03	0.03	0.04	0.03	0.03	0.03	0.02	0.05	0.04	0.02	0.04	0.03	0.03	0.05	0.02	0.02	0.02	0.01	0.01	0.01
Total	98.61	99.13	99.41	98.83	98.77	99.29	98.83	99.17	97.78	98.97	99.97	98.66	98.73	98.76	98.50	99.19	99.08	99.54	99.22	99.84	99.42	99.77	100.23	99.48
FeO*/MgO	0.79	1.50	1.16	1.02	1.02	1.09	1.05	1.01	1.03	1.01	1.01	1.13	1.16	1.15	1.22	1.24	1.24	1.22	1.19	1.21	1.44	1.75	1.11	1.81
Fo%	88.2	79.9	83.7	85.3	85.4	84.5	85.0	85.5	85.2	85.5	85.5	84.0	83.7	83.8	82.9	82.7	82.7	82.9	83.4	83.0	80.5	77.2	84.3	76.7
An%	75.5	75.4	76.8	74.9	74.5	74.6	75.1	75.0	75.4	74.2	75.3	72.5	72.9	72.9	75.5	75.8	75.2	74.5	74.3	74.4	75.8	81.1	81.3	83.1

TABLE 4c

Electron microprobe glass analyses for the N–S segment. For details, see Table 4a

Station	S2	S4	S4	S4	S4	S4	K14	K14	K14	K14	K14	K14	K14	K15	K15	K15	K15	K15	K15	K15
Sample	2	01	02	03	04	05	1	2	5	6	7	8	10	2	5	6	7	8	9	10
Lava Type	3-III	3-II	3-II	3-II	3-II	3-II	3-II	3-II	3-II	3-IV	3-II	3-II	3-IV	3-III	3-III	3-III	3-III	3-III	3-III	3-II
Mode	MPH	SA	SA	SA	SA	SA	SA	SA	SA	SA	SA	SA	A	SA	SA	SA	SA	SA	SA	SA
SiO_2	50.92	51.21	50.50	50.28	49.67	49.80	49.49	49.36	49.77	49.86	49.37	49.43	49.35	48.95	48.80	48.68	48.91	48.92	49.29	49.04
TiO_2	1.84	2.11	1.53	1.51	1.44	1.43	1.48	1.48	1.51	1.73	1.49	1.50	1.72	1.85	1.84	1.82	1.85	1.82	1.85	1.81
Al_2O_3	14.34	13.14	14.60	14.59	15.12	14.83	15.07	15.20	14.86	14.93	15.09	15.26	15.07	15.66	15.60	15.27	15.30	15.52	15.46	15.48
FeO *	11.82	12.42	10.22	11.07	10.71	10.79	10.27	10.30	10.52	10.64	10.29	10.21	10.32	9.79	9.95	9.93	10.19	10.01	10.01	9.99
MnO	0.19	0.26	0.27	0.18	0.18	0.17	0.18	0.20	0.22	0.17	0.18	0.18	0.19	0.13	0.19	0.20	0.24	0.19	0.20	0.18
MgO	7.02	6.38	7.06	7.92	7.92	7.76	8.17	8.28	8.13	7.37	8.23	8.04	7.60	7.83	7.91	8.01	7.92	7.98	8.09	8.19
CaO	11.18	10.88	11.58	12.10	12.09	12.19	11.76	11.71	11.68	11.34	11.56	11.68	11.24	11.55	11.38	11.32	11.32	11.37	11.27	11.34
Na_2O	2.08	2.61	2.66	2.43	2.47	2.41	2.56	2.55	2.68	2.73	2.64	2.49	2.80	2.86	3.01	2.94	2.95	2.89	2.93	2.98
K_2O	0.14	0.19	0.31	0.08	0.07	0.07	0.07	0.08	0.08	0.20	0.07	0.08	0.19	0.17	0.13	0.14	0.12	0.13	0.15	0.13
P_2O_5	0.12	0.23	0.29	0.09	0.10	0.10	0.10	0.10	0.09	0.14	0.09	0.08	0.14	0.15	0.15	0.15	0.13	0.14	0.14	0.15
Cr_2O_3	0.01	0.01	0.02	0.01	0.01	0.01	0.02	0.02	0.02	0.01	0.02	0.03	0.02	0.03	0.03	0.04	0.02	0.03	0.04	0.04
Total	99.66	99.43	99.05	100.24	99.78	99.57	99.16	99.28	99.56	99.11	99.03	98.98	98.63	98.97	99.00	98.50	98.96	99.00	99.43	99.34
FeO*/MgO	1.68	1.95	1.45	1.40	1.35	1.39	1.26	1.24	1.29	1.44	1.25	1.27	1.36	1.25	1.26	1.24	1.29	1.25	1.24	1.22
Fo%	77.9	75.3	80.4	81.0	81.5	81.0	82.5	82.7	82.1	80.5	82.6	82.4	81.4	82.6	82.5	82.7	82.2	82.6	82.8	83.0
An%	79.4	75.0	75.8	78.1	77.8	78.4	76.7	76.7	75.8	75.0	76.0	77.1	74.3	74.4	73.1	73.5	73.4	73.8	73.4	73.2

Station	SDT	SDT	SDT	SDT	SDT	SDT	SDT	SDT	S1	S1	S1	S1	S1	S1	S1	S1	S1	GT
Sample	01	02	03	04	05	07	09	10	01	02	03	04	05	06	07	08	09	104
Lava Type	3-II	3-II	3-II	3-III	3-II	3-II	3-II	3-II	3-II	3-II	3-II	3-II	3-II	3-II	3-II	3-II	3-II	3-I
Mode	A	SA	SA	A	SA	SA	SA	SA	SA	SA	SA	SA	SA	SA	SA	SA	SA	SA
SiO_2	50.01	50.05	50.31	50.67	50.72	50.45	50.25	50.97	51.00	50.14	50.09	50.08	49.85	50.60	50.28	50.25	50.42	49.87
TiO_2	1.59	1.40	1.44	1.65	1.31	1.29	1.28	1.50	1.16	1.75	1.38	1.57	1.57	1.45	1.44	1.42	1.36	1.32
Al_2O_3	14.33	14.47	14.56	14.54	14.56	14.61	14.65	14.20	17.56	15.02	14.86	14.40	14.31	14.95	14.98	15.06	13.76	14.86
FeO *	10.10	9.76	10.01	10.28	9.89	9.82	9.77	10.24	8.34	9.82	10.43	11.44	10.94	10.17	10.06	10.06	10.37	9.03
MnO	0.20	0.20	0.17	0.16	0.17	0.17	0.17	0.21	0.21	0.19	0.18	0.18	0.20	0.18	0.16	0.17	0.15	0.20
MgO	7.69	7.87	7.87	7.76	7.84	7.84	7.89	7.80	5.39	7.40	8.02	7.35	7.58	7.98	8.16	7.96	8.17	8.14
CaO	12.15	12.63	12.54	12.36	12.52	12.38	12.52	11.68	12.37	11.45	12.25	11.95	12.16	11.95	11.93	12.05	11.91	12.75
Na_2O	2.68	2.68	2.56	1.99	2.40	2.64	2.55	2.67	2.65	2.70	2.48	2.58	2.50	2.47	2.62	2.55	2.46	2.76
K_2O	0.10	0.09	0.09	0.09	0.10	0.09	0.09	0.08	0.08	0.29	0.08	0.09	0.09	0.09	0.09	0.08	0.09	0.06
P_2O_5	0.10	0.09	0.09	0.10	0.09	0.10	0.09	0.00	0.11	0.24	0.09	0.10	0.12	0.11	0.11	0.11	0.00	0.08
Cr_2O_3	0.03	0.03	0.03	0.04	0.03	0.04	0.03	0.00	0.01	0.02	0.01	0.01	0.01	0.04	0.04	0.05	0.00	0.05
Total	98.98	99.26	99.66	99.65	99.63	99.42	99.30	99.35	98.89	99.01	99.88	99.74	99.32	100.00	99.87	99.76	98.69	99.11
FeO*/MgO	1.31	1.24	1.27	1.32	1.26	1.25	1.24	1.31	1.55	1.33	1.30	1.55	1.44	1.27	1.23	1.26	1.27	1.11
Fo%	81.9	82.7	82.4	81.8	82.5	82.6	82.7	81.9	79.4	81.8	82.0	79.3	80.4	82.3	82.8	82.5	82.4	84.3
An%	76.5	77.2	77.9	81.7	78.9	77.1	77.9	75.9	77.0	75.3	78.0	76.9	77.8	77.6	76.6	77.3	77.7	76.9

been altered by hydrothermal circulation. This alteration is relatively weak in samples K6A-1, 2, and 3 and in K4A-4 and 1, and no mineral transformations are present; however, hydration in some samples results in K_2O%, Rb, Sr and Ba increases (Table 3b). In samples K4A-3, 7 and 2, this high temperature alteration is more penetrative. Even though plagioclase crystals are still not altered, the vesicle fillings, hydration, and the K_2O%, Rb, Sr and Ba increases are much more significant than in the samples previously mentioned and the Fe_2O_3 content decreases drastically (Table 3b). However, microprobe glass rim analyses for samples K4A-4 and 7 (Table 4b), show that this alteration is not always complete. Few other samples have been strongly transformed by low-temperature alteration, and they have a strong enrichment in volatiles and in K_2O (samples K12-2, 3 and 4, with $H_2O^+ > 0$) (Table 3b). All these altered samples have been discarded from most of our geochemical comparisons. Samples from station S3 (Fig.2) have been weakly altered at low temperature, as observed in some samples from the N160 segment.

The petrography of the 53 basaltic samples collected along the N15 segment is highly variable: they vary from aphyric to highly phyric basalts, and show large variations in their mineralogical assemblages. The range of their bulk rock (Table 3b) and glass rim compositions (Table 4b) is also much wider (Fig.3a) than those from the N160 and N–S segments. The seven following lava types are distinguished:

Type 2-I: Moderately phyric basalts with plagioclase + olivine from station K12. These lavas, which are actually thin lava crusts, have fairly primitive bulk rock and glass compositions (Tables 3b and 4b), with low FeO*/MgO ratios (1.11 ± 0.04), low TiO_2% contents (0.94 ± 0.04), and relatively high Cr (312 ± 13 ppm) and Ni (102 ± 9 ppm) contents, even if their glass TiO_2% (1.25 ± 0.02) content is slightly higher.

Type 2-II: Moderately phyric to phyric basalts with plagioclase + olivine from station S3 (03, 04, 05, 06 and 09). Despite their high crystal content, these lavas have relatively primitive bulk rock and glass compositions, with low FeO*/MgO ratios (1.10 ± 0.05), low TiO_2% contents (1.13 ± 0.04) and high Cr contents (303 ± 12 ppm) (Tables 3b and 4b).

Type 2-III: Sub-aphyric to moderately phyric basalts with plagioclase + olivine ± clinopyroxene for all samples from station K6 and some from station K9 (1, 2, 3 and 4). These lavas have slightly more evolved bulk rock compositions with higher FeO*/MgO ratios (1.28 ± 0.05) and higher TiO_2% contents (1.38 ± 0.10), although rocks from station K6 have relatively high Cr (282 ± 10 ppm) and Ni (89 ± 16 ppm) contents. Samples from station K9 have comparatively lower Cr (166 ± 10 ppm) and Ni (49 ± 1 ppm) contents, and show bulk rock and glass composition results which are somewhat uncorrelatable (Tables 3b and 4b), owing to the modal mineral content.

Type 2-IV: Aphyric to sub-aphyric basalts with plagioclase ± olivine (± clinopyroxene) from station K4. These basalts contain mainly euhedral to skeletal microphenocrysts and the very occasional isolated phenocryst. They have slightly more evolved bulk rock compositions; moderately high FeO*/MgO ratios (1.41 ± 0.03) and TiO_2% contents (1.55 ± 0.03), and low Cr (128 ± 3 ppm) and Ni (51 ± 3 ppm) contents (Table 3b). The high Cr content of sample K4-5 (247 ppm) corresponds to the only occurrence of clinopyroxene microphenocrysts at this station (Table 4b).

Type 2-V: Moderately phyric to phyric basalts with plagioclase + olivine + clinopyroxene from station S3 (01, 02, 07, 08 and 10). These basalts contain mainly euhedral phenocrysts and the occasional xenomorphic phenocryst (plagioclase > olivine ≥ clinopyroxene) and a few microphenocrysts. As demonstrated by the occurrence of clinopyroxene, these lavas are much more evolved than the basalts from the first group of the same site (S3, Fig.2), with higher FeO*/MgO ratios (1.58 ± 0.04), high TiO_2% contents (1.63 ± 0.04), and relatively low Cr (134 ± 3 ppm) and Ni (55 ± 2 ppm) contents (Table 3b). These bulk rock characteristics correlate quite well with the glass compositions (Table 4b).

Type 2-VI: Sub-aphyric basalts with plagioclase + olivine + clinopyroxene from station K8 (1, 2, 3 and 4) and K9 (5 and 6). These basalts contain mainly euhedral to skeletal microphenocrysts and many isolated phenocrysts and have slightly more

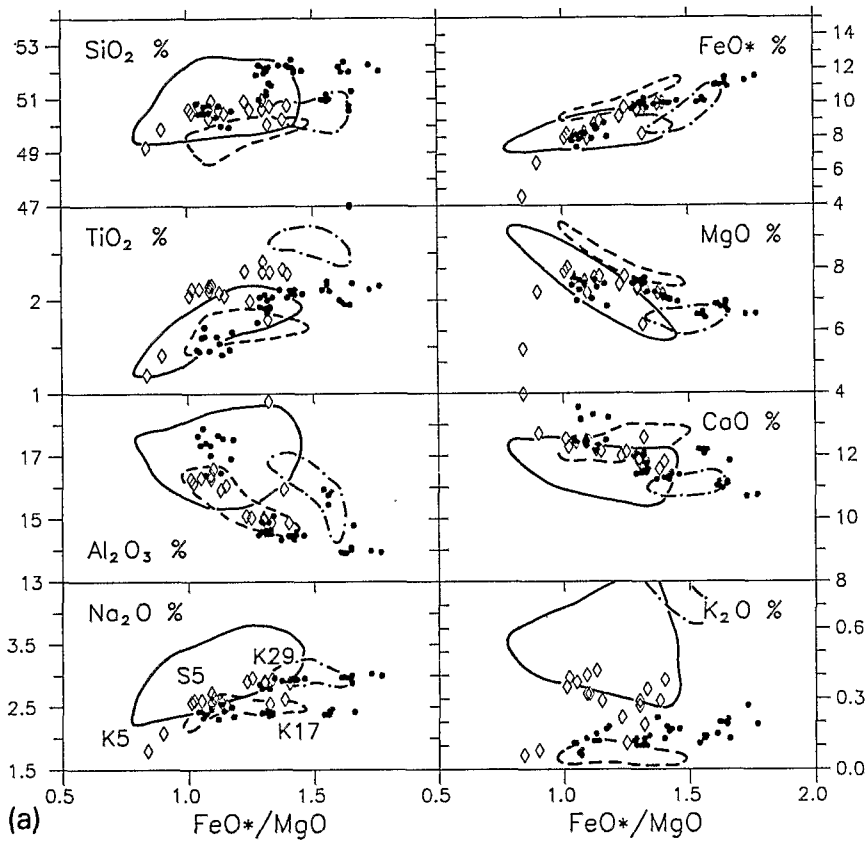

Fig.3. Plot of the main major elements (in weight percent) versus FeO*/MgO showing the general trends of evolution for the NFB basalts (from bulk rock analyses recalculated at 100% without LOI). (a) White diamond = N160 segment (approximate location of basalts from stations K5, S5, K29 and K17 is given in the Na_2O diagram); dot = N15 segment. Fields shown for comparison are: solid line = Mariana Basin BABB (bulk rock analyses, recalculated at 100% without LOI, from Hawkins and Melchior, 1985);

evolved bulk rock compositions, with higher FeO*/MgO ratios (1.66 ± 0.05), medium TiO_2% contents (1.51 ± 0.07), and lower Cr (111 ± 4 ppm) and Ni (41 ± 1 ppm) contents (Table 3b).

Type 2-VII: Sub-aphyric basalts with plagioclase + olivine + clinopyroxene from station K8 (5 and 6). These basalts contain mainly euhedral to skeletal microphenocrysts but very few phenocrysts, the latter being the only visible difference from the other samples from the same station. In terms of FeO*/MgO ratios (1.65) these lavas do not seem to be more evolved than the previous group. However, their bulk rock compositions show much higher TiO_2% contents (2.48), and lower Cr contents (92 ppm) (Table 3b). The two glass rim analyses do not indicate any clear correlation with the bulk rock analyses (Table 4b).

We have not included in this review samples from stations K4A and K4B because they are too altered. However, their higher TiO_2% contents in bulk rock and glass rim compositions indicate that most are more evolved than samples from dredge K4, which was taken in the vicinity of the deep tows. Sample K4B-1, with a lower TiO_2% content (1.10, Table 4b), could be much less evolved. The different groups cannot be well distinguished on the FeO*/MgO variation diagrams (Fig.3a). Compared with basalts from the other segments, they tend to extend more towards an evolved nature, whereas they lack the very primitive terms. The slight scattering observed on some diagrams (SiO_2, Al_2O_3, Na_2O and CaO) might be the result, at least partially, of the modal content of plagioclase (Fig.3a).

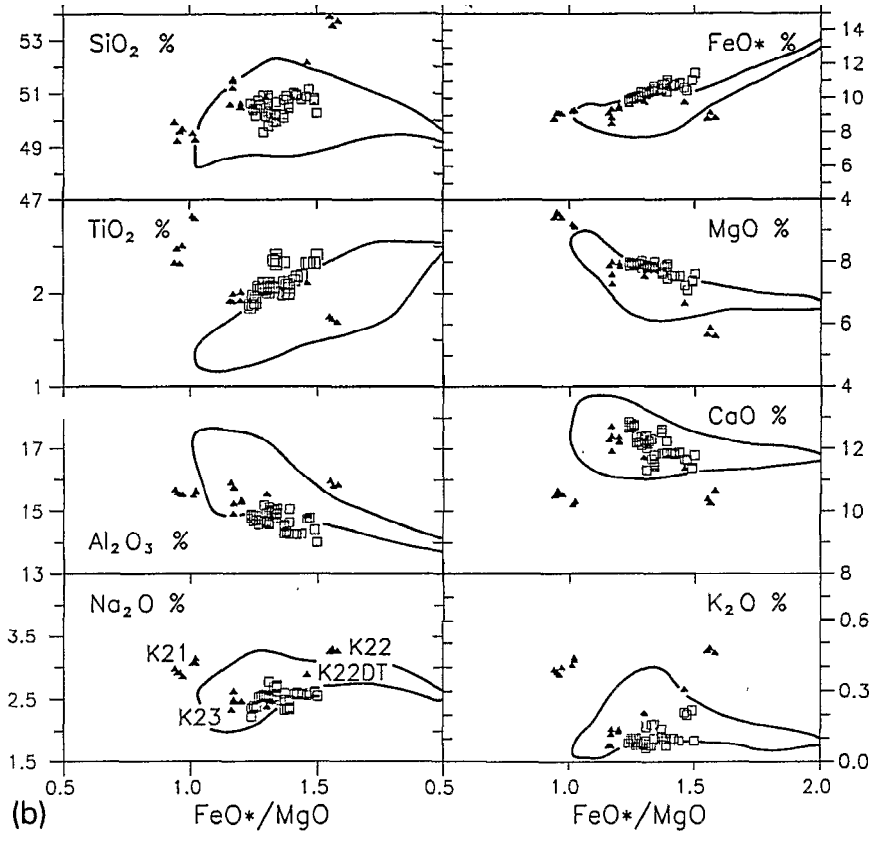

dashed line = MORB and BABB from the northern NFB; dot/dash line = transitional basalts from the South Pandora Ridge (glass analyses, recalculated at 100%, from Sinton et al., in press). (b) White square = N–S segment; black triangle = 174E segment (approximate location of basalts from stations K21, K23, K22 and K22DT is given on the Na_2O diagram). Field shown for comparison is for the Lau Basin BABBs (glass analyses recalculated at 100%, from Hawkins and Melchior, 1985).

N–S segment

This segment is the longest (300 km long) and has a regular morphology. The 49 samples, which were collected at seven stations (Fig.2), turned out to be more homogeneous in terms of mineralogy and geochemistry than the basalts from the other segments. The N–S segment basalts are sub-aphyric, with plagioclase + olivine ± clinopyroxene; they are usually unaltered, except at the slightly off-axis station S2 (Fig.2 and Table 2). Compared with basalts from the other segments, on the FeO*/MgO variation diagrams (Fig.3b) their composition range is strictly restricted to moderately evolved basalts.

Four groups have been distinguished in the N–S segment (Tables 3c and 4c):

Type 3-I: Sub-aphyric plagioclase + olivine + clinopyroxene basalt (sample GT 104). Because of the very small size of this sample, it was only possible to obtain a glass rim composition of the less evolved magma observed along the entire length of the segment (FeO*/MgO = 1.11, TiO_2% = 1.32, K_2O% = 0.06, P_2O_5% = 0.08, Cr_2O_3% = 0.05; Table 4c), despite the fact that this basalt has reached the four-phase cotectic.

Type 3-II: Sub-aphyric plagioclase + olivine (± clinopyroxene) basalts (all samples from station S4 and S1 and some from station K14 (1, 2, 5, 7 and 8), station SDT (01, 02, 03, 05, 06, 07, 08, 09 and 10), and sample K15-10. These basalts contain mainly euhedral to skeletal microphenocrysts of plagioclase and olivine (plus clinopyroxene in basalts from station SDT and S1), and very few

isolated phenocrysts. Their bulk rock compositions show intermediate FeO*/MgO ratios (1.32±0.06) and TiO_2% contents (1.52±0.08), although they have a relatively high Cr content (260±41 ppm) (Table 3c). Glass rim compositions (Table 4c) give coherent results except for sample S4-01 (which has a ferro-basaltic composition very different from the bulk rock composition) and sample K15-10.

Type 3-III: Aphyric to sub-aphyric plagioclase+olivine (±clinopyroxene) basalts (all samples from stations S2 and K15 (not sample 10), and sample SDT-04). The basalts of station K15 contain mainly euhedral to skeletal microphenocrysts and the very occasional isolated phenocryst. Sample SDT-04 is almost aphyric, whereas samples from station S2 are sub-aphyric to moderately phyric plagioclase+olivine+clinopyroxene basalts. The more phyric character of sample S2-1 is mainly due to the coarser grain of this pillow interior or thick lava flow. These lavas have slightly more evolved bulk rock compositions, with medium FeO*/MgO ratios (1.39±0.06), higher TiO_2% contents (1.82±0.04), and slightly lower Cr contents (250±18 ppm) (Table 3c), in agreement with the glass rim analyses (Table 4c).

Type 3-IV: Aphyric plagioclase basalts (samples K14-6 and 10). These basalts contain only a few skeletal microphenocrysts of plagioclase. They have the most evolved bulk rock compositions, with high FeO*/MgO ratios (1.49) and high TiO_2% contents (1.80), and lower Cr contents (137–148 ppm) (Table 3c) in agreement with the glass rim compositions (Table 4c). At station K14 this variation denotes some local heterogeneity.

174E segment

On this relatively short segment (90 km long), only four sampling stations were established during the KAIYO 88 cruise (Fig.2 and Table 2), and eighteen samples were studied. Some of them are slightly altered, with palagonite and Fe–Mn hydroxides in vesicles and along cracks, and positive LOI (Table 3d). Four different lava types were distinguished, each at a different site, based mainly on geochemical characteristics. On the FeO*/MgO variation diagrams (Fig.3b), scattering is quite important compared to the other segments, with negative correlation for TiO_2%. We will therefore list the basalt types on the basis of increasing FeO*/MgO ratios:

Type 4-I: Sub-aphyric plagioclase±olivine basalts (station K21). These basalts have a peculiar chemistry with a fairly primitive character, as shown by their very low FeO*/MgO ratio (0.98±0.03), high Cr (276±30 ppm) and very high Ni (182±5 ppm) contents (Table 3d). The contents of TiO_2% (2.05±0.20), K_2O% (0.40±0.02) and P_2O_5% (0.24±0.02), however, are quite high, as might be expected in an evolved lava. Despite the presence of olivine, it seems that this lava has dominantly, and quite abundantly, fractionated plagioclase; however, there is very little olivine or clinopyroxene. Further, these basalts seem to be little altered, despite their slightly high K_2O%, Rb and Sr contents; the latter could, then, be interpreted as petrogenetic characteristics.

Type 4-II: Sub-aphyric to moderately phyric plagioclase+olivine±clinopyroxene basalt (station K23). These basalts have a relatively primitive composition, although four-phase multiple saturation was reached. The FeO*/MgO ratio is low (1.20±0.04), and TiO_2% (1.44±0.05), Cr (253±17 ppm) and Ni (69±6 ppm) contents are all at a medium level (Table 3d). The closest chemical equivalent of this type in the other segments of the NFB is sample GT 104 (N–S segment; Table 4c) but sample GT 104 is sub-aphyric.

Type 4-III: Sample K22DT-2 is a slightly altered sub-aphyric plagioclase+clinopyroxene basalt intermediately evolved with a medium FeO*MgO ratio (1.47), medium TiO_2% content (1.57) and low Cr (151 ppm) content (Table 3d).

Type 4-IV: Sub-aphyric to moderately phyric plagioclase+olivine+clinopyroxene basalts (station K22). These are the most altered of this segment, with clear H_2O^+, K_2O%, Rb and Sr gains, and extremely low Cr (5±2 ppm) and Ni (27×3 ppm) contents; MgO% is depleted, resulting in an abnormally high FeO*/MgO ratio (1.56±0.01). On the basis of the TiO_2% content (1.19±0.02), these lavas are not very evolved (Table 3d). However, the influence of the subduction process occurring along the Hunter Ridge might have modified the chemistry of these basalts,

which could be intermediate between MORBs and basic andesites.

In summary, the petrology of the basalts of the four segments of the NFB spreading centre present variations which range strictly in the field of basaltic lavas. Most of these basalts have MORB affinities. However, homogeneous basalts from the N–S segment clearly differ from the more varied basalts observed on the N160, N15 and 174E segments. In addition, the most phyric basalts seem to be restricted to a few stations (K5, K17, K9 and S3) of the N15 and N160 segments, and they are all located in distinct structural contexts, which could explain their unusually high phenocryst contents. For example, station K5 (16°53′S) which is located over recent lava flows, from a sidescan sonar data (Kroenke et al., 1987) and station K17 (16°48′S), have sampled basalts erupted in the triple junction area. Station K9 is located near the middle of the N15 segment (17°19′S), just in the area where the ridge starts to rise in the direction of the triple junction. Station S3 is on a small 200 m high volcano at the southern tip of this segment. In this zone, the spreading ridge (which is very well defined towards the north) disappears in an irregular area marked by several volcanoes similar to the one sampled. Thus, there is an apparent correlation between the morphology of the spreading centre and the lavas it produces, with more heterogeneous types on morphologically complex ridges and more restricted types along clearly defined axes.

Mineralogy

In all the 56 lavas in which minerals were analyzed, the morphology, mutual relationships and chemistry of the different minerals of the basalts of the NFB spreading ridge generally exhibit a "normal" evolution from mafic or calcic phenocrysts to more evolved microphenocrysts and microlites. During crystal fractionation, the partition of the elements between the melt and the growing crystals follows the law of mass action, expressed by specific partition coefficients (K_D mineral/liquid). The calculation of the K_D's for some major element pairs using the glass composition and its coexisting minerals provides a guide to gross disequilibrium between phenocryst and host glass. We used the following low-pressure experimental partition coefficients (assuming that $X\mathrm{FeO}_{\mathrm{Liq}} = 0.9 \times X\mathrm{FeO}^*_{\mathrm{Liq}}$):

Olivine: $$\frac{X\mathrm{FeO}_{Ol}}{X\mathrm{MgO}_{Ol}} \times \frac{X\mathrm{MgO}_{Liq}}{X\mathrm{FeO}_{Liq}} = 0.30$$

(Roedder and Emslie, 1970)

Clinopyroxene: $$\frac{\mathrm{XFeO}_{Cpx}}{X\mathrm{MgO}_{Cpx}} \times \frac{X\mathrm{MgO}_{Liq}}{X\mathrm{FeO}_{Liq}} = 0.23 \text{ to } 0.27$$

(Grove and Bryan, 1983; Irving and Frey, 1984)

Plagioclase: $$\frac{\mathrm{XCa}_{Pl}}{X\mathrm{Na}_{Pl}} \times \frac{X\mathrm{Na}_{Liq}}{X\mathrm{Ca}_{Liq}} = 1.2 \text{ to } 1.4$$

(Drake, 1976; Grove and Bryan, 1983)

The clinopyroxene phenocrysts and microphenocrysts are endiopside which does not evolve much towards augitic compositions, as is frequently observed in MORBs (Grove and Bryan, 1983). Their average compositions do not vary along the different segments (Table 5a and Fig.4) and they most commonly occur as sub-euhedral to skeletal microphenocrysts associated in glomerocrysts with plagioclase microphenocrysts and less often with olivine. The NFB clinopyroxenes cover the entire range of experimentally determined K_D's (0.23–0.27) (Table 5a) as described for some of the Mid-Atlantic Ridge basalts near 36°N (Stakes et al., 1985) and the Red Sea Rift basalts near 18°N (Eissen et al., 1989). However, some clinopyroxene microphenocrysts from sample S5-05 (N15 segment) are more evolved (Fig.4a) and in complete disequilibrium with their host glass with K_D's > 0.50 (Table 5a and Fig.5a). Some intersertal clinopyroxene microphenocrysts of sample S2-1 (N–S segment) are also slightly more ferrous, which is probably the resulting of the coarser texture of this doleritic basalt (Fig.5c). Further, samples K8-2, K8-3, K9-4 and K9-5 contain clinopyroxenes that are in general too evolved to have crystallized from their present host glass. This fact seems to indicate that some magma mixing occurred during the genesis of these basalts, although the magmas that mixed were probably closely related. In contrast, several basalts contain clinopyroxenes which are more primitive than would

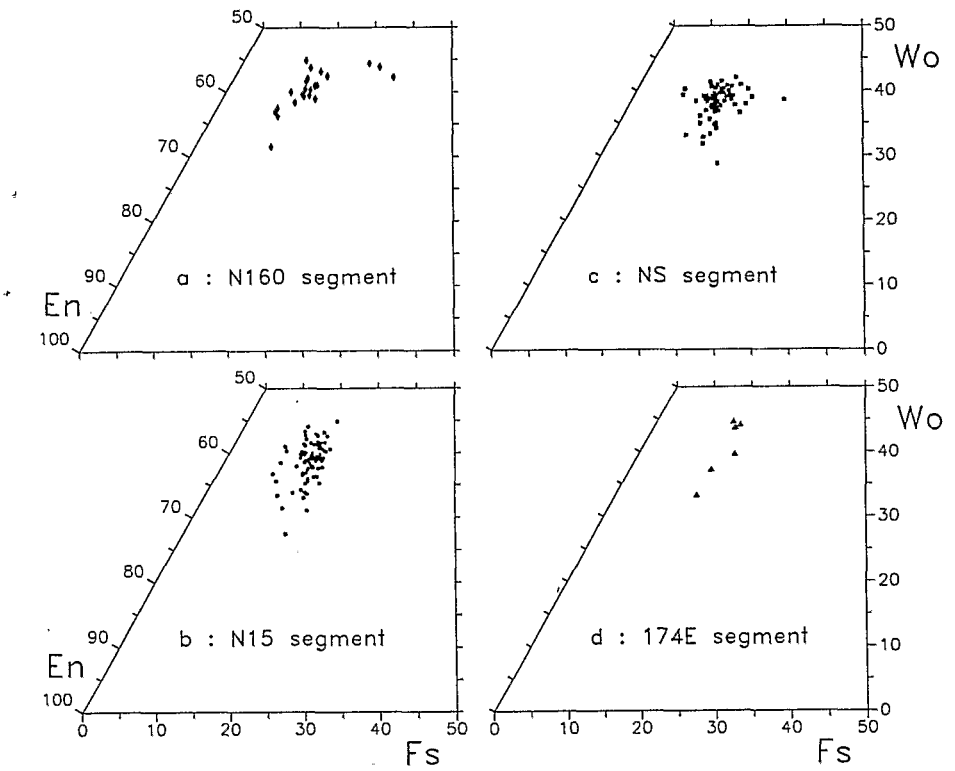

Fig.4. Clinopyroxene compositions plotted in the En%–Wo%–Fs% triangle. (a) N160 segment. (b) N15 segment. (c) N–S segment. (d) 174E segment.

be the case if they were in equilibrium with their host glass. K_D's < 0.20 are observed in sample S5-02 on the N160 segment, in samples K9-1, S3-02 and S3-04 on the N15 segment, and in samples S1-04, S2-1 (zoned phenocryst, Table 5a) and S2-2 on the N–S segment. These clinopyroxenes are mainly euhedral to rounded phenocrysts, and can be considered as xenocrysts. They are possible relics of a higher pressure stage or they may have resulted from the mixing of closely related magma batches.

Olivine crystals show regular behaviour, being lined up (Fig.5) more or less around their theoretical equilibrium with their host glass ($K_D = 0.30$, Roedder and Emslie, 1970). However, their compositional range (Table 5b) varies from one segment to another, with values of $82 < Fo\% < 90$, $78 < Fo\% < 90$, $79 < Fo\% < 87$ and $81 < Fo\% < 88$ being observed for the N160, N15, N–S and 174E segments respectively. Moreover, the range is also variable (Fig.5b) within each of these segments.

In the N160 segment, samples S5-03 and S5-05 have an average olivine composition of $Fo_{85.2 \pm 0.6}$, the composition being relatively homogeneous and close to equilibrium with its host glass (Fig.5b and Table 5b). In sample S5-04, olivine compositions vary between $Fo_{81.7}$ and $Fo_{87.7}$ (Table 5b), with an average ($Fo_{84.6}$) similar to that seen in samples S5-03 and 05 but a much higher standard deviation ($=2.6$). In sample S5-02, olivines are more Mg rich (average $Fo_{87.8 \pm 2.2}$), and not in equilibrium with their host glass. Their strong crystal zonations (Table 5b) suggest the possibility of magma mixing. As frequently observed in MORB, the most magnesian olivines are found in the most phyric basalts, in this case station K5, with euhedral phenocrysts of average composition of $Fo_{89.2 \pm 0.8}$ close to equilibrium with their host glasses.

TABLE 5a

Selected electron microprobe analyses of some microphenocrysts and phenocrysts from the NFB. Clinopyroxene analyses: enstatite (En%), wollastonite (Wo%) and ferrosilite (Fs%) content as relative percentage of the clinopyroxene. K_D = partition coefficient of Mg and Fe between the clinopyroxene and its host glass (bulk rock for sample S2-1). Analyses performed on the CAMEBAX microprobe at the IFREMER Centre at Brest and on the JEOL superprobe at the Geological Survey of Japan at Tsukuba (analysts J.P. Eissen and G. Morvan). Arrows link centre and rim of a single phenocryst. *mph* = microphenocryst; *ph* = phenocryst. The complete set of data is available from J.P. Eissen upon request

	N160 segment				N15 segment													
Station	S5	S5	S5	S5	K29	K17	K17	K8	K8	K8	K8	K8	K9	K9	K9	K9	S3	S3
Sample	02	02	04	05	11	1	2	1	2	3	3	6	1	4	5	5	02	02
	mph	ph	mph	mph	mph	mph	mph	mph	mph	mph	mph	mph	mph	mph	mph	mph	mph	mph
SiO_2	54.21	54.11	51.70	49.15	53.94	50.64	52.19	51.22	53.28	51.32	50.88	53.51	54.16	50.54	52.16	53.16	51.50	53.34
TiO_2	0.23	0.12	0.63	1.90	0.54	1.15	0.81	1.00	0.60	0.60	0.68	0.49	0.29	0.74	0.75	0.53	0.47	0.53
Al_2O_3	2.42	2.15	3.48	4.34	2.47	4.29	4.30	3.99	1.81	3.40	3.47	2.54	1.74	4.37	2.94	1.32	2.31	2.63
FeO	4.99	5.02	6.54	12.44	5.15	7.18	5.79	6.94	7.33	6.76	7.24	6.73	5.28	5.81	7.03	9.27	6.19	6.33
MnO	0.06	0.14	0.23	0.24	0.25	0.26	0.24	0.17	0.24	0.23	0.19	0.11	0.11	0.19	0.23	0.42	0.00	0.16
MgO	19.38	19.46	17.68	12.24	17.92	15.33	16.40	16.29	17.98	17.58	18.10	17.92	19.92	17.15	17.07	19.78	17.80	17.93
CaO	18.13	18.68	19.40	19.73	19.47	20.04	19.07	20.16	19.16	19.17	18.13	18.99	17.70	20.01	20.75	15.86	19.85	20.13
Na_2O	0.25	0.23	0.23	0.52	0.19	0.28	0.28	0.29	0.24	0.26	0.25	0.26	0.19	0.29	0.27	0.19	0.24	0.30
Cr_2O_3	0.49	0.49	0.19	0.16	0.21	0.14	0.72	0.39	0.25	0.21	0.24	0.27	0.50	0.68	0.20	0.02	0.29	0.16
Total	100.16	100.40	100.08	100.72	100.19	99.33	100.74	100.45	100.87	99.53	99.18	100.82	99.89	99.78	101.40	100.55	98.65	101.51
Si	1.955	1.952	1.894	1.849	1.954	1.880	1.831	1.879	1.939	1.893	1.884	1.939	1.960	1.860	1.898	1.942	1.915	1.924
Ti	0.006	0.003	0.017	0.054	0.015	0.032	0.022	0.028	0.016	0.017	0.019	0.013	0.008	0.021	0.020	0.014	0.013	0.014
Al^{IV}	0.045	0.048	0.106	0.151	0.046	0.120	0.105	0.121	0.061	0.107	0.116	0.061	0.040	0.140	0.102	0.057	0.085	0.076
Al^{VI}	0.058	0.043	0.045	0.041	0.060	0.068	0.079	0.051	0.017	0.041	0.035	0.047	0.035	0.050	0.024	0.000	0.016	0.036
Fe	0.150	0.151	0.200	0.391	0.156	0.223	0.176	0.213	0.223	0.209	0.224	0.204	0.160	0.179	0.214	0.283	0.193	0.191
Mn	0.002	0.004	0.007	0.008	0.008	0.008	0.007	0.005	0.007	0.007	0.006	0.003	0.003	0.006	0.007	0.013	0.000	0.005
Mg	1.041	1.046	0.965	0.686	0.968	0.848	0.887	0.891	0.976	0.967	0.999	0.968	1.074	0.941	0.926	1.077	0.987	0.964
Ca	0.700	0.722	0.762	0.795	0.756	0.797	0.778	0.792	0.747	0.758	0.719	0.737	0.686	0.789	0.809	0.621	0.791	0.778
Na	0.009	0.008	0.008	0.019	0.007	0.010	0.010	0.010	0.008	0.009	0.009	0.009	0.007	0.010	0.010	0.007	0.009	0.010
Cr	0.014	0.014	0.006	0.005	0.006	0.004	0.021	0.011	0.007	0.006	0.007	0.008	0.014	0.020	0.006	0.001	0.009	0.005
Total	3.981	3.992	4.010	3.999	3.974	3.991	3.981	4.002	4.002	4.013	4.018	3.990	3.987	4.015	4.016	4.015	4.017	4.003
En%	55.0	54.4	49.9	36.5	51.3	45.2	48.0	46.8	49.9	49.8	51.3	50.6	55.8	49.1	47.3	54.0	50.1	49.7
Wo%	37.0	37.5	39.4	42.3	40.1	42.5	42.1	41.7	38.3	39.1	36.9	38.6	35.7	41.2	41.4	31.1	40.2	40.2
Fs%	8.0	8.1	10.7	21.2	8.7	12.3	9.9	11.5	11.8	11.1	11.8	10.8	8.5	9.6	11.3	14.8	9.8	10.1
KD	0.21	0.19	0.35	0.90	0.21	0.38	0.29	0.29	0.40	0.44	0.46	0.28	0.26	0.48	0.31	0.35	0.22	0.22

			N-S segment												174E segment	
Station	S3	S3	S2	S2	S2	S2	S2	K15	SDT	SDT	S1	S1	S1	S1	K23	K22
Sample	04	04	1	1	1	2	2	17	09	10	04	05	05	07	14	3
	mph	mph	center-->rim		mph	ph	ph	mph	ph	mph	ph	ph	mph	ph	mph	mph
SiO_2	51.57	51.16	52.62	50.65	49.44	50.97	53.00	52.57	51.78	53.74	50.99	52.65	50.42	51.65	51.20	53.66
TiO_2	0.72	0.79	0.48	1.03	1.51	0.93	0.39	0.40	0.68	0.30	0.77	0.81	1.48	0.75	1.08	0.38
Al_2O_3	2.68	3.96	2.86	5.12	5.15	4.59	3.25	1.56	3.87	1.62	3.87	3.20	5.72	3.50	4.41	1.61
FeO	8.05	7.90	6.18	6.52	9.34	6.63	6.21	7.55	5.65	5.45	7.52	6.94	8.84	7.53	6.09	6.64
MnO	0.24	0.24	0.08	0.14	0.19	0.24	0.13	0.24	0.25	0.09	0.28	0.18	0.23	0.28	0.22	0.24
MgO	18.61	16.83	18.10	16.92	15.95	17.45	17.84	18.59	17.36	18.88	19.32	17.11	15.83	17.96	15.49	18.36
CaO	16.60	19.26	19.06	18.56	18.09	17.66	18.50	18.52	18.52	19.07	16.13	18.27	16.79	18.18	21.29	18.27
Na_2O	0.35	0.24	0.21	0.43	0.35	0.31	0.27	0.24	0.26	0.13	0.25	0.24	0.30	0.28	0.29	0.16
Cr_2O_3	0.14	0.32	0.67	0.49	0.15	0.44	1.02	0.00	0.91	0.55	0.42	0.27	0.19	0.01	0.34	0.00
Total	98.96	100.70	100.26	99.87	100.17	99.22	100.61	99.67	99.28	99.83	99.55	99.67	99.80	100.14	100.41	99.32
Si	1.911	1.876	1.918	1.858	1.832	1.877	1.921	1.938	1.901	1.957	1.873	1.929	1.857	1.893	1.877	1.968
Ti	0.020	0.022	0.013	0.028	0.042	0.026	0.011	0.011	0.019	0.008	0.021	0.022	0.041	0.021	0.030	0.010
Al^{IV}	0.089	0.124	0.082	0.142	0.168	0.123	0.079	0.062	0.099	0.043	0.127	0.071	0.143	0.107	0.123	0.032
Al^{VI}	0.028	0.047	0.040	0.079	0.057	0.076	0.060	0.005	0.069	0.026	0.041	0.067	0.106	0.045	0.067	0.038
Fe	0.249	0.242	0.188	0.200	0.289	0.204	0.188	0.233	0.173	0.166	0.231	0.213	0.272	0.231	0.187	0.204
Mn	0.008	0.007	0.002	0.004	0.006	0.007	0.004	0.008	0.008	0.003	0.009	0.006	0.007	0.009	0.007	0.007
Mg	1.028	0.920	0.983	0.925	0.881	0.958	0.964	1.021	0.950	1.025	1.058	0.934	0.869	0.981	0.846	1.004
Ca	0.659	0.757	0.744	0.730	0.718	0.697	0.719	0.732	0.729	0.744	0.635	0.717	0.663	0.714	0.836	0.718
Na	0.013	0.009	0.008	0.015	0.013	0.011	0.009	0.008	0.009	0.005	0.009	0.009	0.011	0.010	0.010	0.006
Cr	0.004	0.009	0.019	0.014	0.004	0.013	0.029	0.000	0.026	0.016	0.012	0.008	0.006	0.000	0.010	0.000
Total	4.008	4.012	3.998	3.996	4.011	3.992	3.984	4.018	3.983	3.992	4.016	3.976	3.975	4.010	3.993	3.987
En%	52.9	47.7	51.3	49.7	46.5	51.3	51.4	51.2	51.1	52.9	54.7	50.0	48.0	50.7	45.1	51.9
Wo%	33.9	39.3	38.8	39.3	37.9	37.3	38.3	36.7	39.2	38.4	32.9	38.4	36.6	36.9	44.6	37.2
Fs%	13.2	13.0	9.9	11.0	15.6	11.3	10.3	12.1	9.7	8.7	12.4	11.7	15.4	12.4	10.3	10.9
KD	0.27	0.29	0.26	0.29	0.44	0.25	0.23	0.35	0.29	0.25	0.28	0.31	0.43	0.38	0.34	0.23

TABLE 5b

Olivine analyses: forsterite (Fo) content as relative percentage of the olivine. K_D = partition coefficient of Mg and Fe between the olivine and its host glass (bulk rock for samples K17-1, S2-1 and SDT-06). For details, see Table 5a

	N160 segment								N15 segment											
Station	S5	S5	S5	S5	S5	S5	S5	S5	K29	K29	K29	K17	K17	K5	K5	K5	K4	K8	K8	K8	K8	K8
Analyse	02	02	03	03	03	04	04	05	3	5	11	1	1	2	2	2	6	1	3	3	4	6
	center-->rim		center-->rim		mph	mph	center-->rim		mph	mph	mph	mph	ph	ph	ph	center	mph	mph	mph	mph	mph	ph
SiO_2	40.56	40.09	40.33	40.24	40.02	40.85	39.71	39.86	40.00	39.89	40.72	39.73	41.04	40.96	40.33	40.50	39.83	38.70	38.12	38.16	40.20	39.52
Al_2O_3	0.00	0.00	0.00	0.00	0.00	0.00	0.00	0.01	0.08	0.05	0.05	0.02	0.06	0.06	0.02	0.00	0.00	0.02	0.06	0.01	0.00	0.01
FeO	9.66	13.86	13.48	12.44	15.27	12.00	17.21	14.28	15.74	14.69	13.02	17.87	11.81	9.46	10.92	11.40	14.56	20.11	18.88	17.98	14.57	18.14
MnO	0.07	0.04	0.11	0.09	0.10	0.13	0.06	0.34	0.22	0.31	0.31	0.41	0.24	0.15	0.71	0.17	0.20	0.35	0.49	0.35	0.28	0.22
MgO	49.72	46.20	47.43	47.45	45.06	47.88	43.13	45.56	43.53	43.87	44.31	41.01	47.06	48.91	47.36	47.99	45.46	41.85	42.15	43.29	45.42	41.33
CaO	0.34	0.21	0.28	0.30	0.34	0.26	0.27	0.23	0.30	0.33	0.35	0.36	0.33	0.33	0.27	0.33	0.31	0.36	0.28	0.32	0.35	0.25
Cr_2O_3	0.04	0.01	0.00	0.00	0.17	0.00	0.00	0.01	0.04	0.05	0.06	0.03	0.13	0.00	0.42	0.10	0.13	0.00	0.00	0.00	0.08	0.05
NiO	0.00	0.00	0.22	0.33	0.00	0.00	0.00	0.00	0.16	0.09	0.14	0.12	0.20	0.00	0.00	0.00	0.00	0.00	0.00	0.00	0.00	0.00
Total	100.39	100.41	101.85	100.85	100.96	101.12	100.38	100.28	100.07	99.28	98.96	99.55	100.87	99.85	100.03	100.48	100.48	101.38	99.99	100.11	100.89	99.52
Si	0.991	0.997	0.989	0.992	0.997	1.000	1.003	0.996	1.007	1.008	1.023	1.016	1.007	1.003	0.997	0.996	0.994	0.984	0.979	0.975	0.999	1.011
Al	0.000	0.000	0.000	0.000	0.000	0.000	0.000	0.000	0.002	0.001	0.001	0.001	0.002	0.002	0.001	0.000	0.000	0.001	0.002	0.000	0.000	0.000
Fe	0.197	0.288	0.276	0.256	0.318	0.246	0.363	0.298	0.331	0.310	0.273	0.382	0.242	0.194	0.226	0.234	0.304	0.428	0.406	0.384	0.303	0.388
Mn	0.001	0.001	0.002	0.002	0.002	0.003	0.001	0.007	0.005	0.007	0.007	0.009	0.005	0.003	0.015	0.003	0.004	0.007	0.011	0.007	0.006	0.005
Mg	1.810	1.712	1.733	1.743	1.672	1.746	1.623	1.696	1.633	1.652	1.658	1.563	1.720	1.786	1.745	1.759	1.691	1.586	1.614	1.649	1.682	1.576
Ca	0.009	0.006	0.007	0.008	0.009	0.007	0.007	0.006	0.008	0.009	0.009	0.010	0.009	0.009	0.007	0.009	0.008	0.010	0.008	0.009	0.009	0.007
Cr	0.001	0.000	0.000	0.000	0.003	0.000	0.000	0.000	0.001	0.001	0.001	0.001	0.003	0.000	0.008	0.002	0.003	0.000	0.000	0.000	0.002	0.001
Ni	0.000	0.000	0.004	0.007	0.000	0.000	0.000	0.000	0.003	0.002	0.003	0.002	0.004	0.000	0.000	0.000	0.000	0.000	0.000	0.000	0.000	0.000
Total	3.009	3.003	3.011	3.008	3.002	3.000	2.997	3.004	2.991	2.991	2.976	2.983	2.991	2.996	2.999	3.003	3.005	3.016	3.020	3.025	3.000	2.988
Fo%	90.2	85.6	86.2	87.2	84.0	87.7	81.7	85.0	83.1	84.2	85.8	80.4	87.7	90.2	88.5	88.2	84.8	78.8	79.9	81.1	84.7	80.2
Fa%	9.8	14.4	13.8	12.8	16.0	12.3	18.3	15.0	16.9	15.8	14.2	19.6	12.3	9.8	11.5	11.8	15.2	21.2	20.1	18.9	15.3	19.8
KD	0.16	0.25	0.25	0.23	0.29	0.24	0.38	0.28	0.28	0.25	0.22	0.36	0.20	0.25	0.30	0.31	0.27	0.32	0.52	0.48	0.46	0.32

	N15 segment (following)															NS segment						
Station	K9	K9	K9	K9	K12	K6A	K6A	K6	S3	S3	S3	S3	S3	S3	S3	S2	S2	S2	S2	S2	S4	S4
Analyse	1	2	4	5	5	2	2	3	01	02	02	03	04	04	04	01	01	02	02	02	01	02
	center	ph	mph	mph	mph	center	center	ph	ph	mph	mph	rim	center	ph	mph	ph	rim	ph	center	rim	ph	ph
SiO_2	39.53	40.09	38.59	38.45	38.83	40.22	40.17	38.87	40.43	38.43	39.62	40.37	39.35	40.76	38.82	39.83	39.65	39.16	40.43	39.26	40.01	39.66
Al_2O_3	0.08	0.06	0.00	0.05	0.05	0.00	0.04	0.01	0.00	0.00	0.00	0.00	0.07	0.00	0.00	0.03	0.09	0.00	0.00	0.00	0.08	0.00
FeO	15.36	14.86	17.12	19.97	20.17	12.01	14.57	14.78	13.41	17.94	19.00	13.00	17.45	10.15	19.03	15.07	17.62	19.61	13.10	17.82	15.15	15.71
MnO	0.34	0.19	0.27	0.30	0.30	0.00	0.29	0.20	0.05	0.29	0.25	0.23	0.25	0.12	0.22	0.27	0.24	0.31	0.14	0.33	0.19	0.18
MgO	44.42	45.00	44.66	40.96	41.37	47.33	45.15	46.20	46.40	43.27	41.60	46.14	43.18	49.14	41.94	45.07	43.07	40.91	46.95	43.54	45.20	44.86
CaO	0.22	0.39	0.36	0.31	0.31	0.30	0.31	0.27	0.35	0.30	0.39	0.51	0.29	0.38	0.41	0.30	0.27	0.25	0.30	0.26	0.26	0.34
Cr_2O_3	0.00	0.00	0.00	0.00	0.00	0.00	0.00	0.00	0.00	0.00	0.00	0.08	0.11	0.00	0.00	0.13	0.00	0.00	0.11	0.03	0.10	0.05
NiO	0.00	0.00	0.00	0.00	0.00	0.00	0.00	0.00	0.00	0.19	0.08	0.00	0.00	0.28	0.18	0.00	0.00	0.00	0.00	0.00	0.00	0.00
Total	99.96	100.58	100.99	100.04	101.04	99.86	100.53	100.34	100.64	100.42	100.93	100.33	100.70	100.82	100.60	100.69	100.94	100.24	101.03	101.24	100.99	100.80
Si	0.996	1.000	0.973	0.990	0.990	0.997	1.001	0.975	1.000	0.979	1.004	1.002	0.994	0.994	0.990	0.995	0.998	1.003	0.996	0.988	0.996	0.992
Al	0.002	0.002	0.000	0.001	0.001	0.000	0.001	0.000	0.000	0.000	0.000	0.000	0.002	0.000	0.000	0.001	0.003	0.000	0.000	0.000	0.002	0.000
Fe	0.324	0.310	0.361	0.430	0.430	0.249	0.304	0.310	0.278	0.382	0.403	0.270	0.368	0.207	0.406	0.315	0.371	0.420	0.270	0.375	0.315	0.329
Mn	0.007	0.004	0.006	0.007	0.007	0.000	0.006	0.004	0.001	0.006	0.005	0.005	0.005	0.002	0.005	0.006	0.005	0.007	0.003	0.007	0.004	0.004
Mg	1.668	1.673	1.678	1.572	1.572	1.749	1.677	1.727	1.711	1.642	1.571	1.706	1.625	1.787	1.594	1.677	1.616	1.561	1.724	1.633	1.676	1.673
Ca	0.006	0.010	0.010	0.008	0.008	0.008	0.008	0.007	0.009	0.008	0.011	0.014	0.008	0.010	0.011	0.008	0.007	0.007	0.008	0.007	0.007	0.009
Cr	0.000	0.000	0.000	0.000	0.000	0.000	0.000	0.000	0.000	0.000	0.000	0.002	0.002	0.000	0.000	0.003	0.000	0.000	0.002	0.001	0.002	0.001
Ni	0.000	0.000	0.000	0.000	0.000	0.000	0.000	0.000	0.000	0.004	0.002	0.000	0.000	0.005	0.004	0.000	0.000	0.000	0.000	0.000	0.000	0.000
Total	3.003	2.999	3.027	3.009	3.009	3.003	2.998	3.025	3.000	3.021	2.996	2.998	3.004	3.006	3.010	3.004	3.000	2.997	3.003	3.011	3.002	3.007
Fo%	83.7	84.4	82.3	78.5	78.5	87.5	84.7	84.8	86.0	81.1	79.6	86.3	81.5	89.6	79.7	84.2	81.3	78.8	86.5	81.3	84.2	83.6
Fa%	16.3	15.6	17.7	21.5	21.5	12.5	15.3	15.2	14.0	18.9	20.4	13.7	18.5	10.4	20.3	15.8	18.7	21.2	13.5	18.7	15.8	16.4
KD	0.33	0.40	0.54	0.36	0.33	0.24	0.31	0.29	0.22	0.26	0.29	0.28	0.25	0.13	0.28	0.25	0.31	0.32	0.18	0.27	0.19	0.27

TABLE 5b (*continued*)

	NS segment (following)																	174E segment		
Station	S4	S4	K14	K14	K15	K15	SDT	SDT	SDT	SDT	SDT	SDT	S1	S1	S1	S1	S1	S1	K21	K23	K22
Analyse	04	04	1	5	7	7	02	05	06	06	10	10	03	03	04	04	05	09	27	14	3
	center-->rim		mph	mph	mph	mph	center	ph	center	rim	ph	mph	center	ph	ph	ph	mph	ph	mph	mph	mph
SiO_2	39.61	39.38	39.48	39.73	38.94	38.86	39.53	39.58	39.53	39.80	40.31	39.22	39.06	40.16	39.57	39.82	40.49	40.08	40.78	40.19	39.82
Al_2O_3	0.00	0.00	0.10	0.10	0.04	0.11	0.00	0.01	0.09	0.02	0.00	0.00	0.00	0.00	0.00	0.00	0.00	0.00	0.06	0.03	0.04
FeO	15.22	16.04	15.76	14.83	18.24	17.85	13.99	14.84	14.96	14.17	14.28	15.76	17.15	14.85	15.03	17.76	18.09	15.17	11.68	14.99	17.14
MnO	0.29	0.47	0.14	0.22	0.18	0.31	0.25	0.27	0.45	0.26	0.18	0.12	0.24	0.30	0.35	0.21	0.30	0.20	0.25	0.28	0.32
MgO	44.64	43.41	45.07	44.14	42.98	42.89	46.78	45.82	45.89	46.08	45.97	44.41	43.32	45.66	44.65	42.94	42.03	43.03	46.98	43.69	41.48
CaO	0.32	0.38	0.30	0.33	0.34	0.30	0.30	0.31	0.33	0.28	0.33	0.29	0.26	0.39	0.32	0.25	0.30	0.36	0.26	0.34	0.27
Cr_2O_3	0.00	0.00	0.19	0.13	0.16	0.02	0.03	0.00	0.05	0.09	0.00	0.00	0.00	0.10	0.00	0.00	0.00	0.00	0.08	0.05	0.03
NiO	0.00	0.15	0.00	0.00	0.00	0.00	0.00	0.00	0.00	0.00	0.16	0.26	0.00	0.00	0.00	0.00	0.14	0.20	0.29	0.10	0.05
Total	100.08	99.83	101.04	99.48	100.87	100.33	100.89	100.83	101.28	100.70	101.23	100.06	100.03	101.46	99.92	100.98	101.35	99.04	100.38	99.67	99.15
Si	0.996	0.998	0.986	1.002	0.986	0.988	0.982	0.987	0.983	0.990	0.997	0.990	0.992	0.994	0.996	1.002	1.016	1.017	1.005	1.012	1.018
Al	0.000	0.000	0.003	0.003	0.001	0.003	0.000	0.000	0.003	0.001	0.000	0.000	0.000	0.000	0.000	0.000	0.000	0.000	0.002	0.001	0.001
Fe	0.320	0.340	0.329	0.313	0.386	0.379	0.291	0.309	0.311	0.295	0.295	0.333	0.364	0.307	0.316	0.374	0.380	0.322	0.241	0.316	0.366
Mn	0.006	0.010	0.003	0.005	0.004	0.007	0.005	0.006	0.009	0.005	0.004	0.003	0.005	0.006	0.007	0.004	0.006	0.004	0.005	0.006	0.007
Mg	1.673	1.640	1.678	1.660	1.622	1.625	1.731	1.702	1.700	1.708	1.695	1.671	1.640	1.685	1.675	1.611	1.572	1.627	1.726	1.640	1.580
Ca	0.009	0.010	0.008	0.009	0.009	0.008	0.008	0.008	0.009	0.007	0.009	0.008	0.007	0.010	0.009	0.007	0.008	0.010	0.007	0.009	0.007
Cr	0.000	0.000	0.004	0.003	0.003	0.000	0.001	0.000	0.001	0.002	0.000	0.000	0.000	0.002	0.000	0.000	0.000	0.000	0.002	0.001	0.001
Ni	0.000	0.003	0.000	0.000	0.000	0.000	0.000	0.000	0.000	0.000	0.003	0.005	0.000	0.000	0.000	0.000	0.003	0.004	0.006	0.002	0.001
Total	3.004	3.002	3.011	2.995	3.012	3.010	3.018	3.013	3.016	3.009	3.003	3.010	3.008	3.005	3.004	2.998	2.984	2.983	2.993	2.987	2.981
Fo%	83.9	82.8	83.6	84.1	80.8	81.1	85.6	84.6	84.5	85.3	85.2	83.4	81.8	84.6	84.1	81.2	80.5	83.5	87.8	83.9	81.2
Fa%	16.1	17.2	16.4	15.9	19.2	18.9	14.4	15.4	15.5	14.7	14.8	16.6	18.2	15.4	15.9	18.8	19.5	16.5	12.2	16.1	18.8
KD	0.28	0.30	0.31	0.29	0.37	0.36	0.27	0.29	0.29	0.27	0.27	0.31	0.34	0.28	0.24	0.30	0.33	0.30	0.29	0.30	0.27

TABLE 5c

Plagioclase analyses: anorthite (An) content as relative percentage of the plagioclase. K_D = partition coefficient of Ca and Na between the plagioclase and its host glass (bulk rock for samples K17-1, S2-1 and SDT-06). For details, see Table 5a

	N160 segment																								
Station	S5	S5	S5	S5	S5	S5	S5	S5	S5	S5	S5	S5	S5	S5	S5	S5	S5	K29	K29	K29	K17	K17	K17	K5	K5
Sample	02	02	02	03	03	03	03	03	03	04	04	04	04	04	05	05	3	5	11	1	1	2	2	2	
	ph	center-->	rim	center	center-->	rim	mph	center-->	rim	ph	center-->	rim	center-->	rim	ph	ph	ph	mph	mph	ph	ph	mph	ph	ph	
SiO_2	50.86	47.17	46.71	50.30	47.75	49.46	52.59	47.49	49.46	50.86	47.51	46.46	46.47	47.39	52.84	50.47	51.60	51.35	52.88	47.07	46.47	51.91	46.36	46.87	
Al_2O_3	31.13	33.89	33.86	30.62	32.31	31.01	28.01	34.05	32.30	31.12	33.15	34.61	33.83	33.64	31.65	31.46	30.47	29.86	29.56	32.99	33.29	29.83	34.10	33.73	
FeO	0.27	0.21	0.53	0.37	0.41	0.33	1.17	0.21	0.24	0.57	0.28	0.38	0.29	0.36	0.19	0.44	0.41	0.42	0.45	0.19	0.28	0.62	0.16	0.34	
MgO	0.28	0.22	0.24	0.27	0.22	0.25	0.53	0.19	0.19	0.26	0.26	0.22	0.24	0.31	0.21	0.27	0.23	0.22	0.24	0.17	0.17	0.20	0.20	0.19	
CaO	13.89	17.26	16.89	15.70	16.99	16.43	14.01	17.54	15.53	14.65	16.70	17.70	17.41	16.99	14.78	14.93	14.83	13.98	14.23	18.01	18.17	13.91	18.56	17.77	
Na_2O	3.35	1.58	1.66	2.80	2.22	2.67	3.97	1.54	2.77	3.10	1.91	1.30	1.47	1.69	3.24	3.00	3.26	3.46	3.70	1.30	1.10	3.56	1.21	1.48	
K_2O	0.00	0.01	0.03	0.04	0.05	0.08	0.12	0.00	0.00	0.02	0.00	0.02	0.01	0.00	0.05	0.04	0.03	0.04	0.03	0.02	0.02	0.05	0.00	0.01	
Total	99.78	100.34	99.92	100.10	99.95	100.23	100.40	101.02	100.49	100.58	99.81	100.69	99.72	100.38	100.78	100.60	100.83	99.33	101.09	99.75	99.50	100.08	100.60	100.38	
Si	2.318	2.159	2.150	2.299	2.199	2.266	2.399	2.160	2.250	2.308	2.184	2.124	2.143	2.168	2.292	2.291	2.334	2.354	2.382	2.171	2.151	2.363	2.125	2.150	
Al	1.672	1.828	1.837	1.650	1.754	1.674	1.506	1.825	1.732	1.664	1.797	1.865	1.839	1.814	1.689	1.683	1.625	1.613	1.569	1.793	1.816	1.600	1.843	1.823	
Fe	0.010	0.008	0.020	0.014	0.016	0.013	0.045	0.008	0.009	0.022	0.011	0.015	0.011	0.014	0.007	0.017	0.016	0.016	0.017	0.007	0.011	0.024	0.006	0.013	
Mg	0.019	0.015	0.016	0.018	0.015	0.017	0.036	0.013	0.013	0.018	0.018	0.015	0.016	0.021	0.014	0.018	0.016	0.015	0.016	0.012	0.012	0.014	0.014	0.013	
Ca	0.678	0.846	0.833	0.769	0.839	0.806	0.685	0.855	0.757	0.712	0.823	0.867	0.860	0.833	0.717	0.726	0.719	0.687	0.687	0.890	0.901	0.678	0.912	0.873	
Na	0.296	0.140	0.148	0.248	0.198	0.237	0.351	0.136	0.244	0.273	0.170	0.115	0.131	0.150	0.284	0.264	0.286	0.308	0.323	0.116	0.099	0.314	0.107	0.131	
K	0.000	0.001	0.002	0.002	0.003	0.005	0.007	0.000	0.000	0.001	0.000	0.001	0.001	0.000	0.003	0.003	0.002	0.002	0.002	0.001	0.001	0.003	0.000	0.001	
Total	4.994	4.997	5.007	5.001	5.024	5.018	5.028	4.996	5.006	4.997	5.002	5.002	5.003	5.000	5.007	5.001	4.997	4.995	4.996	4.991	4.991	4.996	5.007	5.004	
An%	69.6	85.7	84.7	75.4	80.6	76.9	65.7	86.3	75.6	72.2	82.9	88.2	86.7	84.7	71.4	73.1	71.4	68.9	67.9	88.3	90.0	68.1	89.5	86.9	
Ab%	30.4	14.2	15.1	24.3	19.1	22.6	33.7	13.7	24.4	27.7	17.1	11.7	13.2	15.3	28.3	26.6	28.4	30.9	31.9	11.5	9.9	31.6	10.5	13.1	
Or%	0.0	0.1	0.2	0.2	0.3	0.4	0.7	0.0	0.0	0.1	0.0	0.1	0.1	0.0	0.3	0.3	0.2	0.2	0.2	0.1	0.1	0.3	0.0	0.1	
KD	0.9	2.3	2.1	1.2	1.7	1.3	0.8	2.5	1.2	0.9	1.7	2.6	2.3	1.9	1.0	1.1	1.1	1.0	1.0	3.4	4.0	1.0	3.7	2.9	

	N15 segment																						
Station	K4	K4	K4	K4	K4	K8	K8	K8	K8	K8	K8	K8	K8	K8	K8	K8	K8	K9	K9	K9	K9	K9	K9
Sample	1	1	6	6	6	1	1	1	1	2	2	3	4	4	6	6	6	1	1	1	1	1	2
	ph	ph	ph	ph	ph	ph	ph	mph	ph	ph	mph	ph	mph	ph	ph	ph	mph	center-->	rim	center	ph	mph	ph
SiO_2	48.79	49.99	51.55	49.22	48.46	49.18	47.73	52.63	46.07	46.72	52.18	45.73	49.60	48.54	46.31	47.63	52.86	47.28	50.78	45.97	46.73	52.81	46.98
Al_2O_3	32.48	30.97	30.71	32.45	33.21	32.14	33.05	28.96	34.31	33.66	29.33	33.85	31.30	32.26	34.48	33.19	28.98	33.46	30.79	34.22	33.93	29.73	33.80
FeO	0.58	0.51	0.55	0.38	0.37	0.47	0.44	0.76	0.25	0.24	0.65	0.39	0.48	0.53	0.28	0.48	0.91	0.24	0.54	0.18	0.32	0.58	0.44
MgO	0.21	0.28	0.21	0.23	0.23	0.22	0.25	0.27	0.22	0.22	0.27	0.20	0.28	0.20	0.24	0.24	0.33	0.26	0.27	0.20	0.22	0.29	0.26
CaO	14.66	14.16	14.16	15.91	16.90	15.87	17.09	13.47	18.29	18.19	13.63	17.14	15.24	16.61	19.06	17.79	13.32	16.63	13.97	17.25	17.19	12.80	17.98
Na_2O	2.46	3.20	3.38	2.32	2.14	2.55	1.93	4.34	1.38	1.62	4.21	1.45	3.07	2.24	1.28	1.79	3.92	1.48	3.31	1.15	1.30	3.77	1.49
K_2O	0.01	0.04	0.05	0.03	0.01	0.01	0.01	0.08	0.02	0.05	0.02	0.02	0.03	0.00	0.03	0.04	0.02	0.03	0.04	0.00	0.00	0.04	0.00
Total	99.18	99.15	100.61	100.55	101.33	100.43	100.49	100.50	100.54	100.69	100.29	98.78	100.00	100.38	101.68	101.15	100.34	99.38	99.70	98.98	99.70	100.01	100.94
Si	2.244	2.300	2.334	2.240	2.197	2.243	2.184	2.390	2.115	2.141	2.374	2.130	2.272	2.221	2.107	2.171	2.399	2.179	2.320	2.132	2.152	2.394	2.145
Al	1.761	1.680	1.639	1.741	1.774	1.728	1.783	1.550	1.856	1.818	1.573	1.859	1.689	1.740	1.849	1.783	1.550	1.818	1.659	1.871	1.842	1.588	1.819
Fe	0.022	0.020	0.021	0.015	0.014	0.018	0.017	0.029	0.010	0.009	0.025	0.015	0.019	0.020	0.011	0.018	0.034	0.009	0.021	0.007	0.012	0.022	0.017
Mg	0.014	0.019	0.014	0.016	0.016	0.015	0.017	0.018	0.015	0.015	0.018	0.014	0.019	0.014	0.017	0.016	0.022	0.018	0.019	0.014	0.015	0.019	0.018
Ca	0.723	0.698	0.687	0.776	0.821	0.776	0.838	0.656	0.899	0.893	0.664	0.855	0.748	0.814	0.929	0.869	0.647	0.821	0.684	0.857	0.848	0.622	0.880
Na	0.219	0.286	0.297	0.205	0.188	0.225	0.171	0.382	0.123	0.144	0.371	0.131	0.273	0.199	0.113	0.158	0.345	0.132	0.293	0.103	0.116	0.332	0.131
K	0.001	0.003	0.003	0.002	0.001	0.000	0.000	0.004	0.001	0.003	0.001	0.001	0.001	0.000	0.002	0.002	0.001	0.002	0.002	0.000	0.000	0.002	0.000
Total	4.985	5.004	4.996	4.993	5.011	5.005	5.010	5.028	5.019	5.023	5.026	5.006	5.021	5.009	5.026	5.018	4.999	4.979	4.998	4.984	4.985	4.979	5.011
An%	76.7	70.8	69.6	79.0	81.3	77.5	83.0	62.9	87.9	85.9	64.1	86.6	73.2	80.4	89.0	84.4	65.2	86.0	69.8	89.3	88.0	65.1	87.0		
Ab%	23.3	29.0	30.1	20.8	18.6	22.5	16.9	36.6	12.0	13.8	35.8	13.2	26.7	19.6	10.8	15.4	34.7	13.8	29.9	10.7	12.0	34.7	13.0		
Or%	0.1	0.3	0.3	0.2	0.1	0.0	0.0	0.4	0.1	0.3	0.1	0.1	0.1	0.0	0.2	0.2	0.1	0.2	0.2	0.0	0.0	0.2	0.0		
KD	1.7	1.3	1.2	2.0	2.3	1.5	2.1	0.7	3.1	2.4	0.7	2.3	1.1	1.7	3.3	2.2	0.8	2.3	0.8	3.0	2.7	0.7	2.6		

TABLE 5c (*continued*)

	N15 segment (following)																					
Station	K9	K9	K9	K9	K9	K12	K12	K12	K12	K6A	K6A	K6A	K6A	K6A	K6A	K6A	K6	K6	K6	K6	K6	S3	S3
Sample	4	4	4	5	5	1	1	4	4	2	2	2	3	3	3	3	3	3	5	5	5	01	01
	mph	center-->	rim	mph	mph	ph	ph	ph	mph	mph	center-->	rim	center-->	rim	center	ph	center	ph	ph	ph	mph	center	ph
SiO_2	51.45	46.34	47.03	52.62	52.09	47.23	49.03	48.20	51.69	51.99	48.52	50.68	47.43	49.98	50.99	48.46	50.01	50.94	50.31	47.24	51.83	46.83	48.05
Al_2O_3	30.71	33.84	33.49	28.79	29.71	33.28	31.47	32.32	29.22	30.68	32.61	31.61	33.48	32.01	31.09	32.58	31.46	30.25	30.55	32.77	29.90	33.55	33.04
FeO	0.74	0.34	0.32	0.58	0.59	0.29	0.33	0.31	0.42	0.56	0.52	0.32	0.44	0.37	0.47	0.57	0.41	0.72	0.45	0.45	0.40	0.15	0.45
MgO	0.24	0.17	0.25	0.20	0.27	0.14	0.23	0.21	0.25	0.27	0.13	0.23	0.18	0.23	0.27	0.23	0.31	0.38	0.27	0.27	0.14	0.12	0.23
CaO	13.39	17.06	16.80	13.04	13.31	17.73	15.67	16.91	14.43	13.59	15.97	14.26	17.19	15.39	14.69	16.37	15.45	14.14	14.41	16.08	13.27	17.54	17.23
Na_2O	3.64	1.75	2.05	4.53	4.06	1.44	2.50	1.86	3.33	3.48	2.39	3.00	1.43	2.51	3.12	2.21	2.57	3.22	3.42	2.05	3.68	1.61	1.96
K_2O	0.03	0.00	0.03	0.04	0.01	0.00	0.10	0.02	0.04	0.11	0.02	0.11	0.06	0.07	0.10	0.06	0.04	0.02	0.03	0.01	0.00	0.00	0.01
Total	100.22	99.50	99.97	99.80	100.04	100.11	99.33	99.83	99.38	100.68	100.16	100.22	100.21	100.55	100.74	100.47	100.26	99.67	99.45	98.87	99.22	99.80	100.97
Si	2.337	2.143	2.163	2.401	2.370	2.170	2.259	2.215	2.370	2.348	2.221	2.302	2.174	2.270	2.310	2.214	2.279	2.331	2.310	2.192	2.372	2.158	2.189
Al	1.645	1.844	1.816	1.549	1.594	1.802	1.709	1.751	1.579	1.633	1.759	1.693	1.809	1.713	1.660	1.755	1.690	1.632	1.654	1.792	1.612	1.822	1.774
Fe	0.028	0.013	0.012	0.022	0.023	0.011	0.013	0.012	0.016	0.021	0.020	0.012	0.017	0.014	0.018	0.022	0.016	0.027	0.017	0.017	0.015	0.006	0.017
Mg	0.016	0.012	0.017	0.014	0.018	0.010	0.016	0.014	0.017	0.018	0.009	0.016	0.012	0.015	0.018	0.016	0.021	0.026	0.019	0.018	0.009	0.008	0.016
Ca	0.652	0.845	0.828	0.637	0.649	0.873	0.774	0.833	0.709	0.658	0.783	0.694	0.844	0.749	0.713	0.802	0.755	0.693	0.709	0.800	0.651	0.866	0.841
Na	0.321	0.157	0.183	0.401	0.358	0.128	0.223	0.166	0.296	0.305	0.212	0.264	0.127	0.221	0.274	0.195	0.227	0.285	0.305	0.184	0.327	0.144	0.173
K	0.002	0.000	0.002	0.002	0.000	0.000	0.006	0.001	0.002	0.006	0.001	0.006	0.004	0.004	0.006	0.004	0.003	0.001	0.002	0.001	0.000	0.000	0.001
Total	5.002	5.014	5.021	5.026	5.012	4.993	5.000	4.993	4.990	4.991	5.006	4.987	4.987	4.986	5.000	5.008	4.990	4.996	5.016	5.005	4.986	5.003	5.011
An%	66.9	84.3	81.8	61.3	64.4	87.2	77.1	83.3	70.4	67.9	78.6	72.0	86.6	76.9	71.8	80.1	76.7	70.7	69.8	81.2	66.6	85.8	82.9
Ab%	32.9	15.7	18.0	38.5	35.5	12.8	22.3	16.6	29.4	31.5	21.3	27.4	13.0	22.7	27.6	19.5	23.1	29.1	30.0	18.7	33.4	14.2	17.1
Or%	0.2	0.0	0.2	0.2	0.0	0.0	0.6	0.1	0.2	0.6	0.1	0.7	0.4	0.4	0.6	0.4	0.3	0.1	0.2	0.1	0.0	0.0	0.1
KD	0.9	2.3	1.9	0.7	0.8	3.0	1.5	2.2	1.0	1.0	1.8	1.3	3.2	1.6	1.3	1.8	1.4	1.0	1.0	2.0	0.9	2.5	2.0

	N15 segment (following)								N-S segment													
Station	S3	S3	S3	S3	S3	S3	S3	S3	S3	S3	S3	S2	S2	S2	S2	S2	S2	S2	S4	S4	S4	S4
Sample	01	02	02	02	02	03	03	04	04	04	04	1	1	1	2	2	2	2	01	01	02	03
	center	center	ph	center	mph	center	ph	center-->	rim	ph	mph	ph	center	mph	ph	ph	center-->	rim	ph	mph	ph	ph
SiO_2	46.26	47.19	47.59	50.98	52.61	46.35	48.37	45.80	47.59	46.10	52.49	51.87	47.53	55.75	49.07	51.48	46.79	52.22	47.58	50.90	51.14	50.75
Al_2O_3	33.71	32.87	32.32	30.70	28.95	34.24	32.94	34.51	32.53	34.37	28.71	29.12	32.04	26.61	31.68	30.89	34.90	30.23	32.51	30.19	31.12	30.76
FeO	0.33	0.45	0.31	0.39	0.70	0.34	0.41	0.44	0.53	0.41	0.70	0.53	0.48	0.84	0.47	0.44	0.26	0.53	0.53	0.47	0.53	0.43
MgO	0.14	0.19	0.26	0.22	0.24	0.10	0.25	0.22	0.26	0.26	0.26	0.31	0.26	0.31	0.18	0.19	0.10	0.27	0.23	0.31	0.29	0.28
CaO	17.43	17.92	18.27	15.21	13.94	17.84	16.16	17.69	16.16	17.87	14.03	13.88	17.32	11.30	16.76	13.56	17.64	13.32	15.85	14.25	14.21	14.49
Na_2O	1.43	1.33	1.53	2.94	3.81	1.37	2.22	1.27	2.19	1.43	3.96	3.40	1.68	4.94	2.04	3.45	1.05	3.79	2.07	3.34	3.33	3.33
K_2O	0.00	0.00	0.01	0.02	0.00	0.00	0.02	0.00	0.00	0.01	0.05	0.04	0.02	0.11	0.01	0.00	0.00	0.01	0.04	0.02	0.00	0.02
Total	99.30	99.95	100.29	100.46	100.25	100.24	100.37	99.93	99.25	100.46	100.20	99.15	99.33	99.86	100.21	100.01	100.74	100.37	98.81	99.48	100.62	100.07
Si	2.143	2.174	2.188	2.317	2.392	2.130	2.209	2.112	2.201	2.116	2.391	2.380	2.202	2.524	2.246	2.339	2.132	2.364	2.207	2.333	2.316	2.314
Al	1.841	1.785	1.751	1.644	1.551	1.854	1.773	1.876	1.773	1.860	1.542	1.575	1.749	1.420	1.709	1.654	1.874	1.613	1.778	1.631	1.661	1.654
Fe	0.013	0.017	0.012	0.015	0.027	0.013	0.016	0.017	0.020	0.016	0.027	0.020	0.018	0.032	0.018	0.017	0.010	0.020	0.021	0.018	0.020	0.016
Mg	0.010	0.013	0.018	0.015	0.016	0.007	0.017	0.015	0.018	0.018	0.018	0.021	0.018	0.021	0.012	0.013	0.007	0.018	0.016	0.021	0.020	0.019
Ca	0.865	0.885	0.900	0.741	0.679	0.878	0.791	0.874	0.801	0.879	0.685	0.683	0.860	0.548	0.822	0.660	0.861	0.646	0.788	0.700	0.690	0.708
Na	0.128	0.119	0.136	0.259	0.336	0.122	0.197	0.114	0.196	0.127	0.350	0.303	0.151	0.434	0.181	0.304	0.093	0.333	0.186	0.297	0.292	0.294
K	0.000	0.000	0.001	0.001	0.000	0.000	0.001	0.000	0.000	0.000	0.003	0.002	0.001	0.006	0.001	0.000	0.000	0.001	0.002	0.001	0.000	0.001
Total	5.000	4.993	5.005	4.991	5.001	5.004	5.003	5.007	5.010	5.018	5.015	4.984	4.999	4.986	4.990	4.986	4.977	4.996	4.998	5.001	4.999	5.006
An%	87.1	88.2	86.8	74.0	66.9	87.8	80.0	88.5	80.3	87.3	66.0	69.1	85.0	55.5	81.9	68.5	90.3	66.0	80.7	70.1	70.2	70.6
Ab%	12.9	11.8	13.2	25.9	33.1	12.2	19.9	11.5	19.7	12.7	33.7	30.6	14.9	43.9	18.0	31.5	9.7	34.0	19.1	29.7	29.8	29.3
Or%	0.0	0.0	0.1	0.1	0.0	0.0	0.1	0.0	0.0	0.0	0.3	0.2	0.1	0.6	0.1	0.0	0.0	0.1	0.2	0.1	0.0	0.1
KD	2.8	2.3	2.0	0.9	0.6	2.2	1.2	2.0	1.1	1.8	0.5	0.9	2.3	0.5	1.5	0.7	3.1	0.7	1.8	1.0	1.0	0.9

TABLE 5c (*continued*)

	N-S segment (following)																					
Station	S4	S4	S4	S4	K14	K14	K14	K14	K14	K14	K14	K15	K15	K15	SDT	SDT	SDT	SDT	SDT	SDT	SDT	SDT
Sample	04	04	04	05	1	1	5	5	6	8	8	2	7	7	02	02	02	05	05	06	06	09	10
	mph	center-->	rim	ph	ph	mph	ph	mph	mph	ph	ph	mph	mph	mph	ph	ph	mph	ph	ph	center-->	rim	mph	center
SiO_2	51.62	46.98	47.74	50.21	48.31	50.81	50.99	52.07	51.89	47.16	51.19	51.90	52.08	52.48	45.53	47.89	49.55	44.74	46.32	44.64	45.51	51.30	44.94
Al_2O_3	29.33	32.77	32.86	30.63	32.83	30.35	31.07	29.85	28.94	32.69	30.02	29.70	29.86	29.46	34.65	32.59	30.99	35.02	33.43	34.86	33.82	30.02	33.79
FeO	0.49	0.50	0.38	0.55	0.58	0.47	0.47	0.92	0.67	0.41	0.58	0.75	0.76	0.63	0.39	0.37	0.39	0.25	0.32	0.44	0.28	0.67	0.13
MgO	0.24	0.23	0.21	0.24	0.24	0.31	0.29	0.46	0.36	0.17	0.27	0.35	0.30	0.30	0.23	0.28	0.25	0.17	0.25	0.15	0.22	0.23	0.13
CaO	14.56	16.79	16.81	15.39	15.70	13.79	14.73	13.88	14.38	17.70	14.81	13.77	13.85	12.94	17.69	16.32	14.15	18.36	17.14	18.53	17.41	14.58	18.59
Na_2O	3.28	1.95	2.20	2.72	2.03	3.54	3.10	3.56	3.47	1.55	3.15	3.50	3.93	4.18	1.35	2.19	3.48	0.99	1.74	0.78	1.42	3.09	0.81
K_2O	0.01	0.01	0.00	0.05	0.02	0.05	0.04	0.04	0.02	0.01	0.03	0.02	0.05	0.04	0.02	0.00	0.02	0.00	0.02	0.01	0.02	0.04	0.00
Total	99.53	99.23	100.20	99.79	99.71	99.33	100.70	100.78	99.73	99.69	100.05	99.99	100.83	100.03	99.87	99.64	98.82	99.52	99.23	99.42	98.68	99.93	98.39
Si	2.365	2.178	2.190	2.301	2.217	2.331	2.310	2.357	2.374	2.178	2.336	2.364	2.358	2.386	2.102	2.205	2.290	2.075	2.149	2.075	2.124	2.342	2.107
Al	1.584	1.791	1.777	1.655	1.776	1.641	1.659	1.593	1.561	1.780	1.615	1.595	1.593	1.579	1.886	1.769	1.688	1.914	1.828	1.910	1.860	1.615	1.867
Fe	0.019	0.019	0.015	0.021	0.022	0.018	0.018	0.035	0.026	0.016	0.022	0.029	0.029	0.024	0.015	0.014	0.015	0.010	0.012	0.017	0.011	0.026	0.005
Mg	0.016	0.016	0.014	0.016	0.016	0.021	0.020	0.031	0.025	0.012	0.018	0.024	0.020	0.020	0.016	0.019	0.017	0.011	0.017	0.010	0.015	0.016	0.009
Ca	0.715	0.834	0.826	0.756	0.772	0.678	0.715	0.673	0.705	0.876	0.724	0.672	0.672	0.630	0.875	0.805	0.700	0.912	0.852	0.923	0.871	0.713	0.934
Na	0.291	0.175	0.196	0.242	0.181	0.315	0.273	0.312	0.308	0.139	0.279	0.309	0.345	0.369	0.121	0.196	0.311	0.089	0.157	0.070	0.128	0.274	0.074
K	0.001	0.001	0.000	0.003	0.001	0.003	0.003	0.002	0.001	0.001	0.002	0.001	0.003	0.002	0.001	0.000	0.001	0.000	0.001	0.001	0.001	0.002	0.000
Total	4.990	5.014	5.019	4.994	4.986	5.007	4.998	5.004	5.000	5.001	4.996	4.994	5.020	5.010	5.016	5.008	5.023	5.012	5.016	5.006	5.011	4.988	4.996
An%	71.0	82.6	80.9	75.5	80.9	68.1	72.2	68.1	69.5	86.3	72.1	68.4	65.9	62.9	87.8	80.4	69.1	91.1	84.4	92.8	87.0	72.1	92.7
Ab%	28.9	17.4	19.1	24.2	18.9	31.6	27.5	31.6	30.4	13.7	27.7	31.5	33.8	36.8	12.1	19.6	30.8	8.9	15.5	7.1	12.8	27.7	7.3
Or%	0.1	0.1	0.0	0.3	0.1	0.3	0.3	0.2	0.1	0.1	0.2	0.1	0.3	0.2	0.1	0.0	0.1	0.0	0.1	0.1	0.1	0.2	0.0
KD	0.9	1.8	1.6	1.1	1.7	0.8	1.1	0.9	1.0	2.4	1.0	1.0	0.9	0.8	2.8	1.6	0.9	3.6	1.9	4.4	2.3	1.0	4.7

	N-S segment (following)																			174E segment			
Station	SDT	S1	S1	S1	S1	S1	S1	S1	S1	S1	S1	S1	S1	S1	S1	S1	S1	S1	S1	K23	K23	K22	K22
Sample	10	03	03	03	03	04	04	04	05	05	05	07	07	07	09	09	09	09	09	14	14	3	3
	ph	center-->	rim	center	mph	ph	ph	mph	ph	center-->	rim	mph	ph	center-->	rim	center-->	rim	ph	mph	ph	mph	ph	mph
SiO_2	50.32	45.33	50.96	47.83	52.04	47.88	47.91	53.05	46.77	45.68	53.04	52.71	52.47	44.36	48.18	45.85	49.54	47.76	53.77	47.66	50.31	48.17	52.27
Al_2O_3	30.45	34.93	30.87	32.70	30.00	32.83	33.14	29.46	32.69	34.16	28.46	28.21	29.43	35.65	32.87	34.10	31.04	33.16	28.43	32.14	29.85	31.79	29.52
FeO	0.42	0.35	0.46	0.41	0.80	0.38	0.42	0.48	0.50	0.44	0.85	0.72	0.60	0.38	0.40	0.47	0.47	0.46	0.67	0.26	0.41	0.51	0.56
MgO	0.23	0.10	0.29	0.22	0.42	0.17	0.17	0.25	0.22	0.13	0.33	0.35	0.18	0.09	0.17	0.16	0.23	0.18	0.26	0.19	0.25	0.13	0.22
CaO	15.04	18.37	14.77	16.55	13.34	16.20	16.81	13.12	17.58	18.63	13.24	12.80	13.23	18.74	17.37	17.87	15.21	17.33	13.15	17.47	15.33	17.33	14.12
Na_2O	2.73	1.01	3.31	2.11	3.70	1.90	1.62	4.12	1.24	0.69	3.59	3.99	4.20	0.53	1.98	0.83	2.32	1.51	3.89	1.60	2.98	1.99	3.66
K_2O	0.02	0.00	0.00	0.02	0.00	0.01	0.02	0.00	0.02	0.00	0.06	0.02	0.00	0.01	0.04	0.01	0.01	0.02	0.00	0.02	0.02	0.00	0.02
Total	99.21	100.09	100.66	99.84	100.30	99.37	100.09	100.48	99.02	99.73	99.57	98.80	100.11	99.76	101.01	99.29	98.82	100.42	100.17	99.34	99.15	99.92	100.37
Si	2.314	2.090	2.312	2.200	2.361	2.207	2.195	2.398	2.174	2.113	2.420	2.423	2.385	2.054	2.195	2.125	2.288	2.185	2.436	2.205	2.321	2.219	2.373
Al	1.651	1.898	1.651	1.773	1.605	1.783	1.790	1.569	1.791	1.863	1.531	1.529	1.577	1.945	1.765	1.863	1.689	1.788	1.518	1.753	1.623	1.726	1.580
Fe	0.016	0.013	0.017	0.016	0.030	0.015	0.016	0.018	0.019	0.017	0.032	0.028	0.023	0.015	0.015	0.018	0.018	0.017	0.026	0.010	0.016	0.020	0.021
Mg	0.016	0.007	0.020	0.015	0.028	0.012	0.012	0.017	0.015	0.009	0.022	0.024	0.012	0.006	0.012	0.011	0.016	0.012	0.018	0.013	0.017	0.009	0.015
Ca	0.741	0.907	0.718	0.816	0.649	0.800	0.825	0.635	0.875	0.923	0.647	0.631	0.644	0.930	0.848	0.888	0.753	0.850	0.638	0.866	0.758	0.855	0.687
Na	0.243	0.090	0.291	0.188	0.326	0.170	0.144	0.361	0.112	0.062	0.318	0.356	0.370	0.048	0.175	0.075	0.208	0.134	0.342	0.144	0.267	0.178	0.322
K	0.001	0.000	0.000	0.001	0.000	0.001	0.001	0.000	0.001	0.000	0.003	0.001	0.000	0.001	0.002	0.001	0.001	0.001	0.000	0.001	0.001	0.000	0.001
Total	4.983	5.006	5.009	5.008	4.999	4.987	4.983	4.998	4.987	4.987	4.975	4.991	5.012	4.998	5.011	4.981	4.972	4.988	4.976	4.991	5.002	5.007	4.999
An%	75.2	91.0	71.1	81.2	66.6	82.4	85.0	63.8	88.6	93.7	66.8	63.9	63.5	95.1	82.7	92.2	78.3	86.3	65.1	85.7	73.9	82.8	68.0
Ab%	24.7	9.0	28.9	18.7	33.4	17.5	14.8	36.2	11.3	6.3	32.8	36.0	36.5	4.9	17.1	7.7	21.6	13.6	34.9	14.2	26.0	17.2	31.9
Or%	0.1	0.0	0.0	0.1	0.0	0.1	0.1	0.0	0.1	0.0	0.4	0.1	0.0	0.1	0.2	0.1	0.1	0.1	0.0	0.1	0.1	0.0	0.1
KD	1.1	3.7	0.9	1.6	0.7	1.8	2.2	0.7	2.9	5.5	0.8	0.7	0.7	7.8	1.9	4.9	1.5	2.6	0.8	2.3	1.1	2.7	1.2

Fi
0.(
(c)
(=
lig
in
K_t

FeO/MgO in Olivine FeO/MgO in Pyroxene An% in Plagioclase FeO/MgO in Olivine FeO/MgO in Pyroxene An% in Plagioclase

at
Ir
of

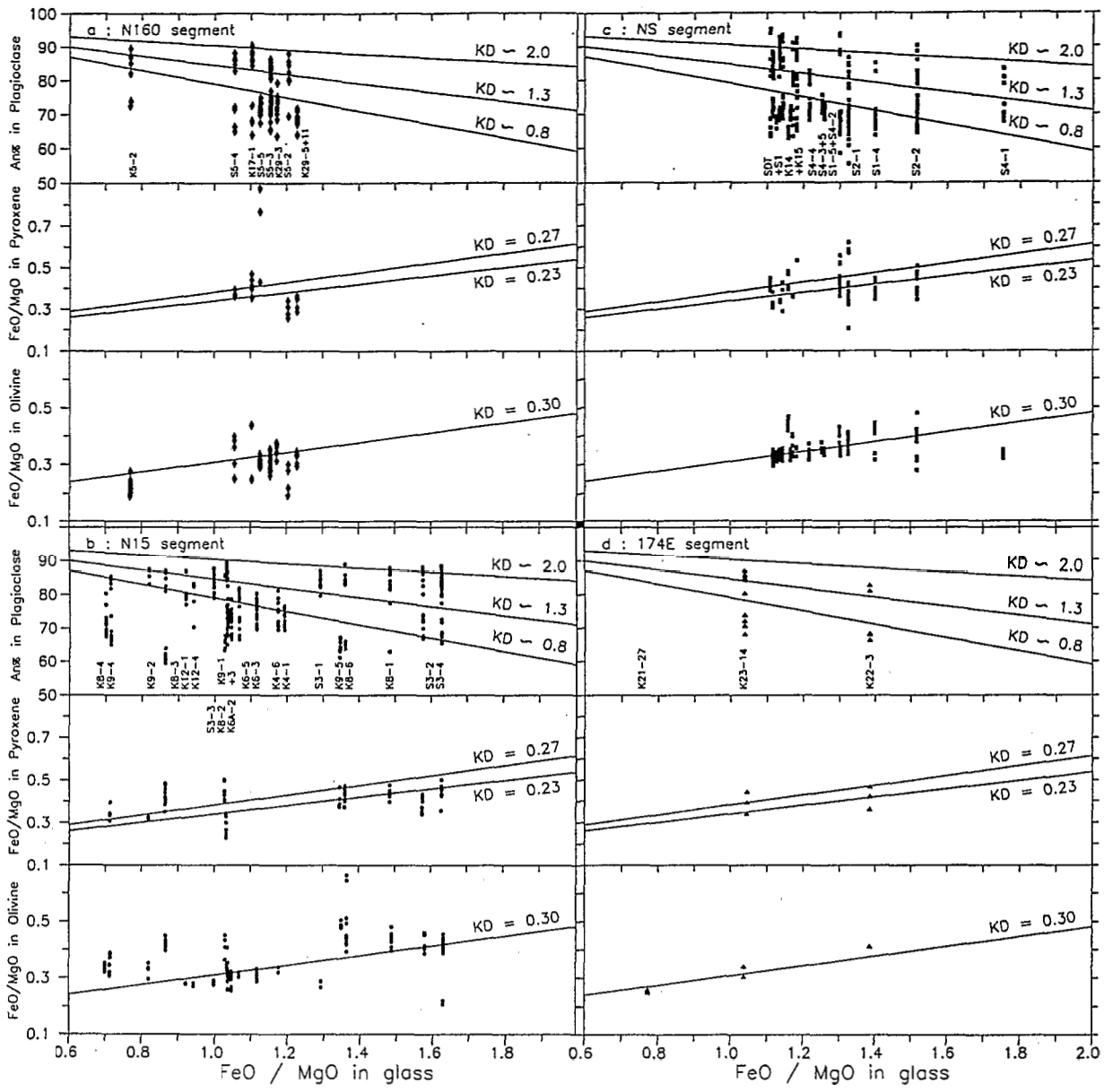

Fig.5. Composition of the minerals as a function of the degree of evolution of their host glass given by FeO/MgO ratio (FeO = 0.9 × FeO*). The range of the calculated partition coefficients (K_D) is given for each sample. (a) N160 segment. (b) N15 segment. (c) N–S segment. (d) 174E segment. *Olivine*: Line indicates the experimentally determined low-pressure K_D olivine/liquid equilibrium (=0.30, Roedder and Emslie, 1970). *Clinopyroxene*: Lines give the range of experimentally determined low-pressure K_D clinopyroxene/liquid equilibrium (=0.23, Grove and Bryan, 1983; or=0.27, Irving and Frey, 1984). *Plagioclase*: Lines give approximate variations in the K_D plagioclase/liquid as a function of the evolution of the glass composition. The experimentally determined low-pressure K_D plagioclase/liquid equilibrium should be around 1.3 (after Drake (1976) and Grove and Bryan (1983)).

The compositional variations of the olivine are at their most important along the N15 segment. In sample S3-04, a few rounded olivine phenocrysts of Mg rich composition ($\sim Fo_{89}$) occur and in sample S3-01 (Table 5b) some less "primitive" ($\sim Fo_{86}$) olivine phenocrysts are apparently not in equilibrium with their host glass. They could be xenocryst relics from a higher pressure stage or

the result of mixing of closely related magma batches, as observed for the clinopyroxene in sample S3-04. In all other samples from the N15 segment, the composition of euhedral to subeuhedral olivine phenocrysts and of the skeletal microphenocrysts is either near Fo_{84-86} (e.g. K4-6, K8-4, K9-1, K9-2, K9-3, S3-01, S3-03, and all the K6 samples) or near Fo_{80-81} (e.g. K8-1, K8-3, K8-6, S3-02 and S3-04). Some slightly more Fe-rich olivines in a few samples of stations K8 and K9 (Table 5b), and the even more fayalitic olivines in samples K8-6 ($Fo_{73.5}$), K9-5 ($Fo_{78.5\pm0.4}$) and K6-3 ($Fo_{77.8}$) (Table 5b), are in disequilibrium with their host glass. These latter crystals correspond to the generally skeletal microphenocrysts which crystallized very rapidly in the later stages of fractionation, such as during magma ascent before eruption, or just after basalt extrusion.

Along the N–S segment, the olivine compositions are much more homogeneous, all the samples but two (K15-7 and S1-05) containing mainly, if not exclusively, phenocrysts and microphenocrysts with compositions around $Fo_{84\pm0.7}$ (Table 5b). Some Fe-rich olivine crystals, like those found in the samples K15-7 and S1-05, can coexist with more Mg-rich olivines as in samples S2-1 and S2-2 (with a few slightly zoned crystals, Table 5b) and in samples S1-03 and S1-04. In sample S2-2, more evolved skeletal microphenocrysts are also found ($Fo_{78.8}$) (Table 5b). Olivines from this segment are generally close to equilibrium with their host glass (Fig.5b). However, some of them may be either less evolved than their host glass (e.g. S1-04, S2-2 and S4-01), or more evolved (as in samples S2-2 and K15-7). For sample S4-01, although there is a difference between glass and bulk rock analyses, this disequilibrium would disappear if the bulk rock was taken as the reference in the calculation. For the other samples, the relatively small discrepancies between K_D's are probably related to mixing of compositionally closely related, mostly differentiated, magma batches, as would occur inside a magma reservoir.

The olivines from the 174E segment are relatively magnesian and very homogeneous ($\sim Fo_{87.5}$) in sample K21-27, and close to equilibrium with their host glass; samples K23-14 and K22-3 are slightly more evolved (Table 5b and Fig.5d).

Plagioclase is by far the most abundant mineral in the NFB basalts, being present in all the 138 studied samples (Table 2), although in highly variable modal abundance. Even when plagioclase crystals are optically zoned, their cores are commonly homogeneous. However, frequent normal zoning (e.g. S5-03, K9-1 and S2-2) (Table 5c) and occasional reverse zoning (e.g. S5-04) are observed between crystal cores and rims. In the case of normal zoning, rim compositions can be below An_{70} (e.g. $An_{60.8}$ in S2-1, or $An_{66.8}$ in S1-05, Table 5c). Usually, the more sodic compositions (even below An_{60}) correspond to the crystals of the mesostasis mainly represented by microlites and skeletal microphenocrysts. A distribution comprising a group of calcic phenocrysts separated by a gap in composition from the more sodic microphenocryst group is commonly observed along the four segments of the NFB spreading centre (Fig.5).

For the N160 segment, plagioclase compositions range between An_{88} and An_{65} in samples S5-02, S5-03 and S5-04 (Table 5a), the phenocrysts being concentrated near An_{84-85} and the microphenocrysts around An_{70-75}. Strong normal and reverse zoning are observed in several of the analyzed crystals (Table 5c) and even some oscillatory zoning is observed in sample S5-04. When the phenocrysts are relatively close to equilibrium with their host glass, the microphenocrysts are in disequilibrium with it, being much too evolved ($K_D < 0.9$) (Fig.5c). Both the last two facts support the hypothesis of magma mixing which has already been suggested by the clinopyroxene and olivine analyses. In sample S5-05, plagioclase microphenocrysts are predominantly very homogeneous ($An_{71.8\pm1.6}$). The most calcic plagioclase phenocrysts/megacrysts (An_{80-90}) are found in the most phyric basalts of stations K5 and K17 (Table 5c), and these crystals are relics of higher pressure stages not in equilibrium with the glass (Fig.5a).

Along the N15 segment, the compositional variations in plagioclase are significant, and disequilibrium between crystals and their host glass is common. In MORB, high-temperature minerals are commonly restricted to the most phyric lavas (Bryan, 1983; Stakes et al., 1985; Eissen et al., 1989). Here, the most calcic plagioclases (An_{88-90}),

as with the most magnesian olivines (Fo_{80-90}), appear in some sub-aphyric (e.g. K8-1 and 6) and moderately phyric (e.g. K9-1) basalts and in the most phyric basalts of station S3 (Fig.5b and Table 5c). They might represent xenocrysts, at least for samples K8-1, S3-02 and S3-04 where complex oscillatory zoning is observed. The similarity in xenocryst core compositions to those of the surrounding phenocrysts suggests that they are cognate xenocrysts produced in a slightly cooler and more crystalline part of the magma chamber, or alternatively that they equilibrated at a slightly higher pressure (Bender et al., 1978). The majority of the other plagioclase phenocrysts can be separated into two chemically coherent groups even when they cannot be distinguished morphologically, being always euhedral to sub-euhedral crystals. The first group consists of calcic plagioclase (An_{85-87}) which is dominantly found in the most phyric samples (e.g. K9-1 and K9-2 and the samples of station S3), but also in some less phyric lavas (e.g. K8-1, K8-2, K8-3, K8-6 and K6A-4). The second group is made up of less calcic plagioclase (An_{80-84}) and is generally found associated with the previously described group (e.g. K8-1, K8-3, K9-2, K6A-4, S3-02 and S3-04). In some samples (e.g. K8-4, K8-6, K9-4, K6-3 and K6-5), the first group of plagioclases is absent. The plagioclase microphenocrysts, which occur as long skeletal to sub-euhedral laths, are present in all these samples and commonly form skeletal glomerocrysts with clinopyroxene and/or olivine. Their composition range (An_{72-79}) is generally the composition of the rim of the larger plagioclases. Few of these microphenocrysts and microlites can reach much more sodic compositions (down to An_{61} in K9-5 and K8-3; Table 5c). Intermediate plagioclase phenocrysts ($_{78<}An_{<86}$) are frequently close to equilibrium with their host glass, but most of the more sodic plagioclases are in complete disequilibrium ($K_D << 1.3$), except in the most evolved basalts. At several stations (S3, K8 and K9) basalts with different degrees of fractionation coexist. These basalts often have similar plagioclase "populations" exhibiting normal, reverse or oscillatory zoning, or any combination of the three, and a similar range of compositions; this supports the important role of magma mixing in their petrogenesis. As suggested above by some of the olivine and clinopyroxene mineral chemistry, the different components of the mixing must have been closely related magmas, i.e. more or less differentiated magma batches within a zoned magma reservoir.

The plagioclases of the N–S segment show the widest range of compositions, from An_{47} to $An_{95.1}$ and a relatively large amount of very calcic xenocrysts (An_{90-95}) in almost all the basalts sampled near 20°S (stations S1 and SDT) and in sample S2-2. These more or less rounded crystals, which are in complete disequilibrium with their host glass (with $K_D >> 2.0$), are probable relics of deep levels of fractionation. A deep magma reservoir may therefore exist below the spreading ridge near 20°S. However, as noted on the N15 segment, the majority of the plagioclase phenocrysts are moderately calcic (An_{80-88}) with, in most samples from stations S2, DT and S1, a bimodal distribution around An_{86} or An_{84}. The microphenocrysts present in almost all these basalts usually have compositions in the sodic labradorite range (An_{70-76}). They are the dominant plagioclases in the basalts of stations S4 and K14, because the more calcic phenocrysts are very rare in these samples. The microliths and the most skeletal microphenocrysts reach bytownite compositions (An_{60-66}). They are present in all the samples but for the station SDT set and are the only plagioclases in the basalts of station K15. An_{47} plagioclase was found only in the massive basalt of station S2, where intergranular plagioclase could reach a higher degree of evolution in the liquids isolated between the larger phenocrysts. As noted in the N15 segment, the phenocrysts in the basalts from the N–S segment are close to equilibrium with their host glass, whereas the more sodic plagioclases are often in complete disequilibrium ($K_D << 1.3$).

Plagioclases were analyzed only in two basalts from the 174E segment. In sample K23-14, the phenocryst composition is moderately calcic ($An_{84.9-87.1}$), whereas the microphenocrysts are more sodic ($An_{68.2-73.9}$), but close to equilibrium with the glass. In sample K22-3, the plagioclases were all more evolved, and the phenocrysts were less calcic ($An_{82.8-81.1}$), as were the microphenocrysts ($An_{66.4-68.4}$) (Table 5c and Fig.5c).

Abundances, crystal shapes and the mutual rela-

tionships between all the mineral phases indicate that plagioclase was probably the liquidus phase in the majority of these basalts. Its crystallization was closely followed by olivine, which is present in 87% of the samples, and then only by clinopyroxene. In only two samples (SDT-04 and K22DT-2), was plagioclase obviously followed by clinopyroxene crystallization (olivine is absent in both of these samples). Interestingly, 52% of the NFB basalts reached the four-phase saturation of co-crystallization of plagioclase, olivine and clinopyroxene (+liquid), behaviour that is not common in MORBs.

Geochemistry

Bulk rock and microprobe analyses permit the recognition of, respectively, 4, 6, 4 and 4 geochemical groups in 4, 9, 7 and 4 sampled stations from the N160, N15, N–S and 174E segments of the NFB central spreading centre. The observed major element variations are due essentially to low-pressure magmatic processes affecting magma compositions, which are dominantly controlled by crystal fractionation (Fig.3). However, other processes, such as magma mixing, may locally play an important role. Discrepancies between the bulk rock and glass compositions of stations K5, K8, K9 and S3 can be attributed to the mineral modal content (essentially plagioclase) on the bulk rock compositions.

Variations observed in the alkali elements, volatiles (only very locally masked by alteration) and LILEs suggest that the mantle sources involved in the petrogenesis of these basalts are distinct or heterogeneous.

MORB versus BABB (back-arc basin basalt)

The NFB spreading ridge is located between 300 and 600 km behind the active New Hebrides subduction zone, which is characterized by a high rate of convergence (12–15 cm/yr; Louat and Pelletier, 1989). The 174E segment is the segment closest to the subduction zone, but in an area where the subduction is oblique and relatively slow (1.5 cm/yr; Louat and Pelletier, 1989; Maillet et al., 1989). Thus, it would seem to be difficult to involve material coming directly from the subducted slab in the petrogenesis of the NFB basalts. However, the coexistence of MORB and BABB has been described in the NFB north of 16°S (Aggrey et al., 1988; Sinton et al., 1991). Since BABBs are enriched in LILEs (K, Rb, Ba, etc.) and possibly volatiles relative to MORB (Saunders and Tarney, 1984; Hawkins and Melchior, 1985; Sinton and Fryer, 1987; Sinton et al., 1991), we will use some of these elements for a comparison between our data and results from other back-arc basins.

In the Na_2O+K_2O vs. Mg number diagram (Fig.6), the NFB basalts are compared to basalts from two very well studied back-arc basins, the Mariana Trough (Fig.6a), and the Lau Basin (Fig.6d) (Hawkins and Melchior, 1985), and to some basalts from the northern NFB (Fig.6c) (Sinton et al., 1991). The Mariana Trough, which is one of the most typical back-arc basins, produces exclusively typical BABBs. In the Lau Basin, Hawkins and Melchior (1985) describe an initial phase with BABB followed by the production of MORB. Sinton et al. (1991) also propose that during its early history the NFB was characterized by the production of BABB. Its recent activity (post 3 m.y.), however, has only produced typical N-MORB, except along the South Pandora Ridge (Fig.2) which is considered to be a reactivated, older, intra-oceanic lineament.

Our data (excluding the most altered samples) indicate that the present-day distribution of basalts is more complex than previously proposed (Sinton et al., 1991; Eissen et al., 1990). Along the N160 segment (Fig.6a), all but two basalts from stations S5 and K29 are in the BABB field, but are not as alkali rich as the typical Mariana BABBs. Two samples with a very low total alkali content correspond to the most phyric samples of station K5 (enriched in phenocrysts). As already suggested, the N15 segment is much more complex (Fig.6b). Basalts from stations K6, K12 and S3 lie in the MORB field, whereas those from stations K4 and K8 are in the BABB field. Basalts from station K9 are in the BABB field (samples K9-5 and K9-6), or straddle the boundary between the two fields. By contrast, all the samples of the N–S segment plot in the MORB field, demonstrating that this segment is not only the most mature morphologi-

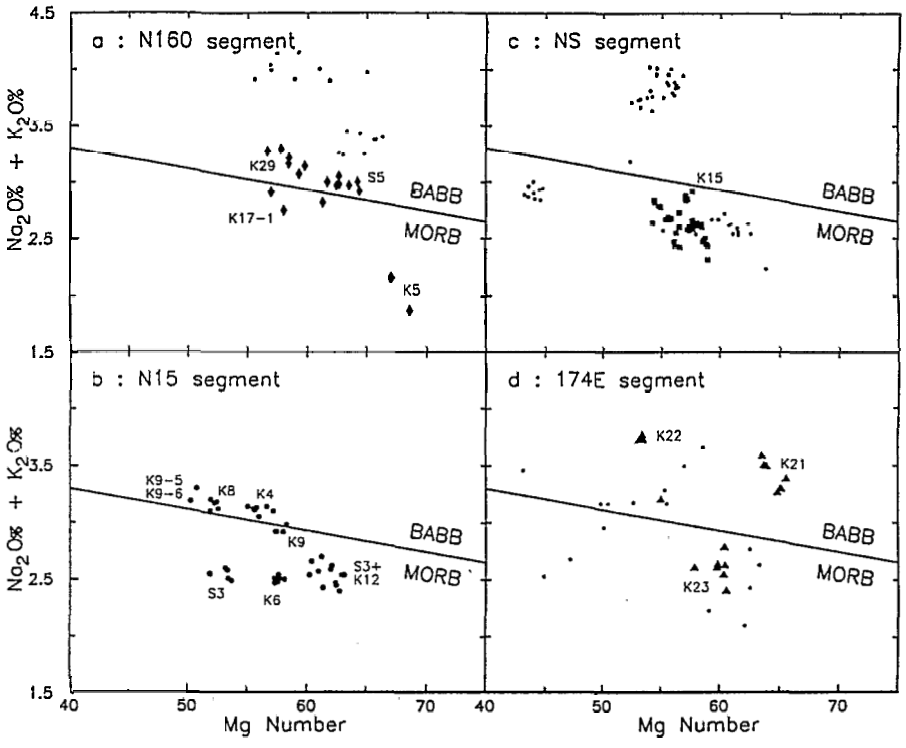

Fig.6. Distinction between BABB and MORB for the NFB basalts based on total alkali content (Na_2O+K_2O in weight percent of bulk rock analysis) vs. Mg number (atomic 100Mg/Mg+Fe; calculated with all Fe as FeO). See text for explanation. The MORB–BABB field boundary is delineated using the set of data shown. (a) Basalts from the N160 segment = diamonds (approximate location of basalts from stations K5, S5, K29 and K17 is given); basalts from the Mariana Trough = small dot (Hawkins and Melchior, 1985). (b) Basalts from the N15 segment = large dot (approximate location of basalts from stations K9, K8, K4, S3, K6 and K12 is given). (c) Basalts from the N–S segment = square (approximate location of basalts from station K15 is given); basalts from the northern NFB = small dot (Sinton et al., 1991). (d) Basalts from the 174E segment = triangle (approximate location of basalts from stations K22, K21 and K23 is given); basalts from the Lau Basin = small dot (Hawkins and Melchior, 1985).

cally but also petrogenetically. These samples are in the same range of composition as the typical MORBs (groups 16A, 16B and 16C defined by Sinton et al. (1991) in the northern NFB). The only slightly alkali enriched basalts from this N–S segment are those from station K15. Geochemical types observed along the 174E segment are highly variable from one station to the next. Basalts from station K23 are typical MORBs, whereas lavas from the three other stations look like more typical BABBs, with a high total alkali content, as observed in the Mariana Trough or during the early opening of the Lau Basin (Fig.6d).

These results are confirmed in the Rb/Sr vs. K/P diagram (Fig.7), where our NFB data are compared to the Mariana Trough basalts (Hawkins and Melchior, 1985). Here, more than half of the basalts from the N160, N15 and 174E segments are in the BABB field, whereas most of the basalts from the N–S segment are in the MORB field.

Preliminary rare earth elements (REE) data (Table 6) show quite large variations in REE contents (normalized to chondrite using data from Sun and McDonough, 1989) (Fig.8), demonstrating the wide variations in the LILEs and especially in the LREE contents of the basalts produced along this back-arc spreading centre. On the N160 segment (sample K29-4, Table 6), the REE pattern is quite flat to slightly LREE depleted (Fig.8), as is also observed in BABB (Saunders and Tarney, 1984; Hawkins and Melchior, 1985; Sinton et al., 1991). On the N15 segment (sample K4-1, Table 6), the REE pattern is again quite flat to slightly LREE depleted (Fig.8), but complementary analy-

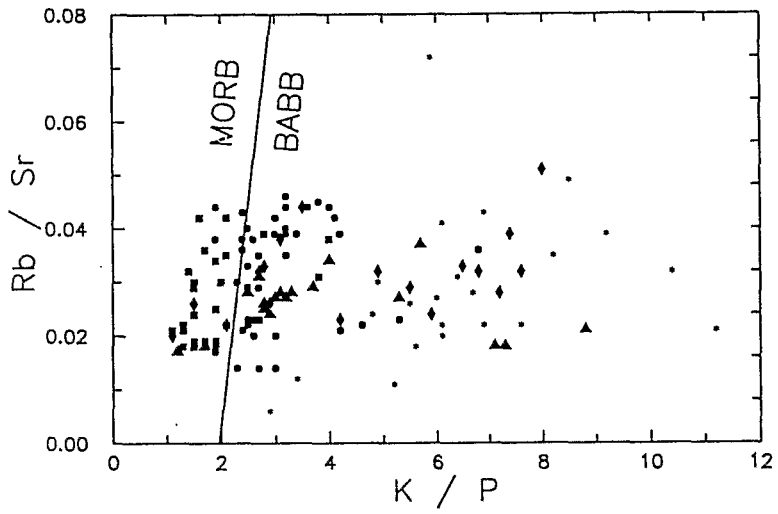

Fig.7. Distinction between BABB and MORB for the NFB basalts based on Rb/Sr vs. K/P diagram (in ppm). Diamond = N160 segment; dot = N15 segment; square = N–S segment; triangle = 174E segment; asterisk = Mariana Trough basalts (Hawkins and Melchior, 1985). The MORB–BABB field boundary is delineated using the set of data shown.

TABLE 6

Rare earth elements analyses of eight basalts from the NFB. Analyses performed by ICP at the Geological Survey of Japan at Tsukuba (analyst M. Nohara)

Sample	K29-4	K17-1	K4-1	K14-7	K15-6	K21-9	K23-1	K22-1
La	3.67	3.69	3.28	1.97	3.67	6.79	1.02	5.40
Ce	11.60	10.72	10.22	7.19	11.49	18.26	3.67	14.63
Pr	1.89	1.62	1.61	1.29	1.85	2.63	0.74	2.27
Nd	9.87	9.04	9.17	7.09	10.06	12.19	4.76	11.40
Sm	3.37	2.92	3.09	2.70	3.47	3.54	1.84	3.25
Eu	1.22	1.12	1.17	1.04	1.29	1.33	0.75	1.17
Gd	4.56	4.23	4.35	4.05	4.60	4.49	2.91	4.08
Tb	0.75	0.71	0.74	0.75	0.84	0.79	0.58	0.71
Dy	5.19	5.04	0.51	5.07	5.59	4.87	3.85	4.48
Ho	1.07	1.05	1.11	1.11	1.26	1.05	0.88	0.99
Er	3.13	3.13	3.25	3.19	3.57	2.91	2.56	2.89
Tm	0.42	0.44	0.47	0.48	0.51	0.41	0.40	0.39
Yb	2.66	2.94	3.05	3.19	3.43	2.54	2.48	2.05
Lu	0.36	0.46	0.46	0.48	0.55	0.39	0.41	0.28

ses should show that LREE-depleted basalts also coexist in this segment, as suggested above. On the N–S segment, a N-MORB with typical LREE-depleted pattern is found at station K14 (Fig.8), but a flat REE pattern is found at station K15 indicating that some BABB affinity might persist even on this more mature segment. On the short 174E segment, basalts showing depleted, flat and slightly LREE enriched patterns coexist, showing that the mantle source is probably quite heterogeneous below this segment, as it is also below the N160 and N15 segments. $^{87}Sr/^{86}Sr$ and $^{143}Nd/^{144}Nd$ ratios show the presence of small but distinct regional scale variations, which support similar conclusions (Nohara et al., 1989).

Along-strike variations

Another means by which the geochemical variations in the NFB basalts can be observed is by plotting selected parameters as a function of the latitude of the sampling site (Fig.9). The first of these parameters is the axial bathymetry of the spreading centre (Fig.9a). The different morpho-

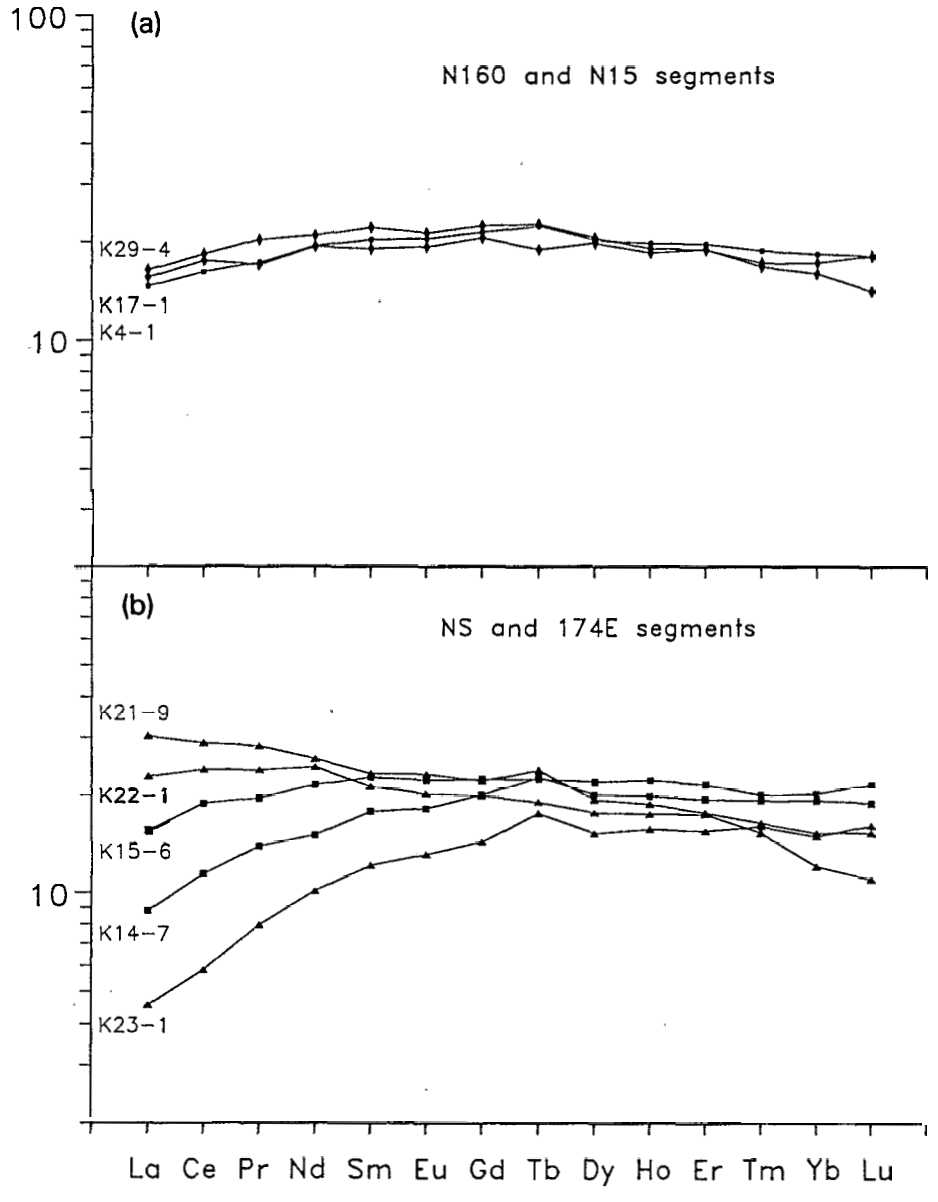

Fig.8. Rare earth element abundances normalized to chondrite (chondrite values after Sun and McDonough, 1989) for selected samples from the NFB. (a) N160 segment = diamond; N15 segment = dot. (b) N–S segment = square; 174E segment = triangle.

logical styles of the four segments clearly appear, with a smooth morphology for the N–S segment, whereas strong bathymetrical irregularities appear along the others, like the rise towards the triple junction or the roughness of the 174E segment.

Preliminary results related the chemical along-strike variability in the N15 segment to a heterogeneous mantle source below this segment (Eissen et al., 1990). The present new data allow us to clarify the situation. The most striking feature in Fig.9 lies within the N–S segment, which shows relatively low and uniform Ba, Rb, K/P and $(K/Ti)_N$ contents/ratios, as expected for N-MORBs. By contrast, the basalts of the N160, N15 and 174E segments show much higher average K/P ratios (between 1 and 8 instead of ca.2 for the N–S

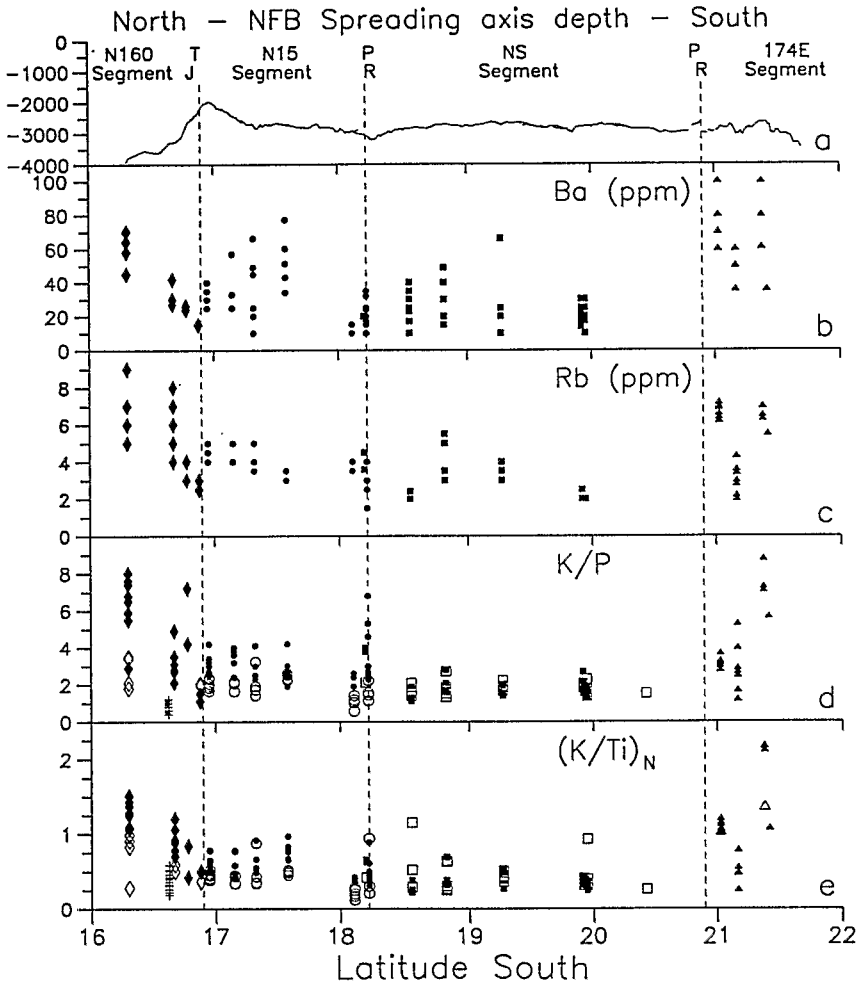

Fig.9. Variations as a function of latitude in terms of five parameters. (a) Bathymetry (m) (Lafoy, 1989). (b) Ba (in ppm). (c) Rb (in ppm). (d) K/P (in ppm). (e) $(K/Ti)_N$ (chondrite normalized) ratio. Diamond = N160 segment; plus sign = data from Sinton et al. (1991); circle = N15 segment; square = N–S segment; triangle = 174E segment. (Open symbols for glass and closed symbols for bulk rock analyses.) *TJ* = triple junction; *PR* = propagating rift.

segment). All segments except the N–S segment display more variable Ba and Rb contents and $(K/Ti)_N$ ratios (this latter ratio varies with Nb/Zr and La/Sm ratios; Romeur, 1987). Therefore, a large proportion of these basalts have a BABB affinity. Moreover, the mantle source of the N15 segment is probably heterogeneous because MORB and BABB presently coexist on this segment. However, the presence of N-MORB just east of the N160 axis (station T16; Sinton et al., 1991; Fig.2) and the variability of the 174E segment probably indicates that these segments also show the presence of heterogeneous mantle sources along them. The morphological and geochemical peculiarities of the N–S segment compared to the others may be explained by its maturity. Indeed, it is the only spreading segment in the NFB which has been functioning in a steady state since 3 m.y. B.P.; it was not affected by the last reorganization (1 m.y. ago) which created the N160 and N15 segments and their triple junction with the North Fiji Fracture Zone (Auzende et al., 1988c).

Because the NFB is a large, old back-arc basin, it is not directly influenced by the New Hebrides subduction. Compared to a back-arc spreading centre situated much closer to an active subduc-

tion, such as the Mariana Trough (Saunders and Tarney, 1984; Sinton and Fryer, 1987), enrichment of LILEs, LREEs and volatiles in the NFB mantle source as the basin gradually opened was much less. However, beneath active spreading segments such as N160, N15 and 174E, NFB upper mantle can be locally slightly enriched in these elements (compared to more typical N-MORB mantle sources) and therefore heterogeneous; this is in particular suggested by the $(K/Ti)_N$ ratio. The N–S segment, which has been in steady state since 3 m.y., produces almost exclusively magmas of the N-MORB type, in which the LILE and LREE component has already been removed during earlier stages of magma extraction. Therefore, the mantle source below this N–S segment is significantly depleted in these elements (Fig.8), as is the case for the classical N-MORB mantle sources.

Summary and conclusion

(1) Oceanic spreading in the North Fiji Basin (NFB) is occurring between 16°S and 21°30′S along four segments which each exhibit a specific morphology. This along-strike variability reflects the lack of stability in this basin. This instability is demonstrated by the 3 m.y. and 1 m.y. reorganizations of the spreading system, and, compared to more classical mid-oceanic spreading centres, has led to a relatively high number of features of local instability such as OSCs and propagating rifts.

(2) Twenty four new sampling stations were established along this spreading centre, and at each plagioclase ± olivine ± clinopyroxene basalts were recovered (plagioclase > olivine > clinopyroxene). The petrogenesis of these basalts is essentially controlled by low-pressure crystal fractionation. However, mixing of more or less differentiated compositionally closely related magma batches may occur locally within a single magma reservoir. These basalts have been described geochemically and mineralogically segment by segment. They have also been compared together with basalts from the Mariana Trough, the Lau Basin and the northern NFB.

(3) The N–S segment of the NFB spreading ridge has a uniform morphology between 18°20′S and 21°S. Basalts from this segment have mineralogical, petrological and geochemical characteristics typical of moderately evolved N-MORBs. This spreading segment is the only one in the NFB that has been functioning in a steady state since 3 m.y. It has therefore reached a mature stage, comparable to the more classical oceanic spreading centres, with a LILE- and LREE-depleted mantle source. However, a limited BABB geochemical signature, such as that observed at station K15, may locally occur along this segment.

(4) North and south of the 16°45′S triple junction respectively the N160 and N15 segments show a steep bathymetrical rise towards the triple junction. Both segments have specific morphological characteristics, i.e. an assymmetrical rift section for the N160 segment and several instability features such as OSCs and propagating rifts on the N15 segment. The basalts are mostly characterized by LILE and slightly LREE-enriched magmas suggesting a BABB affinity, even though MORBs are also found on the N15 and N160 segments. The presence of magma of BABB affinity 500 km east of the active New Hebrides subduction zone might be explained by the youth of these segments. Active spreading started here 1 m.y. ago, in the middle of an older NFB crust with a possible marked BABB affinity. Below these recently formed segments, the mantle source is then heterogeneous, with some BABB affinities being locally retained.

(5) Morphological, petrological and geochemical data from the 174E segment indicate that this segment, the one closest to the subduction zone, is also producing both BABB and MORB magmas. Therefore, the coexistence of basalts with depleted, flat and slightly enriched REE patterns seems to indicate that the mantle sources beneath this segment are also heterogeneous.

(6) Petrogenetically mature processes allow the production of N-MORB magmas only on the most steady-state segment, the N–S segment. BABB still coexist today with MORB on the less stable and more recently created segments. Furthermore, the presence of 12 m.y. old (K/Ar) MORB on the northwestern margin of the NFB (Monjaret et al., 1987) and of ferrobasalts with MORB affinity from the area north of the Fiji Islands (Sinton et al., 1991) indicates that MORBs have been produced since the early development of the NFB.

Acknowledgements

We wish to express our thanks to the captains and crews of the R.V. *Jean Charcot* and *Kaiyo*, and to all the co-chief scientists, scientists and technicians who participated in the sample collection on the SEAPSO Leg 3, KAIYO 87 and KAIYO 88 cruises. We thank also Jo Cotten for the geochemical analyses he performed in his laboratory at the *Université de Bretagne Occidentale* at Brest, Marcel Bohn for his help in performing the microprobe analyses at the IFREMER Centre in Brest, and Masahiro Aoki for his help in performing the complementary microprobe analyses at the GSJ at Tsukuba. We also express our warmest appreciation to Ric Price and John Sinton for their careful review of this paper and their pertinent suggestions. Finally, we thank Jacques Récy, chief of the *Unité de Recherche 1F d'lORSTOM*, for his assistance which allowed us to carry out this work.

References

Aggrey, K.E., Muenow, D.W. and Sinton, J.M., 1988. Volatile abundances in submarine glasses from the North Fiji and Lau back-arc basins. Geochim. Cosmochim. Acta, 52: 2501–2506.

Auzende, J.M., Eissen, J.P., Caprais, M.C., Gente, P., Gueneley, S., Harmegnies, F., Lagabrielle, Y., Lapouille, A., Lefèvre, C., Maillet, P., Mazé, J.P., Ondréas, H., Schaaf, A. and Singh, S., 1986. Accrétion océanique et déformation dans la partie méridionale du bassin Nord Fidjien: résultats préliminaires de la campagne océanographique SEAPSO III du N.O. Jean Charcot (Décembre 1985). C.R. Acad. Sci. Paris, 306: 971–978.

Auzende, J.M., Eissen, J.P., Gente, P., Lafoy, Y., Lagabrielle, Y., Schaaf, A. and Charlou, J.L., 1988a. The accretion system of the central part of the North Fiji Basin (SW Pacific) between 16°S and 21°S (SEAPSO Leg 3 cruise — Dec 1985). Tectonophysics, 146: 317–351.

Auzende, J.M., Honza, E. and the Scientific Party of the Kaiyo 87 Cruise, 1988b. L'accrétion récente dans le Bassin Nord-Fidjien: premiers résultats de la campagne franco-japonaise Kaiyo 87. C.R. Acad. Sci. Paris, 306(II): 971–978.

Auzende, J.M., Lafoy, Y. and Marsset, B., 1988c. Recent geodynamic evolution of the North Fiji Basin (SW Pacific). Geology, 16: 925–929.

Bender, J.F., Hodges, F.N. and Bence, A.E., 1978. Petrogenesis of basalts from the project FAMOUS area: Experimental study from 0 to 15 kbar. Earth Planet. Sci. Lett., 41: 277–302.

Brocher, T.H. (Editor), 1985. Investigations of the Northern Melanesian Borderland. (Circum-Pacific Council for Energy and Mineral Resources, Earth Science Series 3. CPCEMR, Houston, Tex, 199 pp.

Bryan, W.B., 1983. Systematics of modal phenocryst assemblages in submarine basalts: Petrologic implications. Contrib. Mineral. Petrol., 83: 62–74.

Charvis, P. and Pelletier, B., 1989. The northern New Hebrides back-arc troughs: history and relation to the North Fiji Basin based on tectonic and magnetic studies. Tectonophysics, 170: 259–277.

Chase, C.G., 1971. Tectonic history of the Fiji plateau. Geol. Soc. Am. Bull., 82: 3087–3110.

Cherkis, N.Z., 1980. Aeromagnetic investigations and sea-floor spreading history in the Lau basin and northern Fiji plateau. UN ESCAP, CCOP/SOPAC, Tech. Bull., 3: 37–45.

Craig, H. and Poreda, R., 1987. Data report, Papatua expedition, legs V and VI. Scripps Ref. Ser., 87:14, 80 pp.

Drake, M.J., 1976. Plagioclase-melt equilibria. Geochim. Cosmochim. Acta, 40: 457–465.

Eissen, J.P., Juteau, T., Dupré, B., Joron, J.L., Humler, E. and Al'mukhamedov, A.I., 1989. Petrology and geochemistry of basalts from the Red Sea rift at 18° north. J. Petrol., 30: 791–839.

Eissen, J.P., Morvan, G., Lefèvre, C., Maillet, P., Urabe, T., Auzende, J.M. and Honza, E., 1990. Pétrologie et géochimie de la zone d'accrétion du centre du Bassin Nord Fidjien (SW Pacifique). C.R. Acad. Sci. Paris, 310(II): 771–778.

Falvey, D.A., 1978. Analysis of paleomagnetic data from the New Hebrides. Aust. Soc. Explor. Geophys. Bull., 9: 117–123.

Gente, P., 1987. Etude morphostructurale comparative de dorsales océaniques à taux d'expansion variés. Schéma d'évolution morphologique de l'axe de dorsales: liaison avec l'hydrothermalisme. Thèse, Univ. Bretagne Occidentale, Brest, 371 pp.

Grove, T.L. and Bryan, W.B., 1983. Fractionation of pyroxene phyric MORB at low pressure: an experimental study. Contrib. Mineral. Petrol., 84: 293–309.

Hawkins, J.W. and Melchior, J.T., 1985. Petrology of Mariana Trough and Lau Basin basalts. J. Geophys. Res., 90: 11431–11468.

Hey, R.N., 1977. A new class of "pseudofaults" and their bearing on plate tectonics: a propagating rift model. Earth Planet. Sci. Lett., 37: 321–325.

Irving, A.J. and Frey, F.A., 1984. Trace element abundances in megacrysts and their host basalts: constraints on partition coefficients and megacryst genesis. Geochim. Cosmochim. Acta, 48: 1201–1221.

Karig, D.E., 1971. Origin and development of marginal basins in the western Pacific. J. Geophys. Res., 76: 2542–2561.

Karig, D.E., 1974. Evolution of arc systems in the western Pacific. Annu. Rev. Earth Sci., 2: 51–75.

Kroenke, L.W., 1984. Cenozoic tectonic development of the southwest Pacific. UN ESCAP, CCOP/SOPAC, Tech. Bull., 6: 122 pp.

Kroenke, L.W. and Eade, J.V. (Editors), 1991. Basin Formation, Ridge Crest Processes and Metallogenesis in the North Fiji Basin. (Circum-Pacific Council for Energy and Mineral Resources, Earth Science Series Vol. 12.).

Kroenke, L.W. and Shipboard Scientific Party, 1987. Cruise report. CCOP/SOPAC North Fiji Basin expedition. R/V Moana Wave cruise MW 87-01. 37 pp.

Lafoy, Y., 1989. Evolution géodynamique des bassins margi-

naux Nord-Fidjien et de Lau (Sud-Ouest Pacifique). Thèse, Univ. Bretagne Occidentale, Brest, 261 pp.

Lafoy, Y., Auzende, J.M., Gente, P. and Eissen, J.P., 1987. L'extrémité occidentale de la zone de fracture fidjienne et le point triple de 16°40'S: Résultats du Leg III de la campagne SEAPSO du N.O. Jean Charcot (Décembre 1985) dans le bassin Nord-Fidjien (SW Pacifique). C.R. Acad. Sci. Paris, 304(II): 3: 147–152.

Larue, M.B., Pontoise, B., Malahoff, A., Lapouille, A. and Latham, G.V., 1982. Bassins marginaux actifs du sud-ouest Pacifique: plateau Nord-Fidjien, bassin de Lau. In: Equipe de Géologie–Géophysique du Centre ORSTOM de Nouméa (Editors), Contribution à l'Etude Géodynamique du Sud-Ouest Pacifique. Trav. Doc. ORSTOM, 147: 363–406.

Louat, R. and Pelletier, B., 1989. Seismotectonics and present-day relative plate motions in the New Hebrides–North Fiji basin region. Tectonophysics, 167: 41–55.

Maillet, P., Eissen, J.P., Lapouille, A., Monzier, M., Baleivanualala, V., Butscher, J., Gallois, F. and Lardy, M., 1986. La dorsale active du Bassin Nord-Fidjien entre 20.000°S et 20.53°S: Signature magnétique et morphologie. C.R. Acad. Sci. Paris, 302(II): 135–140.

Maillet, P., Monzier, M., Eissen, J.P. and Louat, R., 1989. Geodynamics of an arc–ridge junction: The New Hebrides arc/North Fiji Basin case. Tectonophysics, 165: 251–268.

Malahoff, A., Feden, R.H. and Fleming, H.S., 1982. Magnetic anomalies and tectonic fabric of marginal basins north of New Zealand. J. Geophys. Res., 87: 4109–4125.

Monjaret, M.C., Bellon, H., Maillet, P. and Récy, J., 1987. Le volcanisme des fossés arrière-arc des Nouvelles-Hébrides (campagne SEAPSO Leg 2 du N/O Jean Charcot dans le Pacifique Sud-Ouest): Datations K–Ar et données pétrologiques préliminaires. C.R. Acad. Sci. Paris, 305(II): 605–609.

Nohara, M., Urabe, T., Joshima, M. and Honza, E., 1989. REE and isotope constraints on the origin of back-arc basalts in the North Fiji Basin. CCOP/SOPAC Misc. Rep., 79: 95.

Pelletier, B., Charvis, P., Daniel, J., Hello, Y., Jamet, F., Louat, R., Nanau, P. and Rigolot, P., 1988. Structure et linéations magnétiques dans le coin Nord-Ouest du bassin Nord-Fidjien: résultats préliminaires de la campagne Eva 14 (août 1987). C.R. Acad. Sci. Paris, 306(II): 1247–1254.

Presnall, D.C., Dixon, J.R., O'Donnell, T.H. and Dixon, S.A., 1979. Generation of mid-ocean ridges tholeiites. J. Petrol., 20: 3–35.

Roedder, P.L. and Emslie, R.F., 1970. Olivine–liquid equilibrium. Contrib. Mineral. Petrol., 29: 275–289.

Romeur, M., 1987. Variabilité locale de la composition des MORB. Etude du rapport K/Ti dans les verres basaltiques des axes des rides Médio-Atlantique et Est-Pacifique. Rapp. D.E.A., Univ. Bretagne Occidentale, Brest, 91 pp.

Ruellan, E., Auzende, J.M., Honza, E. et al., 1989. L'accrétion dans le bassin Nord Fidjien méridional: premiers résultats de la campagne franco-japonaise STARMER/KAIYO 88. C.R. Acad. Sci. Paris, 309: 1247–1254.

Saunders, A.D. and Tarney, J., 1984. Geochemical characteristics of basaltic volcanism within back-arc basins. In: B.P. Kokelaar and M.F. Holwells (Editors), Marginal Basins: Geology, Volcanism and Associated Sedimentary and Tectonic Processes in Modern and Ancient Marginal Basins. Blackwell, Oxford, pp.59–76.

Sinton, J. and Fryer, P., 1987. Mariana Trough lavas from 18°N: Implications for the origin of back-arc basin basalts. J. Geophys. Res., 92: 12782–12802.

Sinton, J., Price, R.C., Johnson, K.T.M., Staudigel, H. and Zindler, A., 1991. Petrology and geochemistry of submarine lavas from the Lau and North Fiji Basins. In: L.W. Kroenke and J.V. Eade (Editors), Basin Formation, Ridge Crest Processes and Metallogenesis in the North Fiji Basin. (Circum-Pacific Council for Energy and Mineral Resources, Earth Science Series, 3.) Vol. 12, pp. 155–177.

Stakes, D.S., Shervais, J.W. and Hopson, C.C., 1985. The volcano-tectonic cycle of the FAMOUS and AMAR valleys, Mid-Atlantic ridge (36°47'N): evidence from basalt glass and compositional variations for a steady state magma chamber beneath the valley midsections, AMAR 3. J. Geophys. Res., 89: 6995–7029.

Staudigel, H. and Bryan, W.B., 1981. Contrasted glass-whole rock compositions and phenocryst redistribution, IPOD sites 417 and 418. Contrib. Mineral. Petrol., 78: 255–262.

Sun, S.S. and McDonough, W.F., 1989. Chemical and isotopic systematics of oceanic basalts: implications for mantle composition and processes. In: A.D. Saunders and M.J. Norry (Editors), Magmatism in the Ocean Basins. Geol. Soc. Spec. Publ., 42: 313–345.

Walker, D., Shibata, T. and DeLong, S.E., 1979. Abyssal tholeiites from the Oceanographer Fracture zone. II: Phase equilibria and mixing. Contrib. Mineral. Petrol., 70: 111–125.